Respiratory syncytial virus replication: Inhibition by influenza A virus defective interfering particles

Piagnani, Elena

UNIVERSITY OF RIJEKA
DEPARTMENT OF BIOTECHNOLOGY
Graduate programme
"B*iotechnology for the Life Sciences"*

Elena Piagnani

"Respiratory syncytial virus replication: Inhibition by influenza A virus defective interfering particles"

Master's Thesis

Rijeka, 2022

UNIVERSITY OF RIJEKA
DEPARTMENT OF BIOTECHNOLOGY
Graduate programme
"B*iotechnology for the Life Sciences"*

Elena Piagnani

"Respiratory syncytial virus replication: Inhibition by influenza A virus defective interfering particles"

Master's Thesis

Rijeka, 2022

Mentor: Dr.-Ing. Sascha Young Kupke

Co-mentor: Doc. dr. sc. Nicholas James Bradshaw

Supervisor: Lars Pelz, M. Sc.

SVEUČILIŠTE U RIJECI
ODJEL ZA BIOTEHNOLOGIJU
Diplomski sveučilišmi studij
"Biotehnologija za znanosti o životu"

Elena Piagnani

"Replikacija respiratornog sincicijalnog virusa: Inhibicija interferirajućim česticama defektnog virusa gripe A"

Završni rad

Rijeka, 2022

Mentor: Dr.-Ing. Sascha Young Kupke

Co-mentor: Doc. dr. sc. Nicholas James Bradshaw

Supervisor: Lars Pelz, M. Sc.

The thesis was defended on: _____

Before a committee comprised of:

1. _____
2. _____
3. _____
4. _____

The thesis contains __ pages, __ pictures, __ tables and __ references.

Abstract

Respiratory syncytial virus (RSV) is a major cause of acute lower respiratory infections in infants and susceptible adults. Although the epidemiology and immunobiology of the virus have been widely investigated, no safe vaccine has yet been approved, and treatment with the antiviral ribavirin is limited to severe cases. Nonetheless, new antiviral agents are undergoing development[1].

A new approach encompasses influenza A virus (IAV) defective interfering particles (DIPs). IAV DIPs have been proposed as an antiviral treatment against interferon (IFN)-sensitive respiratory viruses such as influenza A and B, severe acute respiratory syndrome coronavirus 2 (SARS-CoV-2) and yellow fever virus (YFV). In this study, we established a method for RSV production and assessed the virus' replication dynamics. Moreover, the inhibitory potential of IAV DIPs against RSV propagation was studied in *in vitro* coinfection experiments. Specifically, we investigated the antiviral activity of DI244, a prototypic, well-characterized DIP that harbors a large internal deletion in Segment 1 of the viral genome, and of OP7, a newly discovered DIP that presents 37 point mutations on Segment 7 of the viral RNA (vRNA)[2,3]. We report that DI244 and especially OP7 are able to partially suppress RSV replication in IFN-competent cells. Furthermore, we show that the inhibitory potential of IAV DIPs is dependent on the innate immune response stimulation. It appears that DI vRNAs were recognized by the retinoic acid inducible gene I (RIG-I), leading to upregulation of type I and type III interferons (IFNs). IFNs activated the janus kinase-signal transducers and activators of transcription (JAK/STAT) signaling cascade, which culminated in the expression of interferon stimulated genes (ISGs).

Our results suggest that the IAV DIPs DI244 and OP7 may represent a promising antiviral agent for the treatment and prophylaxis of RSV infection.

Keywords: Respiratory syncytial virus (RSV), influenza A virus (IAV), defective interfering particles (DIPs), antiviral, coinfection, tissue culture infection dose 50 ($TCID_{50}$), reverse transcription quantitative PCR (RT-qPCR)

Sažetak

Respiratorni sincicijski virus (RSV) glavni je uzročnik akutnih infekcija donjeg dišnog sustava u dojenčadi i osjetljivih odraslih osoba. Iako su epidemiologija i imunobiologija virusa opsežno istražene, sigurno cjepivo još nije odobreno, a liječenje antivirotikom ribavirinom ograničeno je na teške slučajeve. Usprkos tome, razvijaju se novi antivirusni lijekovi[1].

Novi pristup obuhvaća defektne interferirajuće čestice (DIP) virusa influence A (IAV). DIP-ovi IAV predloženi su kao antivirusni tretman protiv respiratornih virusa osjetljivih na interferon (IFN) kao što su gripa A i B, teški akutni respiratorni sindrom coronavirus 2 (SARS-CoV-2) i virus žute groznice (YFV). U ovoj studiji smo uspostavili metodu za proizvodnju RSV-a i procijenili dinamiku replikacije virusa. Nadalje, inhibicijski potencijal DIP-a IAV protiv širenja RSV-a proučavan je u *in vitro* eksperimentima koinfekcije. Konkretno, istražili smo antivirusnu aktivnost DI244, prototipskog, dobro karakteriziranog DIP-a koji sadrži veliku unutarnju deleciju u segmentu 1 virusnog genoma, i OP7, novootkrivenog DIP-a koji sadrži 37 točkastih mutacija na segmentu 7 virusne RNA (vRNA)[2,3]. Naši rezultati pokazuju da DI244, a posebno OP7, mogu djelomično suzbiti RSV replikaciju u stanicama kompetentnim za IFN. Nadalje, pokazujemo da inhibitorni potencijal DIP IAV ovisi o stimulaciji urođenog imunološkog odgovora. DI vRNA prepoznaje gen I inducibilan retinoičnom kiselinom (RIG-I), što dovodi do pojačane ekspresije interferona tipa I i tipa III (IFN). IFN-i dovode do aktivacije Janus kinaze i STAT proteina putem JAK/STAT signalnog puta, što kulminira ekspresijom gena stimuliranih interferonom (ISG).

Naši rezultati sugeriraju da su DIP-ovi IAV, DI244 i OP7, obećavajuća antivirusna sredstva za liječenje i profilaksu RSV infekcije.

Ključne riječi: Respiratorni sincicijski virus (RSV), virus influence A (IAV), defektne interferirajuće čestice (DIP), antivirusni, koinfekcija, infekcija kulture tkiva doza 50 ($TCID_{50}$), kvantitativni PCR reverzne transkripcije (RT-qPCR)

Acknowledgments

I would like to thank Doc. dr. sc. Nicholas James Bradshaw, Assistant Professor at the Department of Biotechnology of the University of Rijeka, for being my co-mentor and supporting my decision to participate to the Erasmus+ Traineeship program.

I am profoundly grateful to Prof. Dr.-Ing. Udo Reichl for giving me the opportunity to carry out my master's thesis project at the Department of Bioprocess Engineering at the Max Planck Institute for Dynamics of Complex Technical Systems, Magdeburg.

I would like to express my most sincere gratitude to my mentor Dr.-Ing. Sascha Y. Kupke and to my supervisor Lars Pelz. Words cannot express my appreciation for their guidance and encouragement throughout my stay at the MPI, for their valuable advice during each one of our meetings and for all that I have learned under their supervision over the last year.

Special thanks go to Nancy Wynserski and Claudia Best for their technical assistance during my experimental work, and for the kindness they showed towards me since the first day I entered the lab.

I would also like to extend my deepest gratitude to the Molecular Biology and the Upstream Processing groups, for being such a cohesive team and for creating such a stimulating and welcoming working environment. Working with them has been a real inspiration, and I feel privileged to have had the possibility to be part of such a great group.

Finally, I would like to thank my family, for believing in me and supporting me through every step of my academic journey, and my best friends for being the best second family that a person could ever wish for. My heart is always with you, no matter how many kilometers are between us.

Last but surely not least, I want to wholeheartedly thank my boyfriend Hauke, for being the most caring, loving and supportive partner there is, for helping me get through the difficult moments and for celebrating the happy ones with me.

Table of Contents

List of Figures

List of Tables

List of Abbreviations

AA(s)	Amino acid(s)
AEC(s)	Airway epithelial cell(s)
ANOVA	Analysis of variance
ATCC	American Type Culture Collection
CARD	Caspase activation and recruitment
cDNA	Complementary DNA
CO_2	Carbon dioxide
CIL	Conserved intracellular loop
Ct	Cycle threshold
Df	Dilution factor
DI	Defective interfering
DIP(s)	Defective interfering particle(s)
DMEM	Dulbecco's Modified Eagle's Medium
dNTP	Deoxyribonucleotide triphosphate
dpi	Days post infection
ds	Double stranded
DVG(s)	Defective viral genome(s)
EDTA	Ethylenediaminetetraacetic acid
EtOH	Ethanol
FCS	Fetal calf serum
FFU	Focus forming unit
FI	Formalin-inactivated
FL	Full length
GAPDH	Glyceraldehyde 3-phosphate dehydrogenase
GTP	Guanosine-5'-triphosphate
HIV	Human immunodeficiency virus
hMPV	Human metapneumovirus
hpi	Hour(s) post infection
HPV	Human papillomavirus

hTERT-NEC(s)	Telomerase reverse transcriptase-transfected human primary nasal epithelial cell(s)
IAV	Influenza A virus
ICTV	International Committee on Taxonomy of Viruses
IFITM 1	Interferon-induced transmembrane protein 1
IFN	Interferon
IFNAR	Type I IFN receptor
IFN-β1	Interferon beta 1
IFN-λ1	Interferon lambda 1
IFNLR	IFN lambda receptor
IFNR(s)	Interferon receptor(s)
IRF(s)	Interferon regulatory factor(s)
ISG(s)	Interferon stimulated gene(s)
ISGF3	IFN-stimulated gene factor 3
JAK/STAT	Janus kinase-signal transducers and activators of transcription
LGP2	Laboratory of genetics and physiology 2
mAbs	Monoclonal antibodies
MAVS	Mitochondrial antiviral signaling
MDCK	Madin-Darby canine kidney
MDA5	Melanoma differentiation-associated protein 5
MERS-CoV	Middle East respiratory syndrome coronavirus
MM	Master mix
MOI	Multiplicity of infection
MVA	Modified vaccinia virus Ankara
Mx1	Myxovirus resistance protein 1
NS	Non-structural
ns	Not significant
nt	Nucleotide(s)
OA	Older adults
PAMP(s)	Pathogen-associated molecular pattern(s)
PB2	Basic protein 2

PBS	Phosphate-buffered saline
PCR	Polymerase chain reaction
PRR(s)	Pattern recognition receptor(s)
qPCR	Quantitative polymerase chain reaction
RIG-I	Retinoic acid inducible gene I
RLR(s)	RIG-I-like receptor(s)
RNA	Ribonucleic acid
RNP(s)	Ribonucleoprotein(s)
rpm	Revolutions per minute
RSV	Respiratory syncytial virus
RT	Reverse transcription
SARS-CoV-2	Severe acute respiratory syndrome coronavirus 2
Seg	Segment
SH	Small hydrophobic
ssRNA (-)	Single-stranded negative-sense RNA
STV	Standard virus
$TCID_{50}$	Tissue culture infection dose 50
VCC	Viable cell concentration
WT	Wild type
YFV	Yellow fever virus

1. Introduction

The following chapter presents a comprehensive overview of the theoretical background of this study.

1.1 Respiratory syncytial virus

Respiratory syncytial virus (RSV) was first recovered from chimpanzees affected by a respiratory disease in 1956, and was subsequently isolated in humans in 1957[4,5]. RSV is classified into two subtypes, RSV-A and RSV-B, which include multiple genotypes that co-circulate, switching in dominance almost every year. The two RSV subtypes have evolved separately, and they differ in the amino acid sequence of the G protein. For example, if the RSV strain Long is compared to RSV A2 (both belonging to the RSV-A subtype), they are found to share 94% of their amino acid G protein sequences, while the A2 strain only has 53% amino acid identity with the 18573 strain, an RSV-B subtype strain[6–8]. RSV A2, which will be used in this study, is a laboratory strain first isolated in Australia in 1961. To date, it is a widely used platform for the development of live-attenuated vaccine candidates and it is commonly used to study RSV[9].

1.1.1 Taxonomy

According to the International Committee on Taxonomy of Viruses (ICTV), RSV belongs to the Pneumoviridae family, genus Orthopneumovirus, in the order Mononegavirales[10,11]. This taxon used to be a subfamily of the Paramyxoviridae, but was reclassified as a family of its own in 2016[1,12]. The Orthopneumoviruses infect mammalian species primarily through contact and aerosol droplets. The Pneumoviridae family also includes human metapneumovirus (hMPV) which, like RSV, is a very prominent pathogen in children [13].

1.1.2 Virion morphology

RSV is an enveloped non-segmented single-stranded negative-sense RNA (ssRNA (-)) virus[11]. The RSV genome comprises 10 genes and is 15.2 kB long, encoding for 11 proteins[14]. Unlike influenza viruses, it presents a non-segmented

genome, which limits its capacity to re-assort genomic portions and therefore undergo antigenic shifts [15]. The RSV virion is pleomorphic, and in its spherical form it can measure between 150 and 250 nm in diameter. The virus in its filamentous form can be between 1 and 10 μm in length and has a diameter of around 50 nm[16].

The virus particle presents a lipid bilayer with three surface proteins (Figure 1). Glycoprotein (G) (also called attachment protein) and fusion (F) protein are the most abundant ones and are essential for virion attachment and fusion. F is a surface glycoprotein that allows the fusion of the virion membrane to that of the host cell, while G protein attaches to the host cell receptors[17]. Small hydrophobic (SH) proteins form pentameric ion channels that are believed to play a role in delaying the apoptotic process of infected cells[18]. The matrix (M) protein is found underneath the virus envelope: it is a non-glycosylated protein that can bind to the F protein and is involved in the assembly process of virion structures, as well as their stability[14]. M2-1 protein is a transcription factor able to regulate the switch between ribonucleic acid (RNA) replication and protein transcription; it can also associate with ribonucleoprotein (RNP) complexes and M proteins[19]. The RPN is a complex that encloses the viral RNA (vRNA) in the viral nucleocapsid, forming a helical assembly. It is formed by three proteins: nucleoprotein (N), which participates in the creation of a template to synthesize RNA, large (L) protein, an RNA-dependent RNA polymerase, and phosphoprotein (P), a polymerase cofactor[17,19]. Last, the non-structural (NS) proteins NS1 and NS2 are fundamental in dismantling the host defense systems: they can antagonize apoptotic pathway and suppress interferon (IFN) class I and class III production and signaling, as well as targeting numerous interferon stimulated genes (ISGs)[20,21].

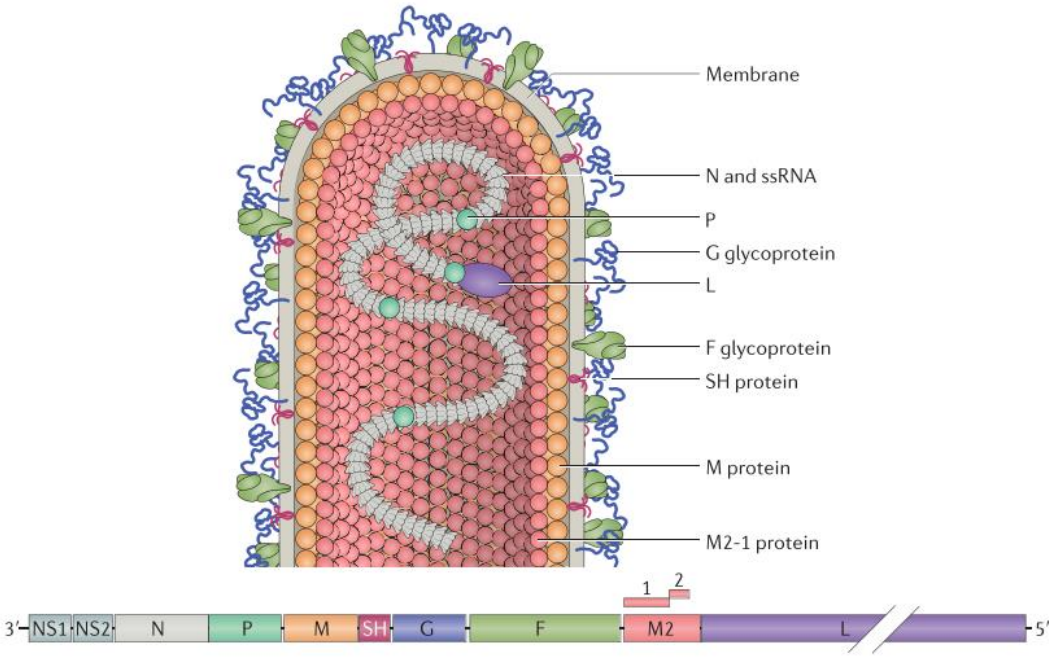

Figure 1 | Schematic structure of RSV virion.

The RSV envelope contains the fusion protein (F), the attachment protein (G) and the small hydrophobic protein (SH). Underneath the envelope are the matrix protein (M) and the M2-1 protein. Viral RNA (vRNA) is encapsulated by nucleoproteins (N), RNA-dependent RNA polymerase (L) and phosphoproteins (P). RSV vRNA is also shown, with genes listed in sense orientation (3' – 5'). (Figure taken from [10])

1.1.3 Replication cycle

RSV enters host cells of the upper and lower respiratory tract via micropinocytosis (Figure 2). When RSV particles attach to the cell membrane through the G protein, they activate several signaling cascades that lead to increased fluid uptake. Actin-mediated membrane protrusion and retraction results in the formation of large vacuoles and a consequent intake of RSV particles. Once the macropinosomes mature into late endosomes and ultimately lyse, RSV vRNA molecules are released into the cell cytoplasm[22,23]. Here, the L, N and P proteins mediate the synthesis of positive-sense mRNA molecules by transcribing all genes from the 3' end to 5' end of the viral genome. Interestingly, there is a gradient of expression by which genes at the 3' are expressed at higher levels than those at the 5' end (Figure 1). As a result, proteins that delay the host's apoptotic and immune responses such as NS and SH proteins are produced in higher amounts starting from early times of infection, delaying the host response against infection and favoring virus proliferation[24–26].

Subsequently, viral RNA is replicated and translated by the host cell machinery, resulting in the production of progeny viral genomes and viral proteins. Newly formed RNP complexes are translocated by the M proteins to the plasma membrane, where they interact with surface glycoproteins F and G. Ultimately, structural proteins and vRNA complexes assemble into infectious filamentous virions prior to detachment from the cell surface; this process is believed to contribute to cell to cell spread of the virus[17,24]. Actin filaments play a fundamental role in this process: RSV can modulate cytoskeletal remodeling and increase actin polymerization and filopodia induction. These processes mediate virion assembly, cell-to-cell spread and virus entry to uninfected cells. The ARP2/3 complex, an actin nucleating and regulatory factor, plays a crucial role in driving actin polymerization, as well as in filopodia formation and cell to cell spreading[17,27].

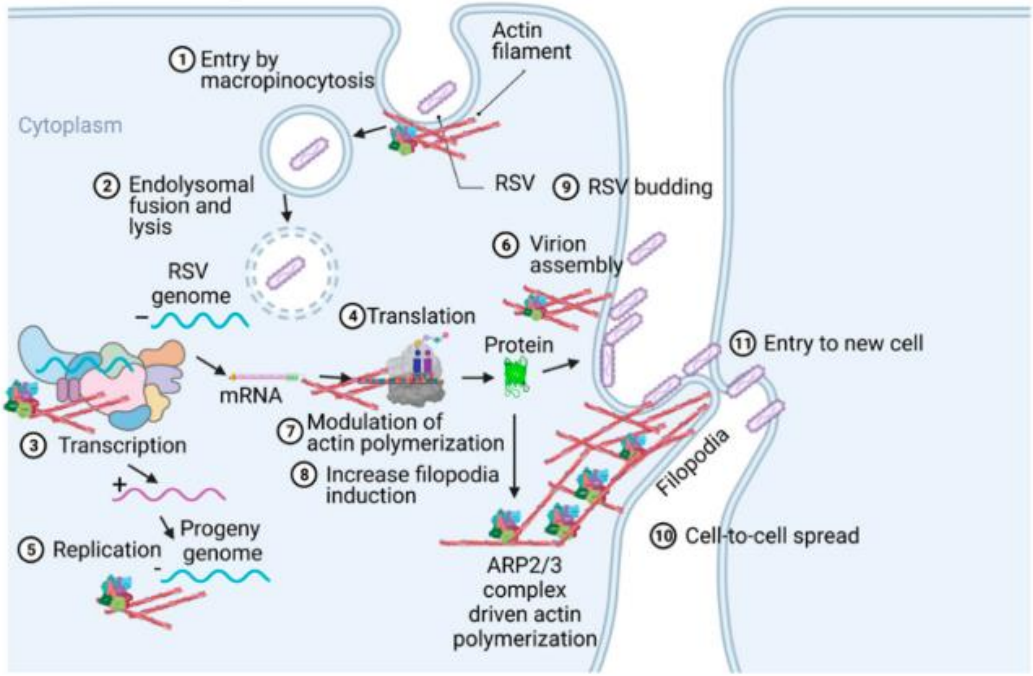

Figure 2 | RSV replication cycle.

RSV particles enter host cells via macropinocytosis and, following endolysosomes lysis, vRNAs are released into the cytoplasm. Here, they undergo transcription, replication and translation, and progeny genomes and proteins are generated. RSV can modulate the polymerization of actin and increase filopodia induction so that actin contributes to the assembly of new filamentous virions, as well as cell to cell spreading of viral particles. (Figure taken from [17])

1.1.4 Transmission and pathogenesis

RSV is the leading cause of bronchiolitis and pneumonia among infants, and each year it causes at least 60000 deaths worldwide among children younger than 5 years. Among the general population, it causes more than 30 million acute respiratory infections per year and it represents an important morbidity and mortality factor[15]. It is estimated that, by the age of 2 years, over 95% of children have been infected with RSV[28]. The seasonality of RSV infection differs across the globe. Temperate climate zones undergo epidemics between late autumn and early spring, while arctic and tropical areas experience less defined variations. On average, epidemics take place in northern areas in the cold and rainy season, while in tropical zones outbreaks occur in rainy and warm seasons[29]. RSV displays seasonality with multiple genotypes: RSV-A and RSV-B types co-circulate and shift in dominance every one to two years. The co-presence of different genotypes is likely one of the reasons why reinfection of previously infected individuals is such a common phenomenon[9].

RSV can be spread through three main modes of transmission: direct contact via physical interaction, indirect contact via touching of contaminated inanimate objects (fomite), and transmission caused by long or short-range interaction with infected individuals with subsequent exposition to infectious aerosols or droplets (Figure 3)[30]. RSV natural strains are highly contagious and they can survive on clothes, objects and skin for extended time periods, in contrast to their heat-sensitive lab-grown counterparts. Inoculation via nose or eyes begins infection in the host, which is followed by 2 to 8 days of incubation[15]. The virus mainly infects ciliated epithelial cells in the respiratory tract, although it has been reported that infection in intraepithelial dendritic cells and pneumocytes can also occur, as well as in basal cells, where RSV can influence the morphogenesis of airway epithelial cells (AECs)[31]. In response to RSV infection, an inflammatory cell infiltrate with T-cell and monocytes is released to the site of infection; this correlates with hyperproduction of mucus, edema of AECs and epithelium necrosis, which eventually lead to narrowing and obstruction of small airways. Disease severity is highly variable within patients, and whether this depends on

the virus strain rather than the host response to viral infection still remains unclear[9,15,32]. Clinical manifestations of RSV disease can range from moderate upper respiratory tract illness to severe lower respiratory tract involvement such as pneumonia and bronchiolitis [11]. Mild symptoms include fever, acute rhinitis or pharyngitis, cough, nasal congestion and shortness of breath. Lower respiratory tract illness can be life-threatening, especially for high risk categories such as infants, elderly and immunocompromised people[15,33]. Bronchiolitis is the most common severe form of RSV disease: patients present fever, lethargy, wheezy cough, noisy breathing and apnea. Other symptoms also include vomiting, general malaise that leads to insufficient feeding and consequent dehydration, subcostal and intercostal retractions and cyanosis[11,15,34]. Diagnoses are normally carried out by analyzing RSV isolates from patients via antigen detection assays. The degree of severity of symptoms is evaluated to determine whether admission to hospital is necessary. An x-ray scan can also be performed in the case of a diagnostic uncertainty, to evaluate the possibility of lower respiratory tract infection[32,35].

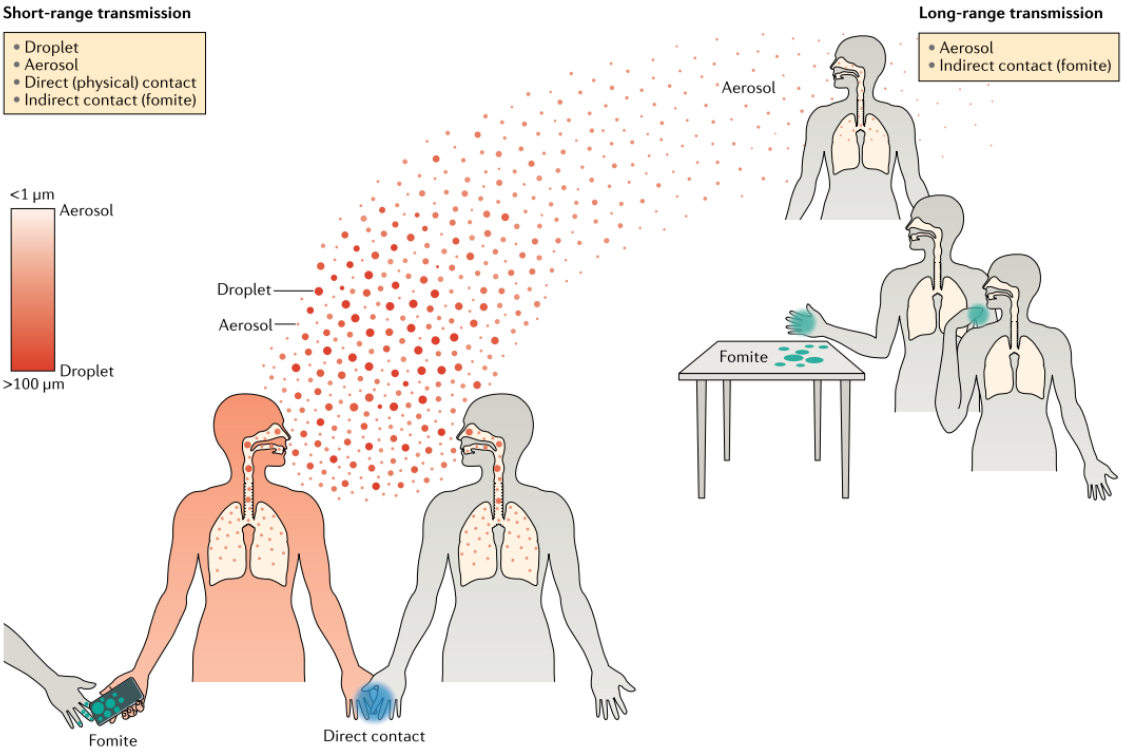

Figure 3 | Modes of transmission of respiratory syncytial virus.

RSV, like many respiratory viruses, can spread through short-range or long-range transmission. The close-range transmission can take place through direct physical contact, indirect contact by touching

contaminated inanimate objects (fomite), or via exposition to infectious aerosols or droplets. Long-range transmission modes include indirect contact via fomite or aerosol inspiration. (Figure taken from [30])

1.1.5 Treatment of RSV infection

To date, aerosolized ribavirin is the only licensed antiviral treatment available to treat RSV infection. Ribavirin is a broad-spectrum antiviral that acts as a guanosine analog. When it is incorporated into the vRNA, it pairs with either uracil or cytosine, introducing mutations. Such hypermutations are lethal for RNA viruses, including RSV[36,3736,37]. Ribavirin's potential has been tested against RSV, as well as the zika virus, hepatitis C virus, sendai virus, influenza A and B viruses and others[37,38]. RSV-infected patients display reduced hospitalization time, limited viral shedding and faster virus clearance following treatment with ribavirin[39,40]. However, the drug is normally only administered in severe cases – especially in immunocompromised children – due to issues with cost, safety and efficacy[41]. The administration process for every aerosol of ribavirin requires a highly specific ventilation system, making the treatment cost-inefficient. On top of that, several cardiovascular-related side effects have been identified following administration, and cases of teratogeny have been reported[39]. Recently, new possible treatments for RSV disease are undergoing development. Seven classes of possible RSV antivirals have been so far identified. There are nucleoside analogues, which introduce mutations that hinder virus replication, monoclonal antibodies (mAbs) that target the N, G and F proteins of RSV, and F and N inhibitors, which interfere with RSV fusion and replication. In addition to these, the potential of inhaled nanobodies, gold nanoparticles and antioxidants is also being investigated[1]. Inhaled nanobodies are variable domains of heavy-chain-antibodies derived from camelids which retain specific antigen binding capacity. Gold nanoparticles can inhibit the virus by hindering viral attachment, entry and budding. Last, antioxidants could ameliorate RSV symptoms and reduce infection by limiting the harmful effects of altered mitochondrial respiratory function caused by RSV[1,39,42].

1.1.6 Vaccine availability

To date, no licensed vaccine is available to prevent RSV infection. The research for the development of an RSV vaccine has been largely delayed by an unsuccessful clinical trial in the 1960s. The protective efficacy of a formalin-inactivated (FI) vaccine was being tested at the time: recipients reported enhanced lung disease and, in some cases, death occurred in patients following RSV infection. Subsequently, it was found that the vaccine did not trigger production of neutralizing antibodies, and it was stimulating an antagonistic Th2 $CD4^+$ T cell response rather than a $CD8^+$ T cell response, which resulted in prolonged virus replication and enhanced immunopathology[43,44]. A further obstacle for the development of a safe and efficient vaccine is the limited duration of immunogenicity conferred by natural RSV infection; the elicited immunity is only transient, and re-infection is very frequent. Moreover, the lack of commonly agreed clinical endpoints due to high variability within different target populations constitutes an additional impairment[45]. Finally, most severe cases in infants occur before 3 months of age, making active immunization not possible[41].

Nowadays, several vaccine candidates are undergoing clinical trials with promising results. It is possible to divide them into four major categories: live-attenuated, subunit-based, vector-based and nanoparticle-based vaccines. The three main target populations that active immunization drugs aim to protect are infants, young children, and adults over the age of 65 [44,45].

Vaccines administered to the parent in the last trimester of their pregnancy have been proposed as a solution for the protection of infants up to 6 months, as transplacental transfer would allow the transmission of antibodies to the fetus[46]. The purified F protein 2 (PFP-2) is a subunit vaccine that showed promising results in phase 1 clinical trials, where 95% of women and their children presented increased levels of anti-F IgG antibodies[47]. Live attenuated vaccines seem to be a promising solution for the immunization of old infants and young children (6-24 months). The LID/ΔM2-2 vaccine is a cDNA-derived version of the RSV A2 strain, in which several regions of M2-2 and SH proteins underwent

deletion. Following administration of LID/ΔM2-2, 90% of recipients displayed a 4-fold increase in neutralizing antibody and anti-F IgG antibody levels, which were maintained by half of the participants also during RSV-season[48]. Several candidates have been tested in the older adults' population as well. The nanoparticle F vaccine is a recombinant near-full length F glycoprotein produced in insect cells with a recombinant baculovirus[49]. It was tested in a phase 1 clinical trial in people over the age of 60. A 60 μL dose triggered a 3.6 to 5.6-fold increase in anti-F IgG expression, and the response persisted until up to one year[50]. Lastly, an RSV vaccine for older adults (RSV OA) recently successfully concluded a phase III clinical trial. RSV OA is a subunit vaccine that contains a recombinant subunit prefusion RSV F glycoprotein antigen combined with the adjuvant AS01. The vaccine candidate induced strong cellular and humoral immune responses that last for at least 6 months following vaccination[51].

Several promising vaccine candidates are currently undergoing clinical trials. Even though more research needs to be carried out regarding a possible maternal vaccination strategy, several live-attenuated, nanoparticle-based and subunit-based vaccines are showing particularly encouraging results for the immunization of older infants, young children and older adults[44].

1.2 Defective interfering particles

Inactive influenza A virus (IAV) particles were first found to interfere with infectious IAV viruses' replication in 1943[52]. In 1954, Preben von Magnus discovered that, when embryonated eggs or other host-cell systems were infected for several passages with IAV at a high multiplicity of infection (MOI), incomplete forms of the virus with the potential to hinder the standard virus (STV) action were produced[53,54]. Finally, in 1970, Huang and Baltimore established a unified description and name for these virus-like particles, by defining them "defective interfering particles" (DIPs)[55].

1.2.1 General overview

Defective interfering particles are virus-like particles presenting at least one large deletion on their genome, which impairs their ability to self-replicate[56]. The mutation, however, does not affect packaging signals at the vRNAs termini, as well as their open reading frames (ORFs) for RNA-polymerase or ribosome recognition[57,58]. Almost all DNA and RNA viruses hold the ability to produce DIPs [59–62]. It has been documented in literature that defective viral genomes (DVGs) influence the course of natural infection and can result in distinct clinical outcomes[63].

DIPs can be formed through two distinct processes. Viral polymerases are purposively error-prone, and they can generate large *de novo* deletions by mistranslocating during replication; this is named "copy-choice" mechanism[64,65]. Alternatively, DIPs can originate from "mosaic" genomes, where non-adjacent sections of the genomic segment are connected together, or from "copyback" genomes, in which some sections of the genome are repeated in a reverse complement form[3]. For instance, OP7, a novel IAV DIP, contains 37 point mutations on segment 7 of the vRNA[3,66].

1.2.2 Interference mechanisms of defective interfering particles

Over the years, DIPs have been shown to be capable of interfering with infectious virus replication through two mechanisms. Upon coinfection, DIPs require the presence of STV in order to replicate. Since the defective interfering (DI) genome is shorter than the full length (FL) genome, DI vRNAs can be produced in greater amount than FL vRNAs [64]. This leads to the accumulation of DI genomes within the infected cells, which eventually interfere with the STV by outcompeting it for cellular and viral resources (Figure 4) [59]. It was believed that DIPs also displayed a packaging advantage over STVs, but this has recently been confuted[67].

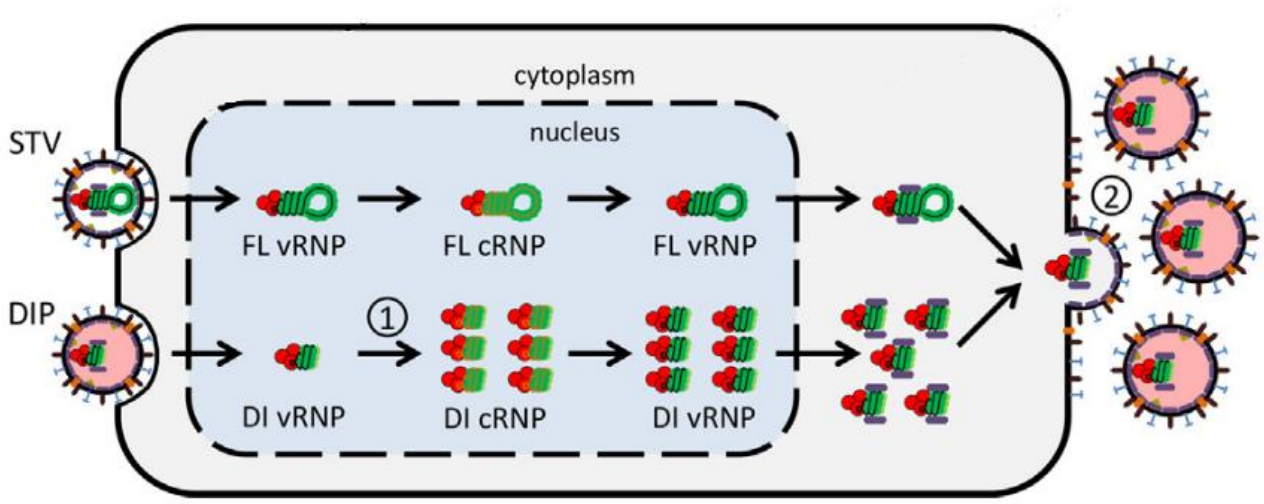

Figure 4 | Schematic representation of IAV STV replication in the presence of DIPs.
In a coinfection scenario, both DIP and STV penetrate the host cell membrane and enter the cytoplasm. Once their vRNPs enter the nucleus, they undergo replication; due to the shorter length of their genomes, defective interfering (DI) cRNPs are synthesized at a faster pace than full length (FL) cRNPs. This leads to a preferential release of DI vRNPs following replication. (Figure taken from [68])

DIPs can also inhibit virus replication by stimulating the host innate immune system (Figure 7). The virus-like particles are detected by pattern recognition receptors (PRRs) such as the retinoic acid inducible gene I (RIG-I), which trigger the upregulation of type I and type III interferons (IFNs)[69,70]. IFNs activate the janus kinase-signal transducers and activators of transcription (JAK/STAT) signaling cascade, which culminates in the downstream expression of interferon stimulated genes (ISGs)[71]. This mechanism confers DIPs a strong antiviral effect, even against non-homologous respiratory viruses like the pandemic SARS-CoV-2 [71].

1.2.3 IAV DIP DI244

IAV DIPs commonly carry a large internal deletion on one of their genome segments [60]. Specifically, DI244 was obtained from the influenza A virus strain A/PR/8/34 (H1N1) and it presents a deletion on segment (Seg) 1 of the vRNA, which only consists of 395 nucleotides instead of the canonic 2341[70] (Figure 5). The ability to replicate and the packaging signals at the 3' and at the 5' of the segment are intact despite the deletion, which contains only the genetic information for the viral polymerase basic protein 2 (PB2)[70,72]. However, the absence of PB2 protein hinders the self-replicative ability of the virus-like

particle. For this reason, cell culture-based DI244 production for use as an antiviral used to be carried out in a coinfection scenario with STV. This was followed by exposition to UV light to inactivate the STV, although this reduced the antiviral activity of the IAV DIP as well[60,70,7341]. Recently, a protocol for the production of DI244 in the absence of STV has been developed. In 2021, Hein *et al*. determined a method of DI244 production: a purely clonal seed virus was first produced by reverse genetics in adherent cells expressing PB2, and genetically engineered MDCK suspension cells expressing PB2 were consequently infected. Finally, steric exclusion chromatography allowed manufacturing of highly concentrated and highly purified material[74]. The antiviral potential of IAV DIP DI244 has been assessed against influenza A virus in mouse and ferret models: in both cases, the animals survived after receiving an otherwise lethal dose of the virus. Moreover, no toxicity was found by only infecting cells with DIPs (without the challenge virus)[70,75].

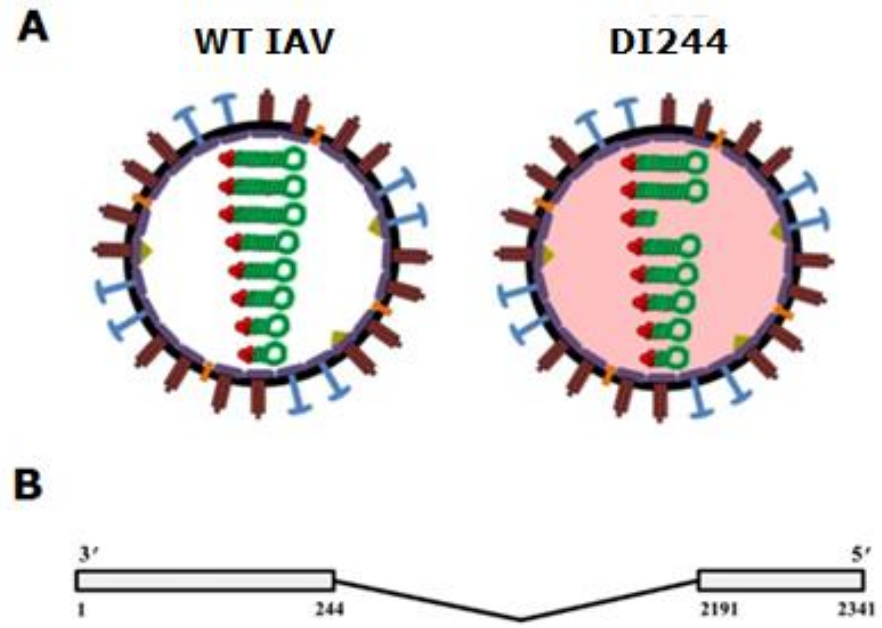

Figure 5 | Schematic structure of IAV DIP DI244.

(A) Structure of DI244 defective interfering particle compared to that of wild type (WT) IAV[76]. **(B)** Schematic structure of the internal deletion on Seg 1 of DI244 (deletion of 1946 nucleotides (nt), 395 nt remaining). The 3' end includes the base sequence 1 to 244, while the 5' end consists of nucleotides 2191 to 2341. (Figure taken from [2])

1.2.4 IAV DIP OP7

Recently, Kupke *et al*. proposed OP7, a newly discovered IAV DIP, as a new antiviral agent for treatment of IAV[3]. While DIPs typically harbor a large deletion on one of their vRNA segments, OP7 presents 37 point mutations on Seg 7 of the viral genome, affecting genome packaging signals, promoter regions and encoding sequences of several proteins (Figure 6). A G3A/C8U substitution in the untranslated region of Seg 7 also results in the creation of a superpromoter, which increases gene expression levels of the segment. The novel IAV DIP was identified via single cell analysis from an influenza virus A/Puerto Rico/8/34 (PR8) strain, and its antiviral potential has already been tested against respiratory viruses such as IAV, severe acute respiratory syndrome coronavirus 2 (SARS-CoV-2) and yellow fever virus (YFV)[3,71,77]. OP7 presents the characteristics that IAV DIPs normally display: it is unable to replicate autonomously, but in a coinfection scenario it can outcompete the WT STV and inhibit infectious virus replication[3,71]. So far, it is not possible to produce pure OP7 material. In order to successfully produce OP7 particles, Hein *et al*. established a new production system in cell culture using MDCK cells. Cells were coinfected with a seed virus containing STV (IAV) and OP7, and the viral material was UV irradiated to neutralize the STV. Subsequently, highly purified and highly concentrated OP7 material was retrieved via steric exclusion chromatography[66]. Administration of OP7 to mice did not display any toxicity and it protected all subjects from an otherwise lethal injection of IAV[66].

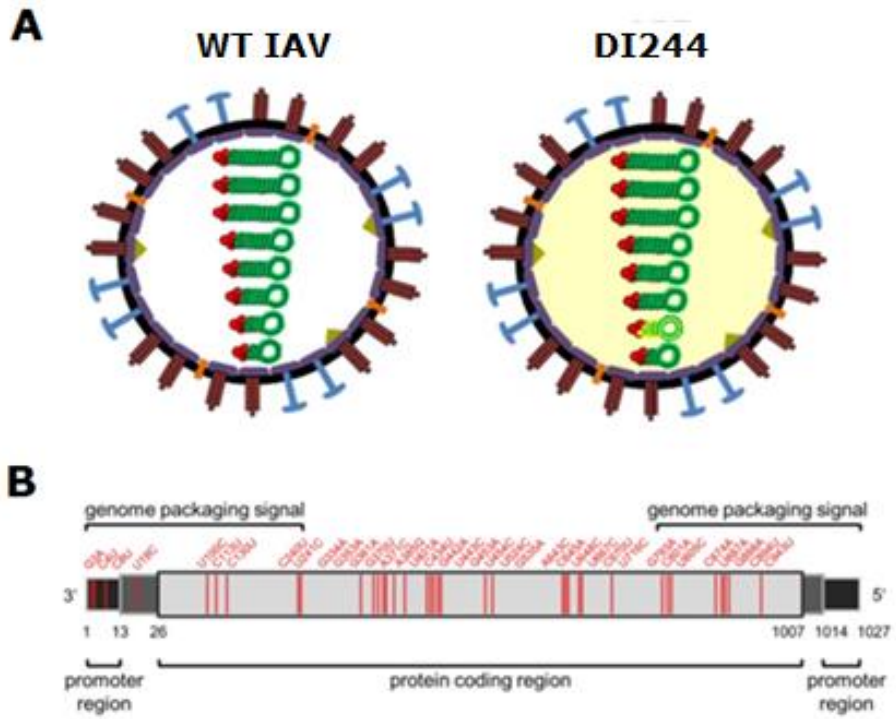

Figure 6 | Structure of IAV DIP OP7.

(A) Schematic structure of OP7 defective interfering particle compared to that of WT IAV[76]. **(B)** The vRNA of segment 7 of OP7 has the same base pair length as the vRNA of segment 7 of WT IAV, but compared to the latter it presents 37 point mutations (represented by red lines) that alter its self-replicating ability. (Figure taken from [3])

1.3 The innate immune response

The innate immune response is the first line of host defense against viral infections. Its induction is crucial for the stimulation of the adaptive immune response and is a key determinant of the infection outcome[78,79]. Defective interfering particles hold the ability to stimulate the innate immune response in an IFN-dependent manner both in natural infections and in *in vitro* studies[56,71].

When a virus-like particle enters the host cell, it can be recognized by pattern recognition receptors (PRRs) such as the cytosolic retinoic acid inducible gene I (RIG-I) (Figure 7). The identification by nucleic acid sensors leads to a signaling cascade which results in the induction of type I and type III IFNs, that can act both in an autocrine and paracrine manner. Once the pro-inflammatory cytokines bind the IFN receptors (IFNRs), they trigger the expression of hundreds of interferon stimulated genes (ISGs) via the Janus kinase-signal

transducer and activator of transcription (JAK/STAT) signaling cascade. Ultimately, this leads to an enhancement of the innate immune response and antiviral activity[78–80].

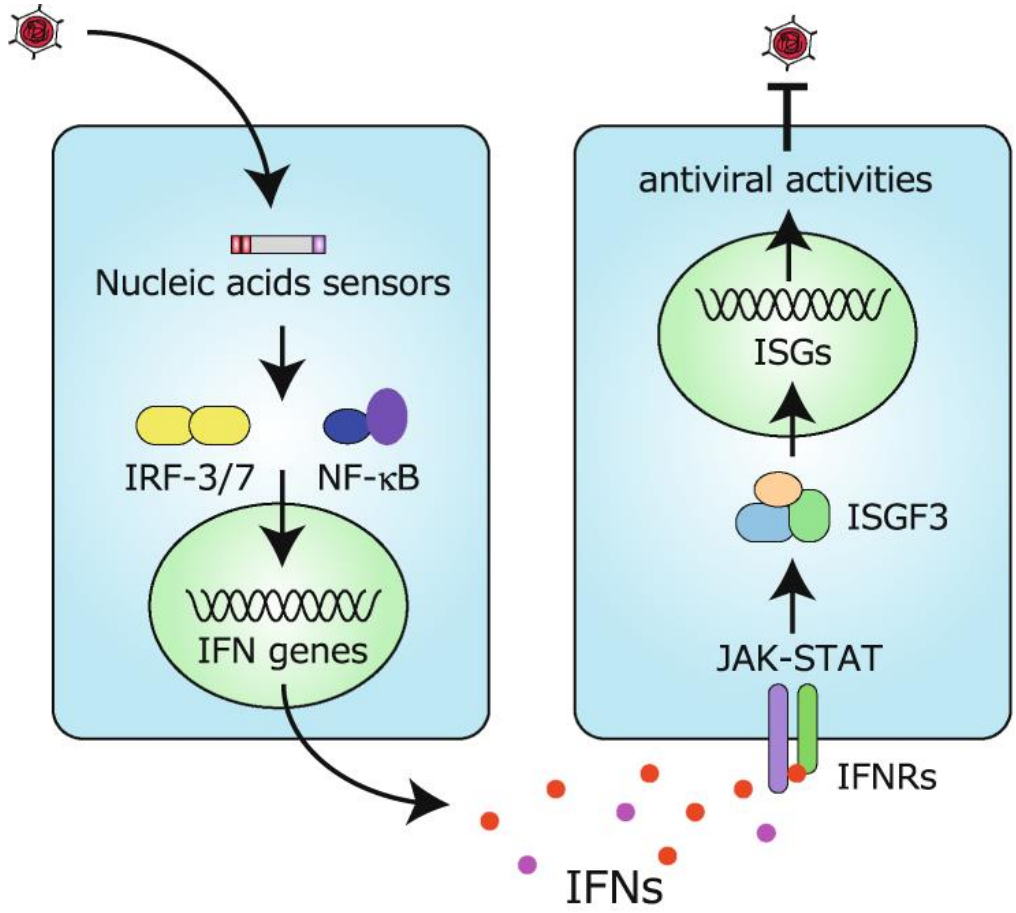

Figure 7 | IAV DIPs elicit IFN-mediated innate immune response in the host.
A virus-like particle penetrates the host cell and is recognized by nucleic acid sensors; factors like the IFN regulatory factor (IRF) 3 and IRF 7 trigger expression of class I and class III IFNs, which bind cell surface IFNRs and activate the JAK/STAT signaling pathway. This ultimately leads to the overexpression of hundreds of ISGs and to antiviral activities by enhancing the host innate immune response. (Figure taken from [81])

1.3.1 RIG-I

The detection of pathogen-associated molecular patterns (PAMPs) by PRRs is crucial for the production of pro-inflammatory cytokines during viral infection[82,83]. RIG-I-like receptors (RLRs) are cytosolic nucleic acid sensors that can activate innate signaling upon recognition of RNA molecules. Three RLRs have been identified: RIG-I, melanoma differentiation-associated protein 5 (MDA5) and laboratory of genetics and physiology 2 (LGP2)[58]. RIG-I is a highly

inducible RNA helicase that recognizes short double stranded (ds) RNAs that are tri- or di-phosphorylated at the 5' end and that are linked to specific secondary structures[78,83]. It possesses a conserved helicase core for RNA-triggered signaling, a C-terminal domain for ligand specificity and two caspase activation and recruitment (CARD) domains at the N terminus. CARD domains can induce downstream signaling by binding to the adaptor protein mitochondrial antiviral signaling (MAVS)[84]. Moreover, when CytARD domains undergo conformational change following interaction with MAVS, IRF3 and IRF7 are activated [85]. IRFs, together with the transcription factor nuclear factor κB (NF-κB), translocate to the cell nucleus and finally elicit expression of IFN molecules[79,81].

1.3.2 Antiviral IFNs

Type I and type III IFNs are critical mediators of the host's innate immunity. They are hallmark antiviral cytokines that play a crucial role in the induction of antivirally active ISGs [86,87]. IFNs bind to their receptors both in an autocrine and a paracrine way[78]. Type I IFNs (IFN-α and IFN-β) bind to type I IFN receptors (IFNAR), activating several signaling pathways. The IFN-stimulated gene factor 3 (ISGF3) complex binds to IFN-stimulated response elements (ISREs) in gene promoters, ultimately inducing expression of ISGs[88]. Class III IFNs (IFN-λ) trigger pathways downstream of IFN-λ receptors (IFNLR) following activation by PRRs or the DNA sensor Ku70[89]. Type I IFNs can modulate the innate immune response and lead to the recruitment of monocytes on the infection site, as well as regulate the adaptive immune response by promoting a Th1 response[90,91]. Type III IFNs are fundamental to elicit an antiviral response in the epithelial cells of the respiratory tract [92,93].

Because RIG-I recognizes short RNA sequences, the truncated genomes of IAV DIP segments are an ideal target for the RLR binding. This mechanism ultimately leads to the expression of IFN genes, and it is one of the factors that motivate the antiviral potential of IAV DIPs. On the other hand, the RSV proteins NS1 and NS2 are potent disrupters of the innate immune response: they can suppress RIG-I mediated antiviral signaling, block the activation of the IRF3, as well as degrade STAT proteins and suppress type I IFNs[94–97].

1.3.3 IFITM 1

Antiviral cytokines such as IFN- β and IFN-λ can activate signal transduction cascades (e.g., through JAK/STAT signaling) that results in the induction of hundreds of ISGs that promote cell-intrinsic antiviral activities as well as antiproliferative defenses and contribute to the stimulation of the adaptive immune response[84,98].

Interferon-inducible transmembrane (IFITM) proteins are one family of ISGs that are functionally conserved across many species and that show antiviral activity against viruses such as IAV, Ebola, dengue and rabies viruses[86,99]. There are three IFITM proteins: IFITM1 is mainly located on the plasma membrane and cytoplasm, IFITM2 is found in late endosomes, and IFITM3 is primarily observed in early endosomes[100]. IFITM1 is made of 125 AAs and it presents an N-terminal domain in the cytoplasm, a C-terminal domain facing the cell surface, a CD225 domain and two membrane domains linked by a conserved intracellular loop (CIL)[100,101]. The CIL-linked domains are crucial for virus restriction, as well as KRRK basic residues. Although KRRK mutant cell lines have displayed a limited antiviral potential, the interference mechanism of IFITM1 proteins has not yet been completely elucidated. However, IFITM proteins are believed to interfere with virus-endosome fusion at the cell entry. In addition to that, IFITM1 can restrict the release of viral particles from late endosomes to the cytosol [100,102].

1.3.4 Mx1

Myxovirus resistance protein 1 (Mx1 or MxA) is a very prominent ISG that is found in most vertebrates. It is a mediator of the IFN-mediated antiviral host response against a wide range of viruses[103]. Mx1 is not directly inducible by viruses but it is regulated by type I and type III IFNs in a JAK/STAT-dependent manner[104,105]. The ISG presents three domains: a GTPase domain at the N-terminus that binds and hydrolyses guanosine-5'-triphosphate (GTP), a C-terminal GTPase effector domain and a central domain responsible for self-assembly. Mx1 is mainly found in the cytoplasm. It can form oligomers in the form of ring-like structures that assemble around viral nucleocapsid structures

and induce liposome tubulation. This impairs the import of nucleocapsid complexes to the nucleus, ultimately leading to the inhibition of viral replication and transcription[106,107]. Oligomerized Mx1 serves as an inflammasome sensor in epithelial airway cells, and it possibly plays a critical role in limiting spreading of progeny viruses in regions that are distant from the initial site of infection[104]. Overall, several IFN-mediated pathways result in the expression of hundreds of ISGs, which are crucial in preventing virus entry, replication and budding and in limiting the spreading of viral infection.

2. Aims

Respiratory syncytial virus (RSV) is a single-stranded negative-sense RNA (ssRNA (-)) virus [11]. RSV is the leading cause of bronchiolitis and pneumonia among infants, and it globally causes significant morbidity and mortality[15]. Because the elicited immunity conferred by natural RSV infection is only transient, and since we lack commonly agreed clinical endpoints due to high variability within different target populations, the development of a safe and effective RSV vaccine has so far been elusive[45]. Treating RSV infection is also challenging: ribavirin, the only drug licensed for RSV treatment, presents limitations regarding its efficacy, safety and cost, and is thus only administered to severely ill patients[41]. In the recent years, several vaccine candidates and potential antiviral agents are undergoing development.

Influenza A virus (IAV) defective interfering particles (DIPs) have been previously reported as a possible antiviral agent against infection caused by interferon (IFN)-sensitive viruses[70]. Recently OP7, a new DIP derived from IAV, was discovered by Kupke *et al*[3]. Its antiviral potential has been assessed in mouse models against otherwise lethal infectious doses of IAV: surprisingly, all infected mice survived and maintained low clinical scores throughout the course of infection. Since OP7 also displayed a strong antiviral potential against SARS-CoV-2 and YFV *in vitro*, this study will assess the antiviral potential of OP7 against RSV and investigate whether it might be implied for RSV treatment and prophylaxis[71,77]. To achieve so, a seed virus production of RSV A2 was first established, and virus replication dynamics were investigated. We therefore established an *in vitro* interference assay to assess the inhibitory effect of IAV DIPs DI244 and OP7 against RSV replication. Ultimately, to determine that the antiviral activity of IAV DIPs is IFN-dependent, we examined gene expression levels of antiviral genes linked to the innate immune response, to confirm their upregulation upon coinfection.

3. Materials and Methods

3.1 Materials

3.1.1 Technical equipment and disposables

Table 1 | List of technical equipment.

Device or instrument (Model)	Manufacturer, Location
Biological safety cabinet (Heraeus HERAsafe SAFE 2020)	Thermo Fisher Scientific, Germany
Cell counter (Vi-Cell XR)	Beckman Coulter, US
Centrifuge (Heraeus Biofuge primo R)	Thermo Fisher Scientific, Germany
CO_2 incubator (HERAcell 240i)	Thermo Fisher Scientific, Germany
Gel electrophoresis mini horizontal chamber (7-0155)	neoLab, Germany
Gel visualizer (BioDocAnalyze)	Biometra, Germany
Heat sealer (Rotor-Disc Heat Sealer)	Qiagen, Germany
Light microscope (Axio Vert.A1)	Zeiss, Germany
Microcentrifuge (iFuge BL08VT)	Neuation, India
Microplate reader (Infinite 200 Pro NanoQuant)	Tecan Trading AG, Switzerland
Mini-plate centrifuge (NG040)	Nippon Genetics Europe, Germany
Multichannel pipette (Research Plus, 8 and 12 channels, 100 µL)	Eppendorf, Germany
Multichannel pipette (Xplorer, 8 channels, 0.5-10 µL and 5-100 µL)	Eppendorf, Germany
Multichannel/multistep pipette (Xplorer, 50-1200 µL)	Eppendorf, Germany
Multistep pipette (Research, 10 and 100 µL)	Eppendorf, Germany
Multistep pipette (Multipipette Plus, 5-25 mL)	Eppendorf, Germany
PCR cabinet (PCR Workstation Pro)	Peqlab, Germany
Pipettes (P10, P100, P200, P1000)	Eppendorf, Germany
Pipettes (Pipetman, P2, P10, P20, P100, P200, P1000)	Gilson, US
Pipette filler (Pipetman)	Hirschmann, Germany
Pipetting robot (QIAgility)	Qiagen, Germany
Real-time PCR cycler (Rotor-Gene Q)	Qiagen, Germany
Test tube vortex shaker (444-1372)	VWR International, US
Thermocycler (T Professional Thermocycler)	Biometra, Germany
Ultrasonic homogenizer (UP200St)	Hielscher, Germany
Water bath (Ultrasonic Cleaner)	VWR, Germany

Table 2 | List of disposables.

Disposable (Model / #Catalog No.)	Manufacturer, Location
6-well plates (CELLSTAR)	Greiner Bio-One, Germany
96-well plates (CELLSTAR)	Greiner Bio-One, Germany
Cell culture flasks (CELLSTAR 75, 175)	Greiner Bio-One, Germany
Cell scrapers (28cm #541070)	Greiner Bio-One, Germany
Cryogenic vials (2 mL #122263)	Greiner Bio-One, Germany
Falcon tubes (CELLSTAR 15 mL, 50 mL)	Greiner Bio-One, Germany
Heat sealing film (Rotor-Disc heat sealing film #981601)	Qiagen, Germany
PCR plates (96-well, 0.2 mL #AB0900)	Thermo Fisher Scientific, Germany
Pipette tips (10, 200, 1000, 1200 µL)	Carl Roth GmbH &Co. KG, Karlsruhe
Reaction tubes (1.5, 2 mL)	Greiner Bio-One, Germany
Reaction tubes (5 mL)	Eppendorf, Germany
Real-time sample discs (Rotor-Disc 100 #981311)	Qiagen, Germany
Serological pipettes 2, 5, 10, 25, 50 mL (CELLSTAR)	Greiner Bio-One, Germany
Sterile pipette tips (10, 30, 100, 200, 1000 µL)	Gilson, US

3.1.2 Solutions, buffers and chemicals

Table 3 | List of cell media and solutions.

Name	Composition
10x TPE buffer	(For 1 L of solution) Milli-Q-water 108g Tris 0,744g EDTA 85% H_3PO_4 to reach pH = 7,5
DMEM (cell culture)	Dulbecco's Modified Eagle's Medium (DMEM) Fetal calf serum (FCS) (10%)
DMEM (infection)	Dulbecco's Modified Eagle's Medium (DMEM)
Phosphate buffered saline (PBS)	(For 10 L of solution) Milli-Q-water NaCl 80g KCl 2g KH_2PO_4 2g Na_2HPO_4 11,5 g
RPMI1640 (cell culture)	RPMI1640 FCS (10%)

	L-glutamine (1%)
RPMI1640 (infection)	RPMI1640 L-glutamine (1%)
V-medium (infection)	Glasgow Minimum Essential Medium (GMEM) FCS (10%) Peptone (1%)
Z-medium (cell culture)	Glasgow Minimum Essential Medium (GMEM) Peptone (1%)

Table 4 | Commercial chemicals, reagents and kits.

Name (Catalog No.)	**Manufacturer, Location**
2-Mercaptoethanol (M6250)	Sigma-Aldrich, Germany
5x Phusion HF buffer (F-518)	Thermo Fisher Scientific, Germany
10x Fast Digest Green Buffer (B72)	Thermo Fisher Scientific, Germany
Agarose (A840004)	Biozym, Germany
Crystal violet (115940)	Merck Millipore, US
Deoxyribonucleoside triphosphate (dNTP) mixture (10 mM each) (R0193)	Thermo Fisher Scientific, Germany
DMEM (41966-029)	Thermo Fisher Scientific, Germany
Ethanol 70 %, 96 % (T868.1 ,P075.1)	Carl Roth GmbH &Co. KG, Karlsruhe
Fetal calf serum (FCS) (10270106)	Sigma-Aldrich, Germany
GeneRuler DNA Ladder Mix (SM0333)	Thermo Fisher Scientific, Germany
L-Glutamine (G8540)	Sigma-Aldrich, Germany
Maxima H Minus Reverse Transcriptase (EP0742)	Thermo Fisher Scientific, Germany
NucleoSpin RNA, Mini kit for RNA purification (740955.250)	Macherey-Nagel, Germany
NucleoSpin RNA virus, Mini kit for RNA purification (740956.250)	Macherey-Nagel, Germany
Recombinant human Interferon beta-1a (11415-1)	Bio-Techne, US
Recombinant human Interferon lambda-1 (1598-IL-025/CF)	Bio-Techne, US
Ribavirin (Cay16757-5)	Cayman Chemical, US
RiboLock RNase inhibitor (EO0381)	Thermo Fisher Scientific, Germany
Rnase H (EN0201)	Thermo Fisher Scientific, Germany
Roti-GelStain (3865.1)	Carl Roth GmbH &Co. KG, Karlsruhe
Ruxolitinib (11609)	Cayman Chemical, US
SYBR Green (204076)	Qiagen, Germany
Trypan blue (93595)	Sigma-Aldrich, Germany

3.1.3 Primers

Table 5 | Primers used for reverse transcription (virus integrity).

Target	Primer name	Sequence (5'→3')
STV RSV	RSV RT STVs	GATAAATATAGGCATGGGGAAAGTG
DVG RSV	RSV RT DVGs (P1)	CTTAGGTAAGGATATGTAGATTCTACC

Table 6 | Primers used for PCR (virus integrity).

Target	Primer name	Sequence (5'→3')
STV RSV	RSV PCR ns1ns2(STV) for	CACTGCTCTCAATTAAACGGTCTA
	RSV PCR ns1ns2(STV) rev	GATAAATATAGGCATGGGGAAAGTG
DVG RSV	RSV PCR DVGs for (P2)	CCTCCAAGATTAAAATGATAACTTTAGG
	RSV PCR DVGs rev (P1)	CTTAGGTAAGGATATGTAGATTCTACC

Table 7 | Primers used for reverse transcription (gene expression).

Target	Primer name	Sequence (5'→3')
PolyA	OligodT	TTTTTTTTTTTTTTTT

Table 8 | Primers used for PCR (gene expression).

Target	Primer name	Sequence (5' → 3')
h RIG-I	RIG-I for	GGACGTGGCAAAACAAATCAG
	RIG-I rev	GCAATGTCAATGCCTTCATCA
h IFN-β1	IFN-β1 for	CATTACCTGAAGGCCAAGGA
	IFN-β1 rev	CAGCATCTGCTGGTTGAAGA
h IFN-λ1	IFN-λ1 for	GGTGACTTTGGTGCTAGGCT
	IFN-λ1 rev	TGAGTGACTCTTCCAAGGCG
h Mx1	Mx1 for	GTATCACAGAGCTGTTCTCCTG
	Mx1 rev	CTCCCACTCCCTGAAATCTG
h IFITM1	IFITM1 for	ATCAACATCCACAGCGAGAC
	IFITM1 rev	CAGAGCCGAATACCAGTAACAG
h GAPDH	GAPDH for	CTGGCGTCTTCACCACCATGG
	GAPDH rev	CATCACGCCACAGTTTCCCGG

3.2 Methods

3.2.1 Cell lines and virus material

Adherent A549 cells

Adenocarcinoma human alveolar basal epithelial A549 cells (ATCC, #CCL-185) were used for coinfection experiments in this study. They were maintained in 175 cm^2 flasks in DMEM supplemented with 10% FCS. Cells were passaged twice a week and discarded after 20 passages. For cell passaging, the cell culture medium was pre-warmed in a 37°C bath prior to use. The cell monolayer was washed twice with PBS and incubated for 5 minutes with 4 mL of 1x trypsin/EDTA solution at 37°C and 5% CO_2. Subsequently, trypsin was neutralized by adding 16 mL of DMEM supplemented with FCS, and cells were resuspended by pipetting. Viable cell concentration (VCC) was determined using a Vi-CELL™ XR. A new flask was therefore filled with 25 mL of pre-warmed fresh DMEM and a seed volume containing $7*10^6$ cells was added (calculated according to Formula 1). The cells were cultivated at 37°C in a 5% CO_2 atmosphere.

$$V_{seed} = \frac{C_{cells(desired)} * V_{cells(desired)}}{C_{cells(counted)}} \qquad (1)$$

V_{seed}	Cell volume necessary for seeding (mL)
$C_{cells(desired)}$	Desired cell concentration (cells/mL)
$V_{cells(desired)}$	Desired volume (mL)
$C_{cells(counted)}$	VCC (cells/mL)

Adherent Vero cells

Vero cells are renal epithelial cells derived from African green monkeys. They were obtained from IDT Biologika in Dessau-Roßlau (Germany)[108]. As a result of mutations, these cells present receptors for IFNs but are unable to produce IFNs on their own, so they are considered IFN deficient. Vero cells were used as a negative control in coinfection studies. They were cultured in 175 cm^2 flasks in Z-medium and passaged twice per week until they reached passage 20. For

passaging, cells were washed twice with PBS; 6 mL of 1x trypsin/EDTA were then used to detach the cells, which were incubated for 5 minutes at 37°C and 5% CO_2. Afterwards, trypsin was neutralized by adding 6 mL of Z-medium, and cells were resuspended using a 10 mL pipette. The VCC was calculated as for A549 cells, and a seed volume of $7*10^6$ cells was added to a new flask previously filled with 25 mL of pre-warmed Z-medium. Vero cells were maintained in a 5% CO_2 atmosphere at 37°C.

Adherent Hep-2 cells

Hep-2 cells (ATCC, #CCL-23) are cervical adenocarcinoma cells derived via HeLa cell contamination. Since they contain human papillomavirus (HPV), they must be handled as infectious material (biosafety level 2). Cells were used for seed virus production and for the $TCID_{50}$ assay. The protocol for maintenance is the same as for Vero cells, with the difference that supplemented DMEM (for seed virus production) and RPMI1640 (for $TCID_{50}$ assay) were used instead of Z-medium. Hep-2 cells were passaged twice per week and discarded after 20 passages. Flasks were kept in an incubator specific for cells containing virus, at 37°C and 5% CO_2.

Cell counting

To measure VCC, we used the automated ViCell XR cell viability analyzer. A cell suspension volume of 0.5 mL was transferred to a ViCell cup that was subsequently inserted in the cell analyzer. By preparing a 1:1 dilution in trypan blue, the instrument identifies viable and dead cells through a dye exclusion method in a series of 50 images per samples, where non-viable cells are stained by trypan blue.

Virus material

Live RSV A2 (ATCC, #VR-1540, biosafety level 2) was used for infections. The strain was isolated in 1961 from the lower respiratory tract of an infant with bronchiolitis and bronchopneumonia and it is propagated in Hep-2 cells. A2 is a live-attenuated strain commonly used in RSV research and development of

possible vaccine candidates and, as many lab-grown strains, it is temperature sensitive[109]. The virus underwent cold passaging, a process in which extensive serial passages are carried out at progressively lower temperatures. Through this modification, RSV A2 can survive in the upper respiratory tract but not in the lower respiratory tract, where the host's body temperature is higher, therefore limiting the risk of severe infections [110]. Because it is heat sensitive, RSV A2 should always be handled on ice[111].

Active and inactive IAV DIPs DI244 and OP7 were provided by Marc Hein (Table 7, Table 8). Production, purification, and UV-inactivation of the material was conducted according to Hein *et al*.[66,74]; these were not conducted by the performing scientist.

Table 7 | Characteristics of IAV DIP DI244.

Description	MODIP	Harvest time (hpi)	HA	$TCID_{50}$ assay ($TCID_{50}$/mL)	vRNAs/mL	Interference (PFU/mL)
STR, 8 min UV, Downstream	1.00E-02	32	3.53	0	1.60E+11	8.40E+04
STR, 24 min UV, Downstream	1.00E-02	32	3.52	0	2.85E+10	8.80E+08

STR = stirred tank bioreactor, MODIP = multiplicity of defective interfering particle, HA assay = hemagglutination assay, PFU = plaque forming units

Table 8 | Characteristics of IAV DIP OP7.

Description	MODIP	Harvest time (hpi)	HA	Plaque assay (PFU/mL)	vRNAs/mL	Interference (PFU/mL)
STR, no UV, Downstream	1.00E-02	24	3.89	3.16E+07	8.89E+10	1.20E+06
STR, 24 min UV, Downstream	1.00E-02	24	3.85	0	1.03E+09	5.20E+08

3.2.2 Seed virus production

For seed virus production, three passages at low MOI were carried out. Hep-2 cells were washed twice with PBS and detached by adding 6 mL of 1x trypsin/EDTA. Flasks were incubated for 5 minutes at 37°C in a 5% CO_2 atmosphere and trypsin was then neutralized by adding 6 mL of DMEM supplemented with FCS. VCC was determined and cells were seeded 24 hours prior to infection in 175 cm^2 flasks at a seed volume of $1.3*10^7$ cells per flask.

On the infection day, one flask was sacrificed to determine VCC, and 6 mL per flask of infection medium (in DMEM) at MOI 10^{-2} were prepared according to Formula 2 by using DMEM without FCS. Flasks were washed twice with PBS and the infection medium was added. The bottles were subsequently incubated at 37°C for 2 hours and were gently rocked every 15 minutes. The infection medium was finally removed, and flasks were incubated at 37°C and 5% CO_2. The seed virus was harvested once the CPE in the flask was ~50%. For this, bottles were kept on ice for 5 minutes and the cells were then scrapped off by using a 28 cm cell scraper and resuspended with a pipette to break cell clumps. The volume was transferred to a 50 mL Falcon tube and centrifuged at 300 g and 4°C for 5 minutes. After this, 19 mL of centrifuged supernatant were transferred to a new Falcon tube. Subsequently, 1 mL of supernatant was used to resuspend the cell pellet, while the rest of the volume was discarded. The supernatant with pellet was moved into a 1.5 mL Eppendorf tube and kept in a bag with ice. The tube was vortexed for 3 minutes at 2500 rpm, and it was then sonicated for 1 minute on a cell disrupter (W= 160, C= 60%, A= 100%). The volume was again centrifuged with the same settings as before to get rid of the cell pellet, and the virus-enriched supernatant was finally added to the 19 mL in the Falcon tube. The volume was additioned with sucrose solution (2% final concentration) and aliquots of 0.5 mL were prepared in cryogenic tubes. For the first passage, RSV stock was used for infection and harvesting was performed after 140 hpi. For the second passage at MOI 10^{-2}, RSV produced during the first low MOI passage was used and flasks were harvested at 96 hpi, while a sample obtained from the second passage was used for infection for the third passage at MOI 10^{-2}, which was sampled at 72 hpi. Aliquots were snap frozen in liquid nitrogen and stored at -80°C until use.

$$V_{virus} = \frac{C_{cells} * MOI}{C_{virus}} \qquad (2)$$

V_{virus}	Virus volume necessary for infection (mL)
C_{cells}	VCC (cells/mL)

MOI	Multiplicity of infection ($TCID_{50}$/mL)
C_{virus}	Established infectious virus titer ($TCID_{50}$/mL)

3.2.3 DIP RT-PCR for seed virus integrity

Total RNA was extracted using a NucleoSpin RNA virus Mini kit for RNA purification, according to manufacturer's instruction. The extracted RNA was stored at -20°C. The protocol for DIP PCR was adapted from the one kindly provided by Yan Sun, University of Rochester Medical Center[69]. cDNA was produced via reverse transcriptase (RT) reaction by using 5 µL of template RNA, 8.5 µL of ddH_2O, 1 µL of primer and 1 µL of dNTPs (master mix 1, MM1). For each sample, one reaction was prepared to analyze the FL genome, while a second one was made for the analysis of the DI genome. Samples were placed in the PCR cycler for 5 minutes at 65°C. A second master mix was prepared with 4 µL of 5x RT buffer, 1 µL of Maxima H Min, 1 µL of ddH_2O and 0.5 µL of Ribolock. A total of 6.5 µL of MM2 was added to each reaction tube and the samples were subsequently placed back in the thermocycler, where the temperature was first set to 50°C for 30 minutes and then at 85°C for 5 minutes. Samples were stored at -20°C for 20 minutes and defrosted again. 1 µL of RNase H was added to each sample to avoid the formation of RNA-cDNA hybrids. Samples were placed in the PCR cycler for 20 minutes at 37°C.

For the polymerase chain reaction (PCR), 2 µL of cDNA were used. For the master mix, for each sample we used 8.8 µL of ddH_2O, 4 µL of 5x Phusion HF Buffer, 2 µL of $MgCl_2$, 1 µL of dNTPs, 1 µL of forward primer, 1 µL of reverse primer (different primers were used for FL and DI genomes) and 0.2 µL of Phusion DNA polymerase. The samples were successively placed in the thermocycler. Samples were denatured at 98°C for 3 min, and this was followed by 35 cycles of 25 s at 98°C (denaturation), 45 s at 54 °C (annealing) and 90 s at 72°C (extension). At the end of the last cycle, samples were kept at 72°C for 10 minutes.

Lastly, DI and FL genomes from each sample were visualized via gel electrophoresis. For this, a 2% agarose gel was prepared with agarose, 1x TPE and Roti GelStain. 2.5 µL of 10x Fast Digest Green Buffer was added to each

sample. The gel was placed in an electrophoresis chamber and 12 µL of FL and DI samples were loaded on the agarose gel. 10 µL of GeneRuler DNA Ladder Mix was also loaded onto the gel. After running for 40 minutes at 70 W, FL and DI bands were visualized using the BioDocAnalyze software.

3.2.4 Virus replication dynamic study

In order to determine the best time points for virus harvesting during our coinfection experiments, we carried out a dynamic study in our cell lines of interest. A549 and Vero cells were seeded in 6-well plates 24 h before infection. To detach the cells, the procedure was the same as for seed virus production. A549 cells were seeded based on Formula 1 with a final cell concentration of $0.5*10^6$ cells/mL (2 mL/well), while the concentration for Vero cells was $0.4*10^6$ cells/mL (2 mL/well): two 6-well plates for A549 cells and two 6-well plates for Vero cells were prepared. On the infection day, two wells for each cell line were sacrificed to determine VCC: wells were washed twice with 1 mL of PBS, and 500 µL of 1x trypsin/EDTA was added to each well. The plates were incubated for 3 minutes, after which trypsin was neutralized by adding 500 µL of media supplemented with FCS. Cells were resuspended by pipetting and 500 µL were finally transferred to a ViCell cup and placed on a Vi-CELL™ XR for cell counting. Cells were washed twice with PBS and infected at MOI 10^{-2} with a volume of 500 µL per well. The infection (at MOI 10^{-2}) volume was prepared based on Formula 2 with non-supplemented DMEM for A549 cells and V-medium for Vero cells. The plates were incubated for 2 hours and rocked every 15 minutes to prevent cell dry-out. Afterwards, the infection volume was removed, cells were washed once with PBS and 2 mL of non-supplemented DMEM or V-medium were added to each well. Samples were taken at 24, 48, 72, 96 and 120 hpi. At harvest time points, the supernatant was pooled and centrifuged for 5 minutes at 300 g and 4°C. Aliquots were snap frozen in liquid nitrogen and stored at –80°C. Infectious virus titers for each time point were subsequently determined via $TCID_{50}$ assay.

3.2.5 Coinfection studies

One day prior to infection, A549 and Vero cells were seeded in 6-well plates as for the virus replication dynamic study. A total of 13 6-well plates for A549 cells and of 5 6-well plates for Vero cells was prepared. On coinfection day, when cells were approximately 90% confluent, two wells for each cell line were sacrificed to determine VCC with the same procedure described in the previous subparagraph. Based on VCC average values, infection volumes were calculated according to Formula 2, to achieve a final MOI of 10^{-2}. Highly concentrated IAV DIP material was diluted in infection media (DMEM for A549 cells and Z-medium for Vero cells) with a dilution factor (Df) of 20 for this experiment.

The experimental setup for time points 0, 6, 24 and 48 hpi was as displayed in Figure 8. Cells were washed twice with 1 mL/well of pre-warmed PBS and infected with RSV at a MOI of 10^{-2}. Alternatively, they were coinfected with RSV and 100 µL of active or inactive IAV DIPs DI244 and OP7 (diluted 1:20 in infection medium). Moreover, cells were infected with 100 µL of IAV DIPs alone, for a total of nine conditions and two 6-well plates per time point. In all cases, wells were filled up using serum-free medium to reach a final volume of 250 µL/well. At 0 hpi, a mock control was also included. The same conditions were included for interference assays at 72 and 96 hpi in A549 cells, together with several controls (Figure 8). Cells were always infected with RSV and cotreated with IFN-β1a with a final concentration of 2000 U/mL (stock concentration = 22500 u/mL)[112], or with either 10 or 100 ng/mL of IFN-λ1 (stock concentration = 6.25 µg/mL)[113]. Moreover, cells were cotreated with ribavirin at a concentration of 409 µM (stock concentration = 20 mg/mL)[114]. To ensure that the antiviral effect of active IAV DIPs is JAK/STAT-dependent, cells were pre-treated for 3 hours with 2 µM of ruxolitinib (stock concentration = 0.25 mg/mL) and treated with ruxolitinib while being coinfected with RSV and either active DI244 or active OP7[115]. Finally, as the JAK inhibitor was dissolved in 96% ethanol (EtOH), cells were also treated with 0.25% v/v of EtOH. Cells were incubated for 2 hours at 37°C in a 5% CO_2 atmosphere, and plates were rocked every 15 minutes to avoid drying.

For Vero cells, sampling was carried out at 72 and 96 hpi and the following conditions were included (Figure 8): cells were infected either with RSV at a MOI of 10^{-2}, or with RSV and 100 µL of active or inactive DI244 and OP7. Furthermore, cells were cotreated with IFN-β1a, ribavirin, ruxolitinib or EtOH as described for A549 cells. The incubation conditions for Vero cells were the same as for A549 cells.

At each time point, the supernatant was pooled for every condition and centrifuged for 5 minutes at 4°C and 300 g. Aliquots of 0.3 mL were prepared and cryogenic tubes were snap frozen in liquid nitrogen and stored at -80°C. Samples from 72 and 96 hpi were used to perform a $TCID_{50}$ assay to investigate the inhibitory effect of IAV DIPs by quantifying infectious virus titers. To assess cell gene expression levels, cell lysate samples were taken at 6, 24, 48, 72 and 96 hpi. After collecting the supernatant, the cells layer was washed once with 1 mL of PBS and 350 µL of 2-mercaptoethanol and RA1 lyses buffer were added (prepared according to manufacturer's instructions – Macherey Nagel, NucleoSpin RNA, Mini kit for RNA purification). After five minutes, cell lysates were transferred to cryogenic tubes and frozen and stored as for supernatant samples. Since at 72 and 96 hpi a considerable amount of cell pellet was found in tubes following centrifugation of the supernatant, the lysis buffer was transferred from the well to the corresponding tube to lyse the pellet before being moved into the cryogenic tube. This way, the maximum amount of intracellular RNA was retrieved.

Figure 8 | Experimental setup for coinfection studies.

At 0, 6, 24 and 48 hpi two 6-well plates for A549 cells were prepared. At 72 and 96 hpi, three 6-well plates were prepared both for A549 and for Vero cells. In total, fourteen 6-well plates for A549 cells and six 6-well plates for Vero cells were prepared for each coinfection experiment. Cells were either infected with RSV alone at an MOI of 10^{-2} or coinfected with RSV and either active or inactive DI244/OP7. Alternatively, cells were infected with one of the active or inactive DIPs alone. Cotreatment with IFN-β1a, IFN-λ1 and ribavirin were used as a positive control, whereas cotreatment with ruxolitinib functioned as a negative control.

3.2.6 Infectious virus titer quantification

The Tissue culture infection dose 50 ($TCID_{50}$) assay was used to determine infectious virus titers. The protocol used in this study was the one published by Sun and Lopez[116], with a few modifications. Hep-2 cells were cultivated to carry out the assay and RPMI1640 was used as cell culture and infection medium (recipes in Table 3). Two days prior to infection, cells were seeded in 96-well plates at a concentration of $0.2*10^6$ cells/mL. For each sample, one 96-well plate was used (8 replicates/sample).

At the day of infection, samples were thawed at room temperature and 1:5 serial dilutions starting from dilution factor 0 were prepared in 96-well plates by adding 240 µL of infection medium and 60 µL of sample. Plates with serial dilutions were stored at 4°C until the time of use. The 96-well plates with Hep-2 cells were subsequently washed twice with 100 µL/well of infection medium, and finally 25 µL of virus dilution was added to each well according to dilution factor by using a 12-multichannel pipette. Plates were incubated for 2 hours at 37°C in a 5% CO_2 environment. After the incubation time, 75 µL/well of infection medium was added to each well and plates were placed back in the incubator for a total of 96 hours.

At 96 hpi, the infectious virus titers were determined. First, plates were visualized under the light microscope and the wells that presented syncytia were scored as positive. Moreover, medium was discarded and plates were stained with 50 µL/well of crystal violet for 20 minutes. Crystal violet was then discarded by submerging the plates in water and by air drying them. Once the plates were dry, the wells that presented CPE were also scored as positive. The infectious virus titer for each sample was calculated by using the Spearman-Karber method based on how many wells per plate scored positive for syncytia and/or CPE.

Please note that when the term "virus titer" is used in this study, it always refers to the infectious virus titer.

3.2.7 Intracellular measurements by RT-qPCR

Cell lysates were thawed and intracellular RNA was extracted using NucleoSpin RNA, Mini kit for RNA purification, according to the manufacturer's instructions. RNA concentration of each sample was measured using a microplate reader to normalize the RNA concentration of all samples to 500 ng. Based on the concentration obtained on Tecan, the volume necessary to achieve RNA concentration of 500 ng was calculated, and the compensation volume of ddH_2O was consequently determined. The samples' volumes were loaded on 96-well PCR plates, together with ddH_2O, 1 µL of dNTPs and 1 µL of oligo-dT primer (MM1). The PCR plate was then positioned in the thermocycler at 98°C for 3

minutes. The MM2 was prepared meanwhile, by adding 4 µL of 5x RT buffer, 1 µL of Maxima H Min, 1 µL of ddH_2O and 0.5 µL of Ribolock for each sample. A total of 6.5 µL of MM2 was added to each tube. The samples were placed back in the PCR cycler, where the temperature was first set to 50°C for 30 minutes and then at 85°C for 5 minutes, followed by cooling at 4°C. After RT, 80 µL of ddH_2O were added to each sample, achieving a total volume of 100 µL. If the qPCR reaction was not performed immediately, samples were stored at -20°C.

For the qPCR, 4 µL of cDNA for each samples were added to a real-time sample disc (Rotor Disc 100), and a master mix was prepared by adding 5 µL of SYBR green PCR mix, 0.5 µL of forward primer and 0.5 µL of reverse primer per sample, for a total of 6 µL of master mix/sample. Two duplicates of each sample were loaded on the disc, followed by two replicates of ddH_2O. After all the samples were loaded, the Rotor Disc was covered with a heat sealing film. The sample disc was finally placed into the Rotor-Gene Q real-time PCR thermocycler. Samples were first denatured at 95 °C for 5 min; this was followed by 40 cycles of 10 s at 95°C (denaturation) and 20 s at 62°C (annealing and extension). Moreover, a melting curve analysis was carried out (65-90 °C).

In order to analyze the data, a threshold of 0.05 was set to determine the cycle threshold (Ct) based on the fluorescent signal. Subsequently, the amplification curves were slope corrected using the Rotor-Gene Q Software. The Ct values of the genes of interest were normalized to the housekeeping gene glyceraldehyde 3-phosphate dehydrogenase (GAPDH). The ΔΔCT method was used to calculate the fold change in gene expression.

3.2.8 Statistical analysis

GraphPad Prism for Windows (version 9.0.0) was used for statistical analysis and graph plotting. To test data for homogeneity of variances, the Brown–Forsythe test was used. The null hypotheses for hypotheses test could be rejected if the p-value was lower than alpha ($p<0.05$). One-way ANOVA (analysis of variance) was performed to assess statistical significance for the interference assays and the gene expression analysis of samples infected with RSV alone of coinfected

with IAV DIPs. This was followed by Dunnett's multiple comparison test in case of significant result. If the Brown-Forsythe test was displaying a significant result, the Welsh ANOVA test was used instead of the one-way ANOVA, and Dunnett's T3 post-hoc test was used instead of the Dunnett's post-hoc test. To assess significance of gene expression analysis of DIP-only samples, Student's t-test was performed by comparing active DI244 with inactive DI244 and active OP7 with inactive OP7.

The P value style used to determine statistical significance was GP (0.1234 (ns), 0.0332 (*), 0.0021 (**), 0.0002 (***), < 0.0001 (****)).

4. Results

In this study, RSV seed production at low MOI was first established, and infection dynamics were investigated in A549 and Vero cells (4.1, 4.2). *In vitro* coinfection experiments were then performed to assess the antiviral potential of IAV DIPs against RSV replication (4.3). Furthermore, expression levels of genes linked to the innate immune response stimulation were measured via real-time RT-qPCR (4.4).

4.1 Seed virus production

To prepare the stock of seed virus, Hep-2 cells were infected with RSV as described in 3.2.2. Because the virus tends to remain highly cell associated[17,117], several harvesting techniques were tested to determine which would grant the greatest infectivity release. To produce a seed virus with a low content of DIPs, several low MOI passages were carried out, and DIP RT-PCR was performed to test for virus integrity.

4.1.1 Testing for different harvesting methods

It is known that RSV assembles into viral filaments at the cell surface, making it difficult to release viral particles[117]. To achieve great virus release in order to produce a seed virus with an elevated infectious virus titer, we tested different harvesting conditions following Hep-2 cells infection at MOI 10^{-2}. At 140 hpi, RSV-infected cells were scraped off the flasks' surface and resuspended in 5mL of DMEM. Harvesting methods were tested by comparing infectious virus titers to that obtained by only centrifuging the supernatant (300 g, 4°C, 5 minutes). The supernatant was centrifuged in all cases prior to aliquoting. The following methods were tested: vortexing the supernatant for 3 minutes at 2500 rpm, sonicating it for 1 minute on a cell disrupter (W=160, C=60%, A=100%), performing both vortexing and sonication, and carrying out three freeze-thawing cycles.

By centrifuging the supernatant, an infectious virus titer of $4*10^6$ $TCID_{50}$/mL was released (Figure 9A). When the cell pellet was vortexed, we reached titers of

5.8*10^6 $TCID_{50}$/mL, and infectious virus titers of 4*10^7 $TCID_{50}$/mL were achieved when cells were sonicated. The combination of sonication and vortexing allowed to reach great virus release, with an infectious virus titer of 5.8*10^7 $TCID_{50}$/mL, which was comparable to that obtained with freeze-thawing cycles (2.7*10^7 $TCID_{50}$/mL). Furthermore, according to visualization on a light microscope, sonicating and vortexing the infectious material allowed us to achieve the greatest cell disruption (Figure 9B), and highest infectious virus titer release, and was thus selected as the harvesting method for seed virus production.

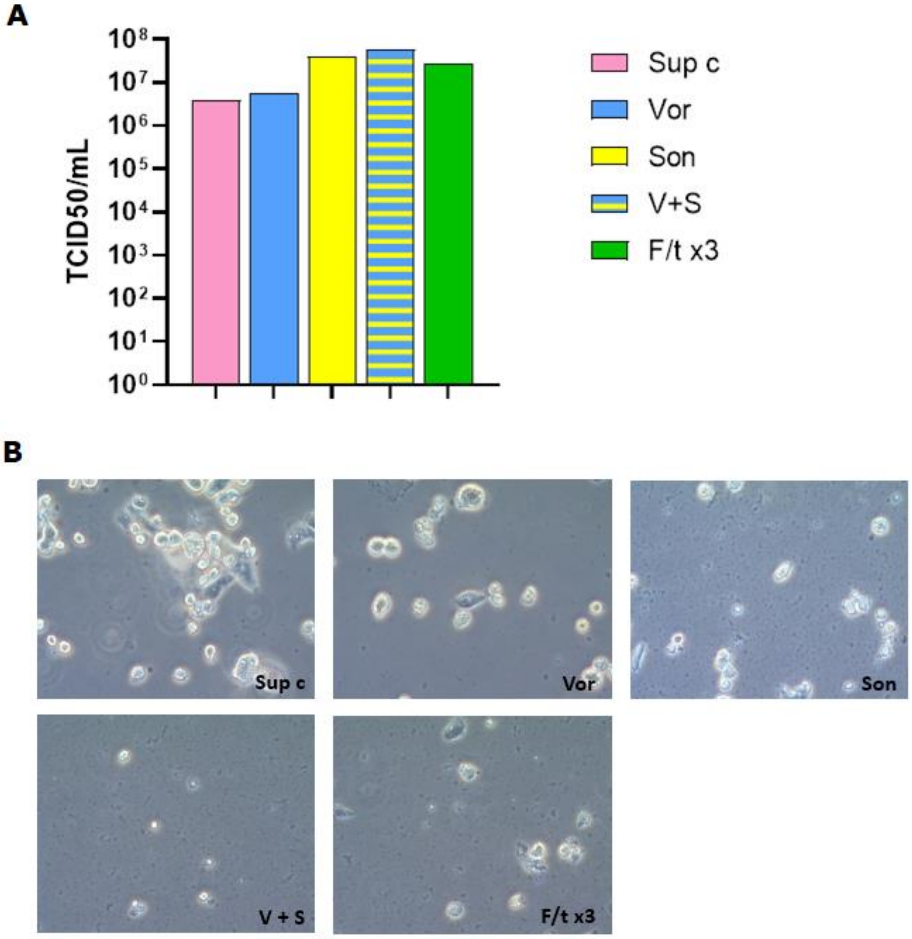

Figure 9 | RSV release from cells achieved with various harvesting methods.
Adherent Hep-2 cells cultivated in 175 cm^2 flasks were infected with RSV A2 at MOI 10^{-2}. At 140 hpi, cells were detached using a cell scraper, and the supernatant was centrifuged to separate it from the cell pellet. Different harvesting methods were subsequently tested: supernatant centrifugation alone, which was used as a negative control (sup c), vortexing (vor), sonication (son), combination of vortexing and centrifugation (v+s), performing three freeze-thawing cycles (f/t x3). **(A)** The infectious virus titers were quantified by $TCID_{50}$ assay ($TCID_{50}$/mL). **(B)** Visualization of cell pellet disruption under the light microscope following testing of different harvesting methods. One single experiment was conducted (n=1).

4.1.2 Assessing integrity of RSV genome via RT-PCR

In order to be able to test the efficacy of IAV DIPs in inhibiting RSV replication, the stock virus must have a low content of RSV DIPs, so that these do not interfere with the effect of the IAV-based antivirals[116]. To reduce the fraction of RSV DIPs, three passages at MOI 10^{-2} were carried out in Hep-2 cells. In a low MOI scenario, less coinfections occur, so DIPs cannot replicate and the STV can outcompete them. On the other hand, high MOIs would result in accumulation of RSV DIPs. We isolated extracellular RNA from each sample, and produced cDNA via RT-PCR. Moreover, bands for FL and DI RSV cDNA were visualized by gel electrophoresis. Four high MOI passages were also performed, and cDNA bands were visualized as for the rest of the samples. High MOI passages served in this experiment as a positive control for the presence of DIPs. For both low and high MOI passages, RSV stock was used to infect the cells in the first passage. For the next passage, virus harvested from the previous passage was utilized for infection.

To visualize FL and DI genome bands, the FL and DI sample from each passage were loaded next to one another. Gel electrophoresis showed that, after four high MOI passages, a very considerable fraction of RSV DIPs is found in the samples. The analysis unveiled the presence of DIPs at 300bp for all three low MOI passages, but at a much lower intensity than that observed in high MOI passages. At the third low MOI passage, we noticed that the presence of RSV DIPs was increasing again. Overall, we confirmed the amplification of the DI genome, as well as the presence of the FL genome at 400 bp (Figure 10). Three independent measurements were carried out to confirm which stock presented the lowest DI content. Ultimately, we chose to use RSV from the second low MOI passage as seed virus for our dynamics study and interference assays, as it appeared to contain the least RSV DIPs.

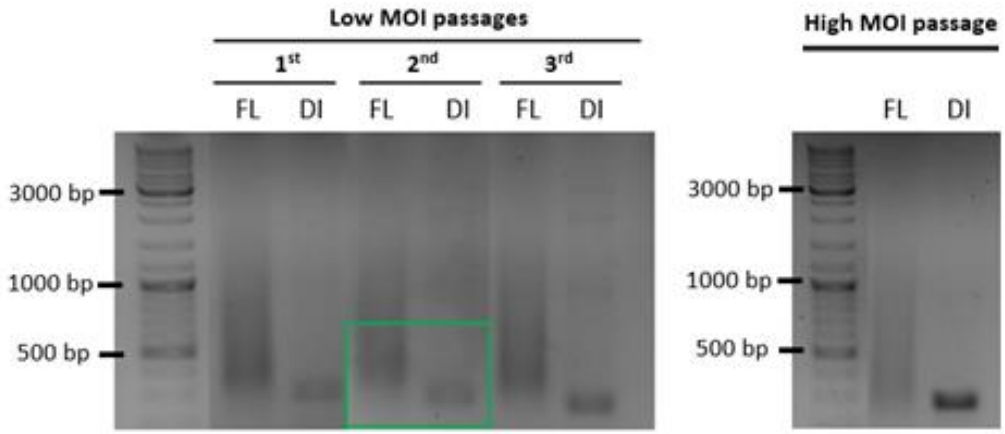

Figure 10 | Selection of a RSV seed virus depleted in DI vRNAs.
Adherent Hep-2 cells cultivated in 175 cm^2 flasks were infected with RSV A2. Over three low MOI passages, RSV was propagated at an MOI of 10^{-2}. As positive control, four high MOI passages were carried out. At various time points, cells were detached, and RSV was harvested as described above. vRNA was subsequently extracted and cDNA was produced via RT-PCR. Samples were loaded on a 2% agarose gel and visualized using the BioDocAnalyze software. For each sample, the FL viral genome and the DI genome were loaded next to one another.

4.2 Assessing RSV infection dynamics

In order to establish our interference assay, we first carried out a dynamic study to assess the kinetics of RSV propagation and to identify the most suitable time points for sampling. We aimed to take samples while infectious virus titers were peaking and comparable in between the two cell lines we will be working with. For this purpose, adherent A549 and Vero cells were seeded in 6-well plates and infected with RSV A2 at an MOI of 10^{-2}. Supernatant was collected at 24, 48, 72, 96 and 120 hpi, and infectious virus titers for each time point were determined via $TCID_{50}$ assay.

Infectious virus titers increased more strongly over time in Vero cells (Figure 11). A549 cells reached the highest infectious virus titer at 120 hpi ($7.11*10^7$ $TCID_{50}$/mL), while Vero cells peaked with a titer of $2.25*10^7$ $TCID_{50}$/mL at 96 hpi, to then decrease at 120 hpi to $1.27*10^6$ $TCID_{50}$/mL due to virus degradation. At 72 hpi, a titer of $1.27*10^7$ $TCID_{50}$/mL was reached both in A549 and Vero cells; at 96 hpi, titers of $7.11*10^6$ $TCID_{50}$/mL and of $2.25*10^7$ $TCID_{50}$ were obtained in A549 and Vero cells, respectively.

Overall, our data provides insights of RSV infection dynamics at low MOI. Infectious virus titers were considered sufficiently elevated and comparable in between cell lines at 72 and 96 hpi, which we chose as final time points for the determination of infectious virus titers in our coinfection studies.

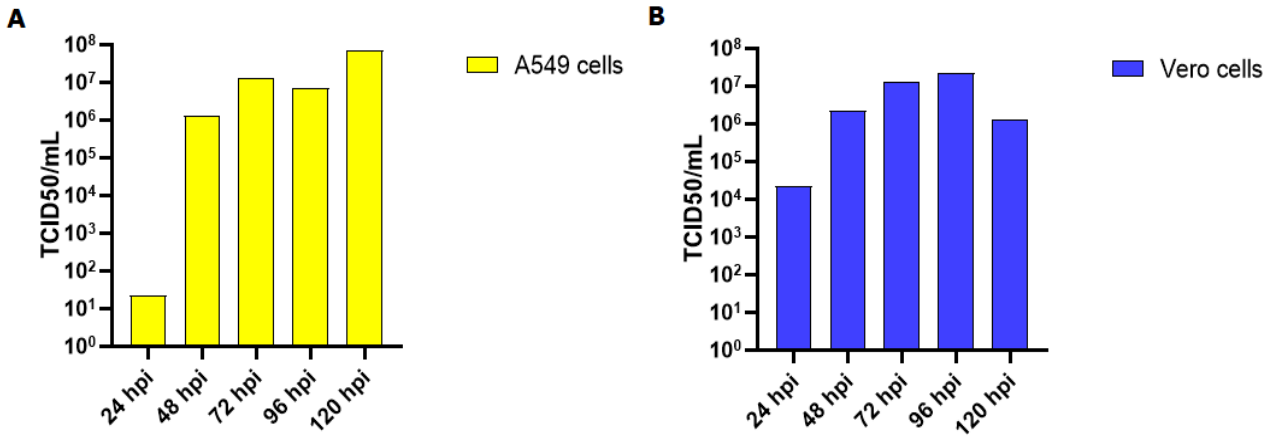

Figure 11 | RSV infection dynamics at low MOI.

Adherent A549 and Vero cells were grown in 6-well plates and infected with RSV at an MOI of 10^{-2}. Samples were taken every 24 hours until 120 hpi to determine infectious virus titer via $TCID_{50}$ assay. One experiment was performed (n=1).

4.3 Inhibitory effect of IAV DIPs against RSV propagation *in vitro*

IAV DIPs have been previously proposed as an antiviral treatment against IFN-sensitive respiratory viral infections due to their capability to stimulate an innate immune system response[66,70,71,77,118]. Literature also shows that RSV DIPs can alter the clinical outcome of patients infected with RSV [63,69]. For these reasons, we decided to test the efficacy of IAV DIPs against RSV replication. Coinfection experiments were carried out using adherent A549 and Vero cells. A549 cells were used as the prominent cell line, because they are lung epithelial cells and possess the ability to secrete IFNs, hence stimulating the innate immune response[83,119,120]. Vero cells, on the other hand, are unable to secrete class I and class III IFNs due to deletion mutations, and were therefore used as a negative control in this study[121–123].

4.3.1 Interference in A549 cells (IFN competent)

According to the literature, IAV DIPs possess the ability to stimulate the host's innate immune response in an IFN-dependent manner, ultimately leading to virus inhibition[70,71]. In this study, we developed an interference assay to test the efficacy of IAV DIPs DI244 and OP7 against RSV replication in A549 cells. Cells were infected with RSV (MOI = 10^{-2}) and infected or coinfected with active or inactive DIPs (fixed volume = 100 µL) derived from a cell culture-based production[74]. We also compared the antiviral efficiency of DIPs with that of other clinically relevant antivirals: specifically, A549 cells were co-treated with either IFN-β1a (2000 U/mL), IFN-λ1 (10 or 100 ng/mL) or ribavirin (409 µM) at the time of infection. To assess whether the inhibitory effect of DI244 and OP7 is IFN-dependent, cells were coinfected with RSV and active IAV DIPs, as well as co-treated with ruxolitinib (2 µM), a janus kinase inhibitor. Lastly, cells were infected with RSV and treated with 96% EtOH (vehicle control). This condition was included because ruxolitinib was dissolved in EtOH, so it was necessary to assess that ethanol would not cause toxicity to either cells or virus. The experimental setup in detail can be found in 3.2.5. Supernatants were sampled at 72 and 96 hpi and infectious virus titers were determined via $TCID_{50}$ assay.

At 72 hpi, cells infected with RSV only exhibited an infectious virus titer of $2.6*10^5$ $TCID_{50}$/mL (Figure 12A). In a coinfection scenario with active DI244, the infectious virus titer was reduced to $5.4*10^4$ $TCID_{50}$/mL. The infectious titer further decreased with active OP7 ($7.07*10^3$ $TCID_{50}$/mL), revealing its stronger inhibitory effect when compared to DI244. Coinfection with inactive DI244 or OP7 showed infectious virus titers of $1.29*10^5$ and $3.36*10^4$ $TCID_{50}$/mL respectively. This suggests that, particularly in the case of OP7, DIPs can show residual inhibitory effects following UV inactivation. When cells were infected with DIPs alone, no infectious virus titer was detectable, as expected.

When A549 cells were co-treated with IFN-β1a, this resulted in a reduction of the infectious virus titer comparable to that of active OP7 ($1.16*10^4$ $TCID_{50}$/mL), while when co-treatment was performed with IFN-λ1, titers of $5*10^4$ $TCID_{50}$/mL and of $2.06*10^4$ $TCID_{50}$/mL were reached with 10 ng/mL and 100 ng/mL,

respectively. Treatment with ribavirin caused the greatest virus inhibition, reaching an infectious virus titer of 6 $TCID_{50}$/mL.
We finally assessed titers of cells coinfected with RSV and active DIPs and treated with ruxolitinib. We measured infectious virus titers of $3.6*10^5$ $TCID_{50}$/mL when cells were coinfected with DI244, and titers of $3.14*10^5$ when coinfection was performed with OP7. The titers were not significantly different compared to the infection with RSV only. This confirms our hypothesis according to which IAV DIPs inhibitory effect is JAK/STAT-dependent.
Lastly, we measured infectious virus titers for cells infected with RSV and treated with EtOH 96%: we calculated titers of $1.86*10^5$ $TCID_{50}$/mL, meaning that the presence of ethanol did not hinder virus propagation.

One-way ANOVA and Dunnett's multiple comparison test were performed to determine statistical significance by comparing infectious virus titers to that obtained by infecting cells with RSV alone. The test unveiled extremely significant p values ($p = < 0.0001$) for coinfection with active DIPs and inactive OP7, for infection with DIPs alone and for co-treatment with IFN-β1a, IFN-λ1 and ribavirin. Coinfection with inactive DI244 resulted in a p value of 0.0088, while treatment with ruxolitinib and EtOH revealed no significance.

At 96 hpi, trends of infectious virus titers were comparable to those seen at 72 hpi (Figure 12B). When we performed Brown-Forsythe test, we found that variances were not homogeneously distributed, and we therefore performed a Welch ANOVA followed by a Dunnett's T3 post-hoc test. This time, the test indicated no statistical significance for any condition, except for coinfection with active DI244 treated with ruxolitinib (p value = 0.0344).

Overall, our results show that active DIPs are able to partially inhibit RSV at MOI 10^{-2}. OP7 reported a stronger inhibitory effect than DI244, comparable to that of IFNs. The FDA and EMA approved ribavirin displayed the strongest inhibitory effect against virus replication. Treatment of coinfected cells with the JAK inhibitor ruxolitinib confirmed that the suppressive effect of IAV DIPs is JAK/STAT-dependent.

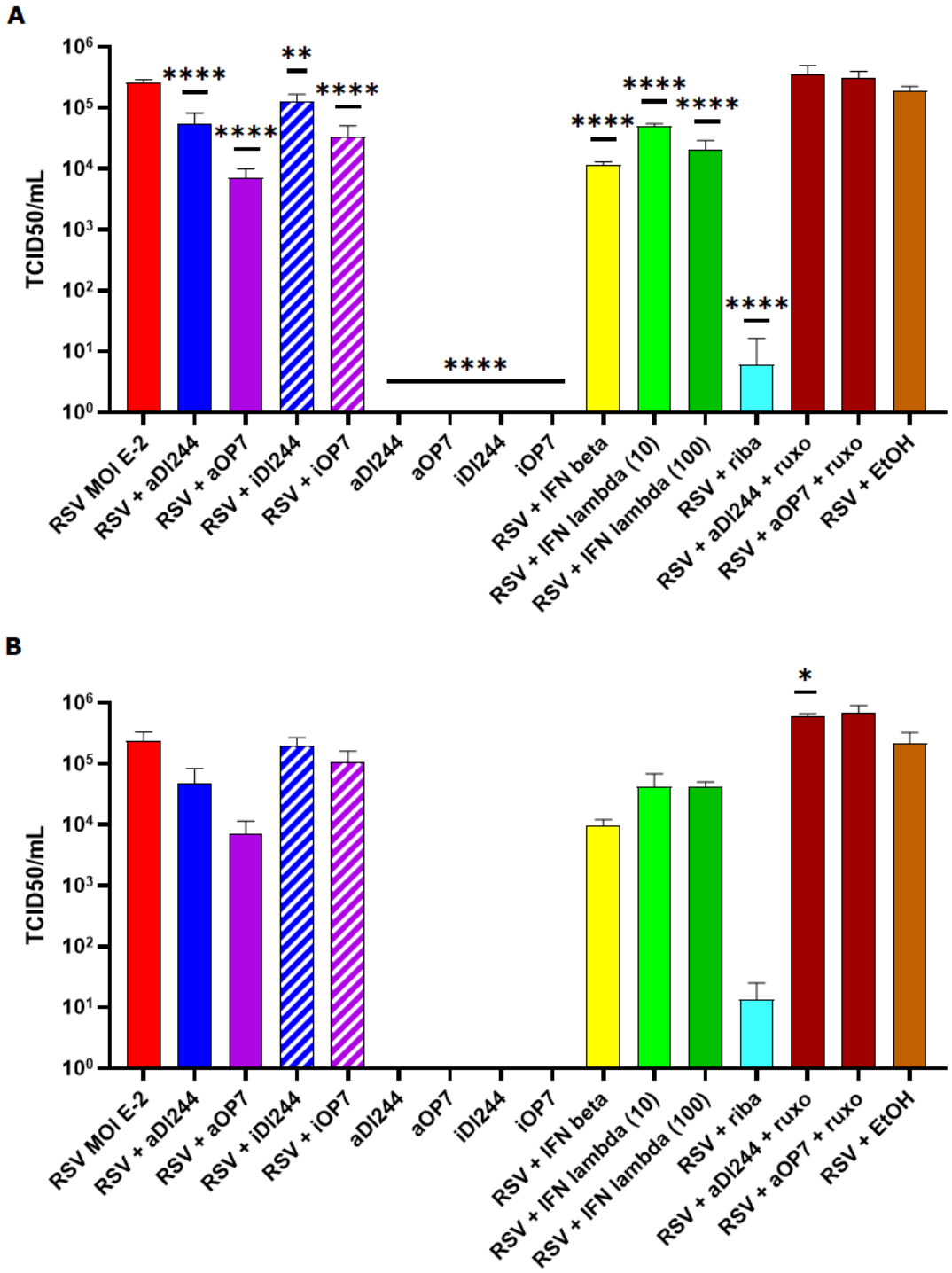

Figure 12 | Interference by IAV DIP coinfection against RSV replication in A549 cells.
Adherent A549 cells were infected with RSV alone, coinfected with RSV and 100 µL of active or inactive IAV DIPs DI244/OP7, or cotreated with one of the control drugs (IFN beta, IFN lambda, ribavirin, ruxolitinib). Supernatants were collected at 72 and 96 hpi. Infectious virus titers were quantified by $TCID_{50}$ assay. **(A)** RSV coinfection at MOI 10^{-2}, 72 hpi. **(B)** RSV coinfection at MOI 10^{-2}, 96 hpi. Three independent experiments were performed (n = 3), and means and sample standard deviations were plotted. Lines above the bars indicate statistical significance (0.1234 (ns), 0.0332 (*), 0.0021 (**), 0.0002 (***), < 0.0001 (****)). Statistical significance was determined by performing one-way ANOVA followed by Dunnett's multiple comparison test for (A) or by carrying out Welsh ANOVA and Dunnett's T3 post hoc test for (B). All conditions were compared to RSV MOI E-2.

4.3.2 Interference in Vero cells (IFN deficient)

In this study, Vero cells were used as a negative control due to their inability to secrete class I IFNs[121–124]. Since it cannot produce antiviral IFNs, we expected no inhibitory effect by IAV DIPs in this cell line.
An interference assay was designed, similar to that for A549 cells. Cells were infected with RSV A2 at an MOI of 10^{-2}, and coinfected with active or inactive DI244 or OP7 (100 µL). Since Vero cells present receptors for class I IFNs but not for class III IFNs[122], only IFN-β1a (2000 U/mL) was used as a positive control, together with ribavirin (409 µM). A negative control with ruxolitinib (2 µM) was also included, to ensure that any potential inhibition by IAV DIPs was not JAK/STAT-dependent.

At 3 days post infection (dpi), Vero cells infected with RSV alone displayed an infectious virus titer of $4.49*10^5$ $TCID_{50}$/mL (Figure 13A). Coinfection with active DI244 and OP7 resulted in infectious virus titers of $3.65*10^5$ $TCID_{50}$/mL and $4.49*10^5$ $TCID_{50}$/mL, respectively, while coinfection with inactive DIPs achieved titers of $7.11*10^5$ $TCID_{50}$/mL for DI244 and $8.75*10^5$ $TCID_{50}$/mL for OP7. There was no significant difference between coinfection with IAV DIPs and infection with RSV alone. The infectious virus titer was reduced to $1.5*10^4$ $TCID_{50}$/mL once infected cells were cotreated with IFN-β1a. Surprisingly, cotreatment with ribavirin barely generated an infectious virus titer reduction ($2.58*10^5$ $TCID_{50}$/mL). Finally, when cells were cotreated with ruxolitinib, titers were comparable to those of cells infected with RSV alone: $5.52*10^5$ $TCID_{50}$/mL for DI244 coinfection and $3.65*10^5$ $TCID_{50}$/mL when cells were coinfected with OP7. EtOH did not have a negative effect on RSV viability.

We performed one-way ANOVA and Dunnett's post-hoc test for statistical analysis. The test unveiled no significance for coinfection with DIPs or co-treatment with ribavirin, ruxolitinib or EtOH, whereas co-treatment with IFN-β1a showed a very significant p value of 0.0097.

At 96 hpi, infectious virus titers were comparable to those obtained at 72 hpi (Figure 13B). No difference in infectious virus titers was observed between cells

infected with RSV alone and coinfected with DIPs. One-way ANOVA and Dunnett's multiple comparison test revealed no significance for any condition.

As we anticipated, coinfection with IAV DIPs did not trigger any inhibition of RSV in the IFN-deficient cell line. This confirms that a functioning IFN system is crucial for successful virus inhibition by DI244 and OP7.

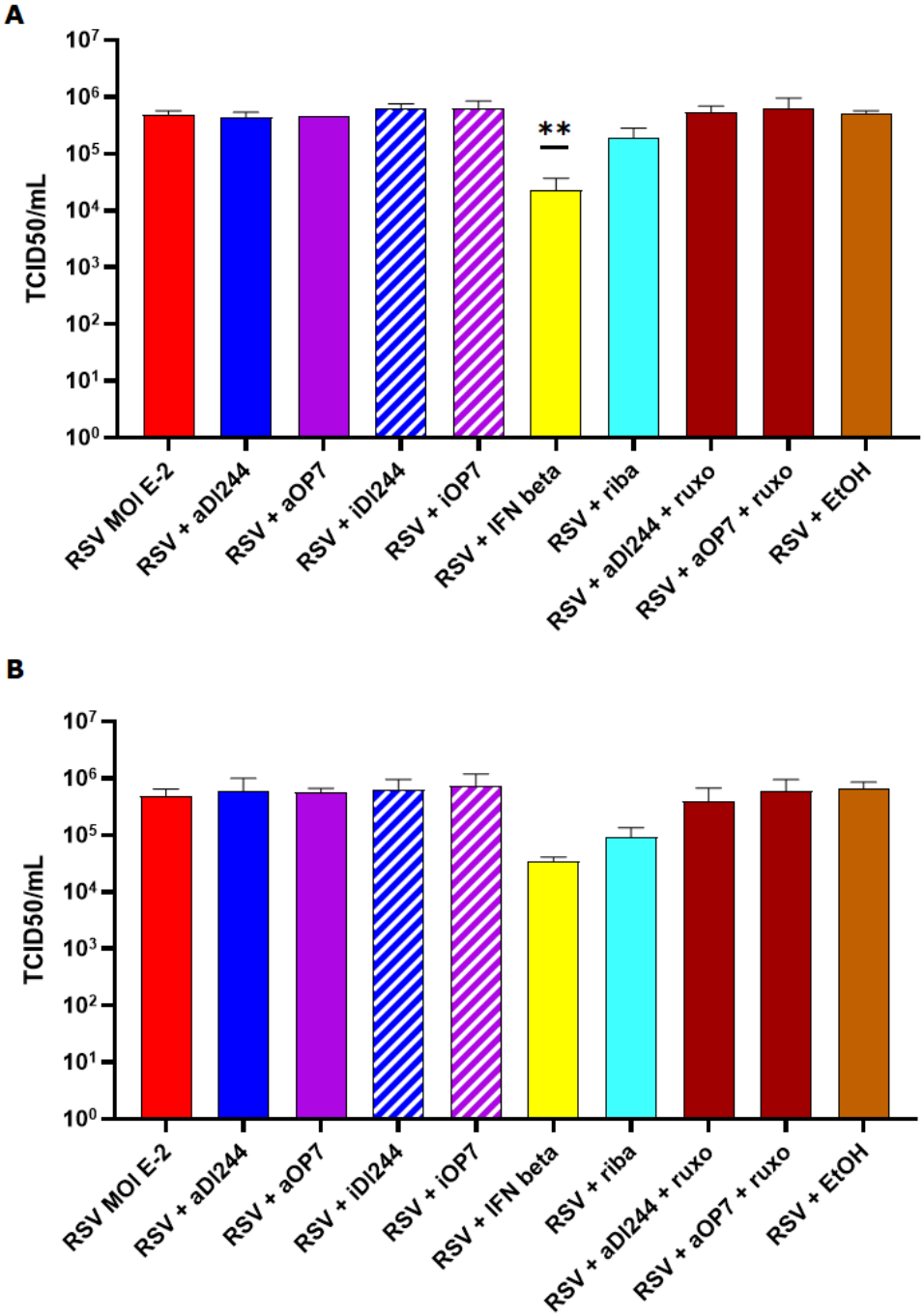

Figure 13 | Interference by IAV DIP coinfection against RSV replication in Vero cells.
Adherent Vero cells were infected with RSV only, coinfected with RSV and 100 µL of active or inactive IAV DIPs, or cotreated with one of the control drugs a fixed volume (100 µL) of active or inactive DI244 or OP7. Supernatants were harvested at 72 and 96 hpi. **(A)** RSV coinfection at MOI 10^{-2}, 72 hpi. **(B)** RSV coinfection at MOI of 10^{-2}, 96 hpi. Three independent experiments were performed (n = 3) and mean values with standard deviations were plotted. One-way ANOVA and Dunnett's post-hoc tests were performed for statistical analysis (0.1234 (ns), 0.0332 (*), 0.0021 (**), 0.0002 (***), < 0.0001 (****)). All conditions were compared to RSV MOI E-2.

4.3.3 Interference of non-diluted IAV DIPs in IFN-competent cells

To test the full antiviral potential of active DI244 and active OP7, we decided to perform a coinfection with non-diluted DIPs in A549 cells. Cells were either infected with RSV alone at an MOI of 10^{-2}, coinfected with 1:20-diluted active DI244 and OP7 (used for the previous coinfection studies, Figures 12 and 13) or coinfected with highly concentrated, undiluted active DI244 or OP7. For all conditions, we used a fixed volume of DIPs of 100 µL/well. Supernatants were sampled at 96 hpi and infectious virus titers were calculated via $TCID_{50}$ assay.

At 4 dpi, cells infected with RSV only revealed an infectious virus titer of $2.14*10^5$ $TCID_{50}$/mL (Figure 14). When cells were coinfected with diluted DIPs, we obtained virus titers of $4.28*10^4$ $TCID_{50}$/mL for DI244 and of $6.32*10^3$ $TCID_{50}$/mL for OP7. In the case of coinfection with non-diluted DIPs, we measured infectious virus titers of $6.62*10^4$ $TCID_{50}$/mL for DI244 and $2.87*10^3$ $TCID_{50}$/mL for OP7.

In conclusion, increasing the concentration of IAV DIPs in a coinfection scenario did not remarkably enhance the inhibitory effect of either DI244 or OP7.

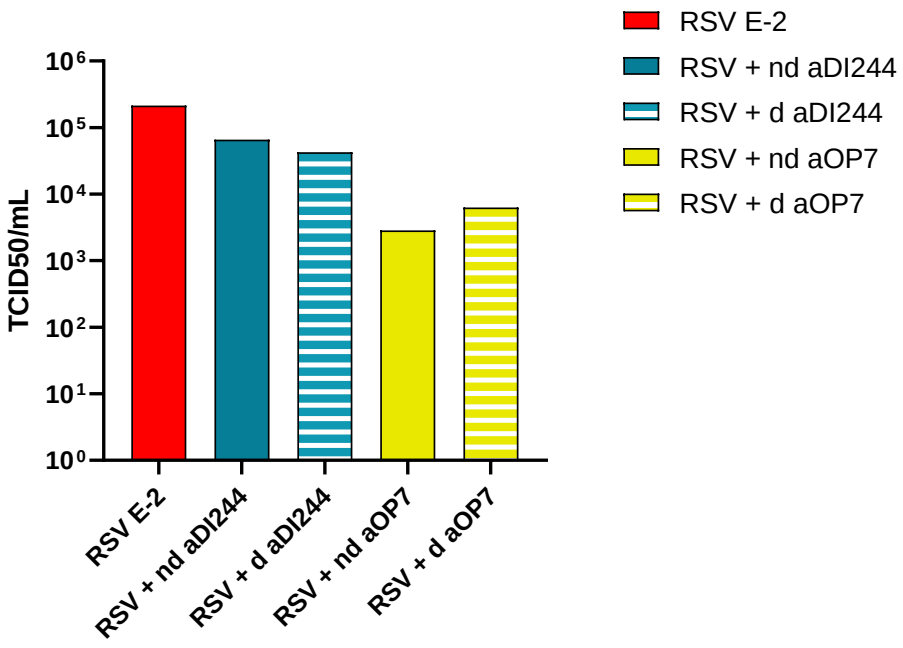

Figure 14 | Interference of non-diluted IAV DIPs against RSV replication.
Adherent A549 cells were infected with RSV alone or coinfected with RSV and 100 µL of diluted (a) or non-diluted (nd) active (a) IAV DIPs. Supernatants were collected at 96 hpi. Infectious virus titers were quantified by $TCID_{50}$ assay. Two independent experiments were performed (n = 2) and means were plotted.

4.4 Innate immune responses to RSV: gene expression analysis

The interference assay demonstrated that IAV DIPs, and especially OP7, can significantly hinder RSV replication in IFN competent cells. This is likely caused by the stimulation of the innate immune response in a JAK/STAT dependent way. In order to assess the impact of the IFN-dependent system on the inhibitory effect of IAV DIPs, mRNA levels of five genes (RIG-I, IFN-β1, IFN-λ1, Mx1 and IFITM1) were investigated via real-time RT-qPCR. The fold change in gene expression level for each gene was calculated by using the ΔΔCt method. Expression levels of the gene of interest in DIP-coinfected cells were always compared to the levels in RSV-infected cells.

4.4.1 Cytosolic PRR RIG-I

RIG-I plays a crucial role in triggering the host antiviral response to contain viral replication [78–80]. The PRR recognizes viral RNA in the cytoplasm and leads to a signaling cascade that results in the induction of type I and type III IFNs, as well as ISGs. In this study, we investigated the gene expression levels of RIG-I by

RT-qPCR: we compared levels of mRNA detected in co-treated A549 cells to the levels found in monolayers infected with RSV only. Adherent A549 cells were infected as reported in 3.2.5 and intracellular mRNA was isolated for subsequent RT-qPCR analysis.

When infected with an MOI of 10^{-2} with RSV alone, A549 cells display no upregulation of RIG-I at 6 hpi, and just a slight fold change increase of 12.7 at 24 hpi (Figure 15A). At later time points, a strong upregulation of the gene is observed, in compliance with the infectious virus titer increase that results in a strong stimulation of the innate immune response: we observed a 93.36-fold change increase at 48 hpi and 82.5-fold change at 72 and 96 hpi. In contrast, coinfection with active DIPs led to a significantly higher increase of gene expression already at 6 and 24 hpi. Coinfection with active DI244 led to an 8.95-fold change increase at 6 hpi, and a significant increase of 77.59-fold at 24 hpi. Active OP7 triggered an even greater upregulation of RIG-I, with values of 17.84 and 114.73-fold at 6 and 24 hpi, respectively. Coinfection with inactive DI244 resulted in RIG-I expression levels being only slightly higher than RSV only, while with inactive OP7 we observed a significant increase of gene expression at 24 hpi, similar to that seen with active DI244. This is likely the result of unspecific innate immune response stimulation by the inactive DIP. At later time points, gene expression levels in cells coinfected with either active or inactive IAV DIPs are congruent with those displayed by cells infected with RSV only. One-way ANOVA and Dunnett's post-hoc tests were performed to compare fold changes in gene expression levels in coinfected cells to those of cells infected with RSV only. These revealed significant differences from the reference curve (RSV E-2) at 6 hpi for active OP7 ($p=0.0281$) and at 24 hpi for active DI244 ($p= 0.0005$), active OP7 ($p= <0.0001$) and inactive OP7 ($p= 0.0097$).

In the case of DIPs only infection (Figure 15B), active DI244 and OP7 displayed a similar trend for RIG-I expression levels compared to the coinfection scenario, with values peaking starting from 24 hpi (81.47 and 113.86-fold, respectively). Gene expression levels kept steadily high for both active DIPs until 96 hpi. Inactive DIPs, on the other hand, displayed a firmly low expression of RIG-I:

fold-change values of 26 for DI244 and 40.58 for OP7 at 24 hpi were the highest registered during the course of the experiment. At later time points, the fold-change values gradually decreased. This confirms that UV inactivation of IAV DIPs generally results in hindered interference and gene expression upregulation. To determine the significance between gene expression levels of active and inactive DIPs, Student's t-tests were performed. Active DI244 was compared to inactive DI244, and the same was done for OP7. Significant to extremely significant values were obtained for both DIPs. Specifically, RIG-I expression levels were significantly higher for active DI244 at both 6 and 24 hpi ($p= 0.0197$ and $p= 0.0438$). At 48 hpi, active DI244 and OP7 showed very significant and significant values ($p= 0.0051$ and $p= 0.0305$ respectively). At 72 and 96 hpi DI244 displayed highly to extremely significant p values of <0.0001 and 0.0005, while OP7 had values of 0.0014 and 0.0114.

To summarize, our results show that, in a low MOI coinfection scenario, DIPs trigger elevated RIG-I upregulation compared to RSV only infection. This is furtherly confirmed by fold change values reported after infection with DIPs alone. Overall, our results suggest that active IAV DIPs can stimulate the host innate immune response.

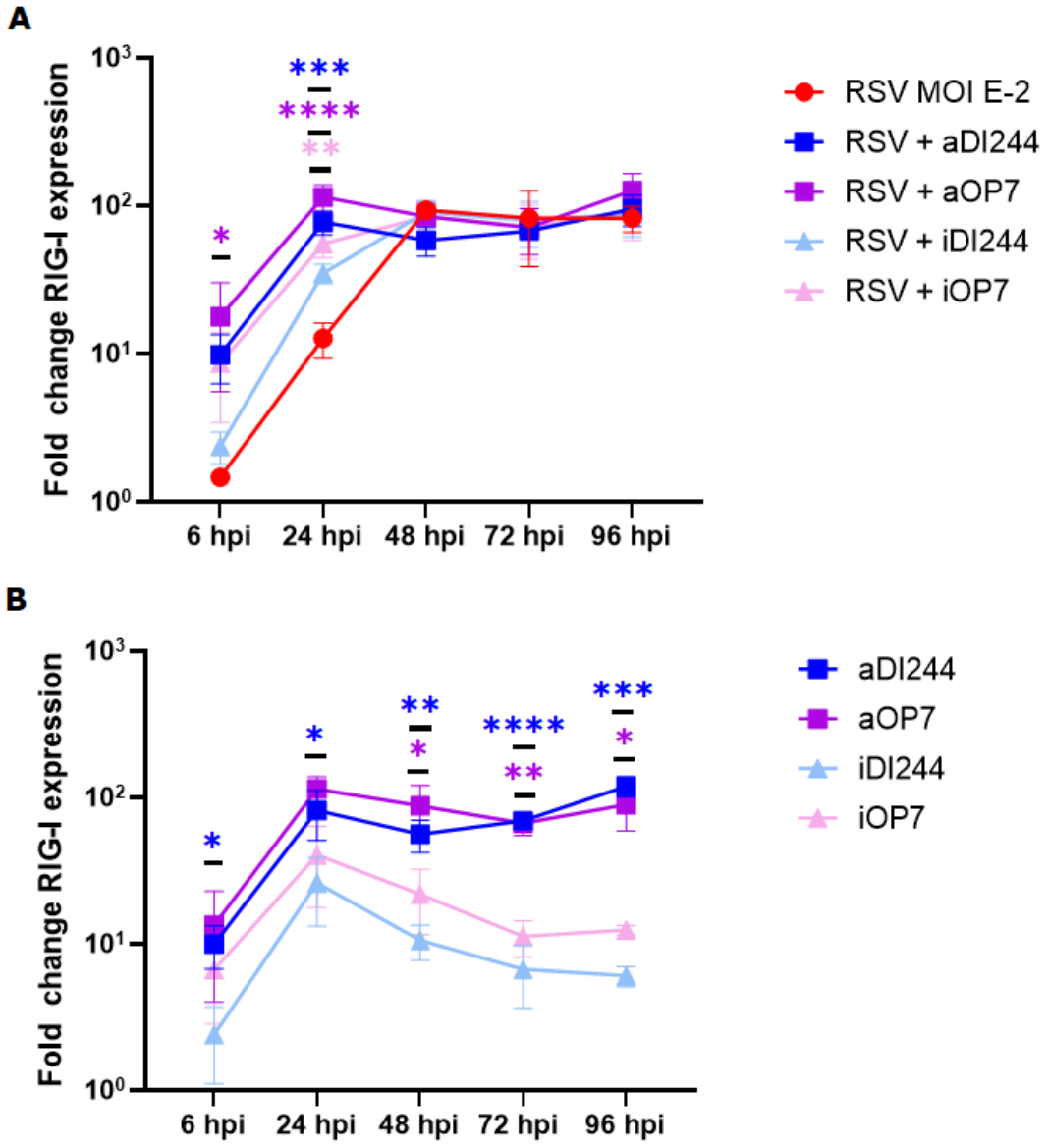

Figure 15 | Stimulation of RIG-I expression.

Adherent A549 cells were either infected with RSV alone, coinfected with active or inactive DI244/OP7 or infected with DIPs alone. At the established time points cells were lysed, and intracellular mRNA was isolated. RIG-I mRNA levels were subsequently measured via real-time RT-qPCR. The ΔΔCt method was used to calculate the fold change in gene expression. **(A)** Infection with RSV alone or coinfection with active or inactive DIPs at MOI 10^{-2}. **(B)** Infection with active or inactive DIPs alone. Means and sample standard deviations were generated from repeated experiments performed independently (n=3). For (A), statistical tests were conducted using one-way ANOVA and Dunnett's post-hoc test. Conditions were compared to RSV MOI E-2. For (B), Student's t-test was carried out. Values of active IAV DIPs were compared to those of inactive IAV DIPs. Asterisks indicate significance (ns $p \geq 0.05$, * (significant) $p < 0.05$, ** (very significant) $p < 0.01$, *** (highly significant) $p < 0.001$, **** (extremely significant) $p < 0.0001$).

4.4.2 Antiviral effects of class I and class III IFNs

Viral detection by PRRs induces production of transcription factors such as interferon regulatory factors (IRFs), which regulate the expression of type I and type III IFNs. Once these pro-inflammatory cytokines bind their receptors, they trigger the expression of hundreds of ISGs via the JAK/STAT signaling cascade, leading to an enhancement of both innate and adaptive immune responses [78,79,82]. Here, we elucidated induction of IFN-β1 (class I IFN) and IFN-λ1 (class III IFN) expression by RT-qPCR. Class I and class III IFNs are fundamental in stimulating the host immune response as they have an antiviral function[113,125].

IFN-β1

At an MOI of 10^{-2}, infection with RSV only did not initially induce a strong upregulation of IFN-β1 (Figure 16A). At 6 hpi, a value of 2.32-fold was detected, which reached 46.75-fold at 24 hpi. Fold-change peaked starting from 48 hpi, when a great upregulation of the gene is detected, with values rising between $3.4*10^3$-fold to $5.35*10^3$-fold. Coinfection with active DIPs resulted in a strong upregulation of IFN-β1 already from early time points. Coinfection with active DI244 resulted in a 717.49-fold change in expression at 6 hpi and upregulation peaked with $4.92*10^3$-fold at 24 hpi. Active OP7 triggered significant upregulation of the gene at 6 hpi ($1.26*10^3$-fold) and reached its peak at 24 hpi with a $1.97*10^3$ fold-change. Values kept steadily high at later time points for both DIPs. Until 48 hpi, coinfection with inactive DIPs displayed upregulation that exceeded that of RSV only infection but was lower than that of active DIPs. For statistical analysis, one-way ANOVA and Dunnett's multiple comparison were carried out as for RIG-I expression analysis. IFN-β1 expression levels were significantly higher for active OP7 at 6 hpi ($p=0.0139$) and very significantly higher at 48 hpi ($p=0.0053$). Active DI244 achieved high significance at 24 hpi with a p value of 0.0008 and significance at 48 hpi with a p value of 0.0116. Increase of gene expression with inactive OP7 at 48 hpi was also registered as significant, with a p value of 0.0157.

For infection with DIPs only, active DIPs displayed a steady and robust upregulation of IFN-β1 starting from 6 hpi; fold-changes peaked at 24 hpi with values of $5.93*10^3$-fold for DI244 and $2.36*10^3$-fold for OP7 (Figure 16B). Interestingly, at 6 hpi the upregulation of the cytokine is stronger with OP7 ($1.58*10^3$-fold) than with DI244 (911.76-fold). This suggests that early upregulation of innate immune responses by active OP7 may explain its stronger inhibitory effect against RSV when compared to active DI244. As expected, inactive DIPs did not induce a strong overexpression of the type I IFN, and fold-change values kept decreasing after 6 hpi. Fold-changes were comparable between the two DIPs. The student's t-test showed a significant difference between active and inactive DI244 at 6, 24 and 48 hpi (respectively, $p=0.04370$, $p=0.0163$ and $p=0.0205$) and a very significant difference at 96 hpi ($p=0.0034$). A significant difference between active and inactive OP7 was registered at 48 hpi ($p=0.0223$).

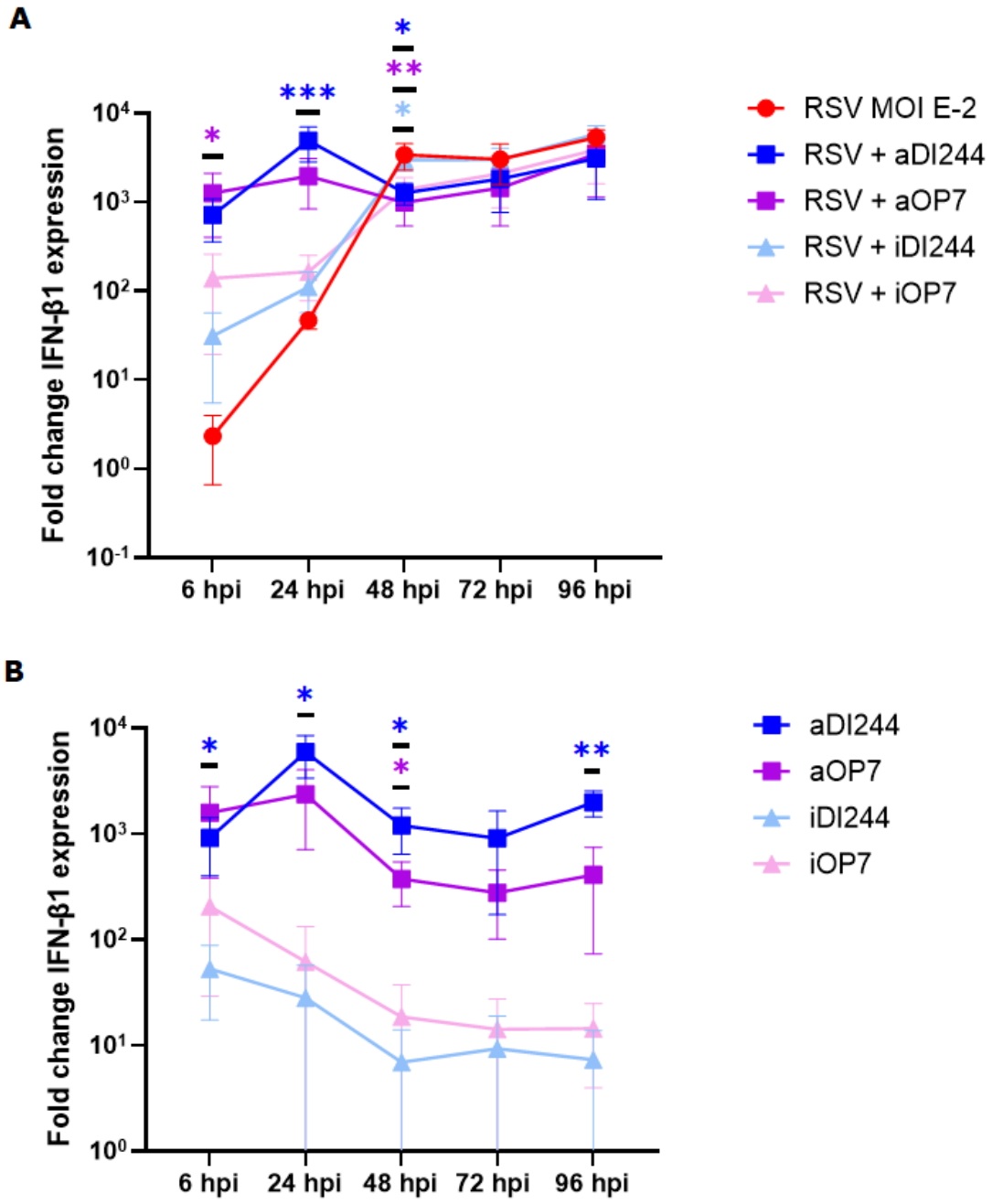

Figure 16 | Stimulation of IFN-β1 expression.

Adherent A549 cells were either infected with RSV alone, coinfected with active or inactive DI244/OP7 or infected with DIPs alone. At the established time points cells were lysed, and intracellular mRNA was isolated. IFN-β1 mRNA levels were determined via real-time RT-qPCR. The ΔΔCt method was used to calculate the fold change in gene expression. **(A)** Infection with RSV only or coinfection with active or inactive DIPs at MOI 10^{-2}. **(B)** Infection with DIPs only. Means and sample standard deviations were generated from repeated experiments performed independently (n=3). For (A), statistical tests were conducted using one-way ANOVA and Dunnett's post-hoc test. Conditions were compared to RSV MOI E-2. For (B), Student's t-test was carried out. Values of active IAV DIPs were compared to those of inactive IAV DIPs. Asterisks indicate significance (ns $p \geq 0.05$, * (significant) $p < 0.05$, ** (very significant) $p < 0.01$, *** (highly significant) $p < 0.001$).

IFN-λ1

In the case of IFN-λ1, it was not possible to determine fold-change values using the ΔΔCt method because the levels of IFN in the mock control were below the limit of detection of the assay. For this reason, we decided that in this study we will be plotting and commenting on the Ct values obtained for each condition at the conventional time points. Please note that lower Ct values correspond to greater gene upregulation, and that a difference in Ct values of ~3.3 corresponds to approximately one log (factor 10).

Upon infection at an MOI of 10^{-2}, A549 cells infected with RSV alone reported a Ct value of 32.81 at 6 hpi, followed by an increase up to 24.52 at 24 hpi (Figure 17A). Ct values peaked at 48 hpi (Ct=16.58) and kept steady for the rest of the experiment, in compliance with what we already observed for the previous targets. In comparison, coinfection with active IAV DIPs resulted in a strong IFN-λ1 expression already from the earliest time point. At 6 hpi, a Ct value of 20.46 was detected in cells coinfected with DI244, followed by 17.13 at 24 hpi. Over later time points, IFN-λ1 levels were comparable to those detected at 24 hpi. A similar course was observed in case of treatment with active OP7. According to Dunnett's multiple comparisons test, both active and inactive DIPs displayed very significant to extremely significant p values at 6 and 24 hpi when compared with RSV only infection. At 48 and 72 hpi, only OP7 showed significant p values (p=0.0148 and p=0.0157). At 96 hpi, both active DIPs presented significantly higher Ct values than RSV alone.

We then examined the effects of DIP only infection on IFN-λ1 expression (Figure 17B). Active IAV DIPs increased fold change of gene expression, while the fold change only declines with inactive DIPs. At 6 hpi, active OP7 presented a Ct value of 19.6. Levels of the type III IFN peaked at 24 hpi, when a Ct value of 18.4 was registered; from 48 hpi, gene expression levels started to decrease. Active DI244 displayed a lower Ct value at 6 hpi (20.32), but if presented the greatest gene upregulation at 24 hpi, with a Ct value of 16.56. Moreover, despite a decrease in gene expression starting from 48 hpi, at 96 hpi the Ct value recorded is 18.76. Last, inactive DIPs exhibited reference curves that were

almost identical to one another. The lowest Ct values were detected at 6 hpi, meaning that in the subsequent time points there was a reduction in IFN-λ1 expression for both DI244 and OP7. The results of the unpaired t-tests indicated high significance for active DI244 at all time points (p values between 0.0003 and 0.0009). OP7 unveiled significance at 6 and 96 hpi (respectively, p=0.0249 and p=0.0186), high significance at 48 hpi (p=0.0011) and very high significance at 72 hpi (p=0.0009).

Finally, high IFN-β1 and IFN-λ1 expression levels were observed upon active IAV DIPs coinfection. This is most likely one of the factors contributing to the inhibitory effect that active DIPs held against RSV. Furthermore, since OP7 showed higher upregulation of both cytokines at 6 hpi, this might be one reason for its stronger effect in limiting RSV propagation.

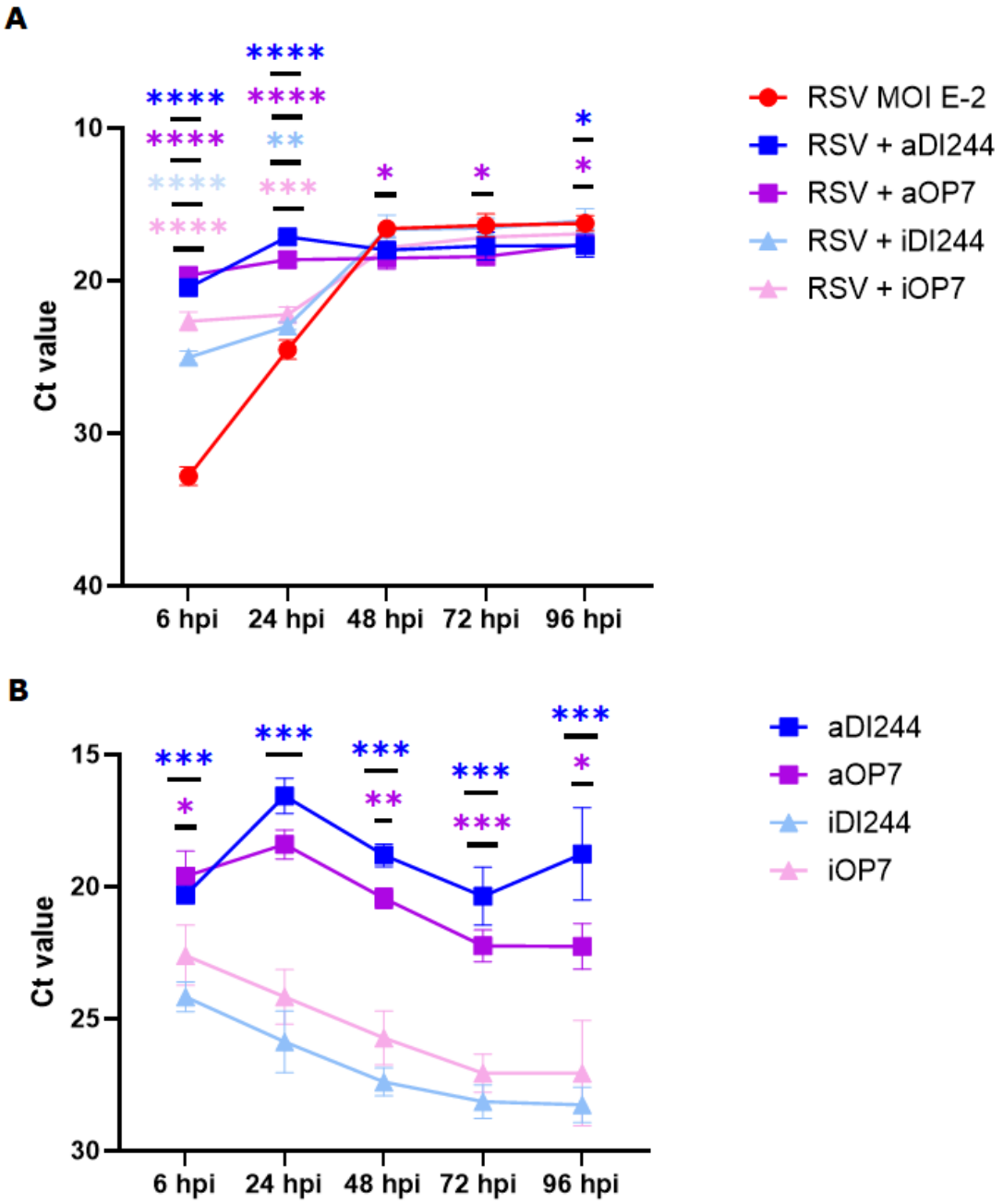

Figure 17 | Stimulation of IFN-λ1 expression.

Adherent A549 cells were either infected with RSV alone, coinfected with active or inactive DI244/OP7 or infected with DIPs alone. At the established time points cells were lysed, and intracellular mRNA was isolated. IFN-λ1 mRNA levels were subsequently measured via real-time RT-qPCR. The Ct values were in this case plotted, as it was not possible to calculate gene expression levels with the ΔΔCt method. **(A)** Infection with RSV alone or coinfection with active or inactive DIPs at MOI 10^{-2}. **(B)** Infection with active or inactive DIPs alone. Means and sample standard deviations were generated from repeated experiments performed independently (n=3). For (A), statistical tests were conducted using one-way ANOVA and Dunnett's multiple comparison test. Conditions were compared to RSV MOI E-2. For (B), Student's t-test was carried out. Values of active IAV DIPs were compared to those of inactive IAV DIPs. Asterisks indicate significance (ns $p \geq 0.05$, * (significant) $p < 0.05$, ** (very significant) $p < 0.01$, *** (highly significant) $p < 0.001$, **** (extremely significant) $p < 0.0001$).

4.4.3 Upregulation of ISGs

The type I and class III IFNs produced in response to the viral infection are able to act both in an autocrine and paracrine way to activate the JAK/STAT signaling cascade. This culminates in the downstream expression of hundreds of ISGs. The antiviral host effector proteins can help cells to resist infection, as well as contain virus propagation in already infected cells[86,98,99]. We quantified the gene expression levels of Mx1 and IFITM1, two ISGs that are reported to be upregulated during infection in the literature[100,126].

Mx1

Infection with RSV only, at an MOI of 10^{-2} revealed an increasing upregulation of Mx1, with 1.99-fold change at 6 hpi and 175.16-fold change at 24 hpi (Figure 18A). Gene expression peaked at 48hpi ($2.57*10^3$-fold), and it remained stable throughout the rest of the assay. Coinfection with active DIPs stimulated a stronger upregulation already from the first time point. Active DI244 registered a fold change of 92.83 at 6 hpi and peaked at 24 hpi with a value of $3.37*10^3$-fold. Gene expression levels remained steadily high for the following time points, with only a slight fold-change decrease. Coinfection with active OP7 stimulated an even stronger upregulation of Mx1: it exhibited 228.51-fold change at 6 hpi, and $3.85*10^3$-fold change at 24 hpi, even though the trend for the remaining time points is comparable to that of DI244. Inactive IAV DIPs presented fold-change values that were lower than those of active DIPs, but notably higher than those of cells infected with RSV alone. One-way ANOVA and Dunnett's post-hoc tests were performed to compare expression levels in coinfected cells to those of cells infected with RSV only. Both active DI244 and OP7 unveiled very significant values at 24 hpi in comparison to RSV alone ($p=0.0089$ and $p=0.0036$, respectively).

In the case of infection with DIPs alone, the two active DIPs showed similar gene expression tendencies, and so did inactive DI244 relative to OP7 (Figure 18B). All four DIPs peaked at 24 hpi: active DI244 exhibited a $3.44*10^3$-fold change expression, active OP7 a $3.73*10^3$-fold change, inactive DI244 an 840.23-fold

change and inactive OP7 a $1.54*10^3$-fold change. Although it is possible to observe a significant difference in gene upregulation between active and inactive DIPs, inactive DI244 and OP7 presented remarkably elevated expression levels of Mx1, which might explain their residual inhibitory effect that is sometimes observed in coinfection scenarios. Student's t-test provided a significant difference between active and inactive DI244 at 24 ($p=0.0280$) and 48 hpi ($p=0.0199$), and a very significant difference at 72 and 96 hpi ($p=0.0046$ and $p=0.0023$, respectively). Active OP7 showed significant p values of 0.0246 at 72 hpi and of 0.0208 at 96 hpi.

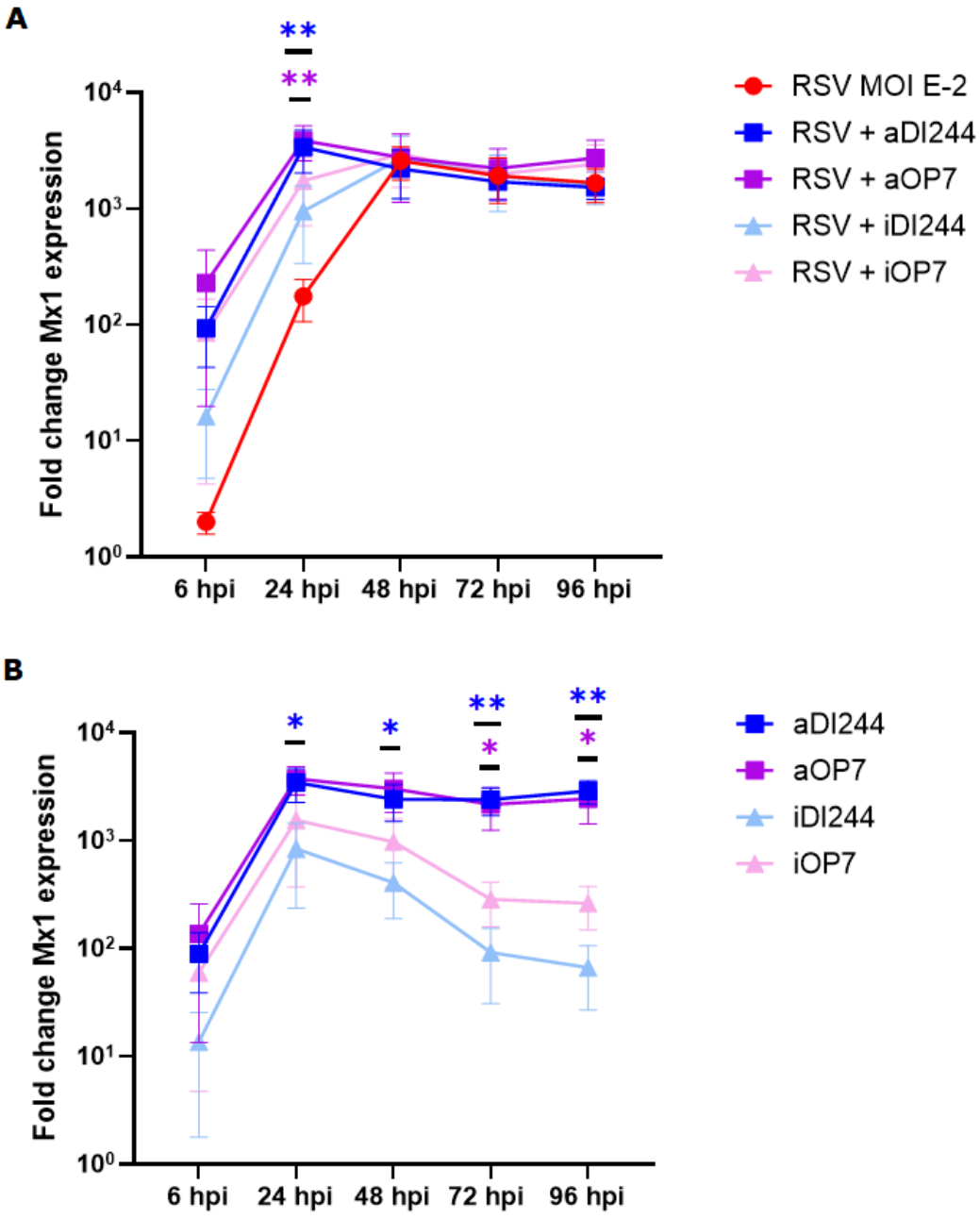

Figure 18 | Stimulation of Mx1 expression.

Adherent A549 cells were either infected with RSV only, coinfected with active or inactive DI244/OP7 or infected with DIPs only. At the established time points cells were lysed, and intracellular mRNA was isolated. Mx1 mRNA levels were determined via real-time RT-qPCR. The ΔΔCt method was used to calculate the fold change in gene expression. **(A)** Infection with RSV only or coinfection with active or inactive DIPs at MOI 10^{-2}. **(B)** Infection with DIPs only. Means and sample standard deviations were generated from repeated experiments performed independently (n=3). For (A), statistical tests were conducted using one-way ANOVA and Dunnett's post-hoc test. Conditions were compared to RSV MOI E-2. For (B), Student's t-test was carried out. Values of active IAV DIPs were compared to those of inactive IAV DIPs. Asterisks indicate significance (ns $p \geq 0.05$, * (significant) $p < 0.05$, ** (very significant) $p < 0.01$).

IFITM1

When infection was carried out at an MOI of 10^{-2}, no upregulation of IFITM1 was found at 6 hpi in cells infected with RSV only (Figure 19A). Fold-change expression levels increased to 37-fold at 24 hpi and peaked at 48 hpi with a value of $2.6*10^3$-fold. The gene of interest remained upregulated also at the following time points, indicating that an infectious virus titer increase results in a stronger stimulation of the innate immune response. In contrast, active DIPs expressed considerably higher levels of IFITM1 already from 6 hpi (14.21-fold for DI244 and 28.47-fold for OP7). A sudden increase was registered at 24 hpi, when active DI244 recorded a $2.05*10^3$-fold change and active OP7 registered a $2.53*10^3$-fold change of expression. From 48 to 96 hpi, gene expression levels remained steadily elevated, in compliance to what we already reported for RSV only infection. Coinfection with inactive DI244 and OP7 resulted in gene expression levels that were considerably higher than those of RSV infection alone, but still lower than those appreciated in a coinfection scenario with active DIPs. One-way ANOVA and Dunnett's multiple comparison test unveiled significant differences in upregulation. Active OP7 showed a significant p value of 0.0393 at 6 hpi, an extremely significant p value of <0.0001 at 24 hpi and a significant value of 0.0289 at 48 hpi. The test presented an extremely significant difference between active DI244 and RSV only at 24 hpi (p=<0.0001) and a significant difference at 96 hpi (p=0.0273). Inactive OP7 displayed a significant p value of 0.0128 at 24 hpi.

Lastly, we examined differences in gene expression levels in A549 cells infected with IAV DIPs alone (Figure 19B). Once again, the two active DIPs displayed trends comparable to one another, and so did the two inactive DIPs. At 24 hpi, we observed strong upregulation of IFITM1 both for active DI244 ($2.41*10^3$-fold change) and active OP7 ($2.55*10^3$-fold change). DI244 stays strongly upregulated at 96 hpi with a fold-change of $4.72*10^3$-fold, while OP7 reported the greatest expression levels at 72 hpi, with a value of $5.5*10^3$-fold. As we noted for Mx1, inactive DIPs also showed copious upregulation of IFITM1 at early time points, even though gene expression levels started decreasing from 48 hpi.

Student’s t-test was conducted to reveal significance between active and inactive variants. The test revealed significance for DI244 at 6 hpi (p=0.0118), and both active DIPs showed very to highly significant p values both at 24 and 48 hpi. In the last time points, active DI244 had extremely significant p values (p=<0.0001), as well as active OP7.

In conclusion, we observed a strong transcription of antiviral host effector genes when A549 cells were coinfected with active IAV DIPs. This most likely contributes to the inhibitory effect of DIPs against virus replication. Moreover, IFITM1, which is primarily found on the cell surface and blocks infection during virus entry, was found to be extremely upregulated with both DI244 and OP7.

Finally, a significant upregulation of RIG-I, type I and type III IFNs and ISGs by active DIPs was assessed via RT-qPCR measurements. In particular, OP7 was able to provide minimally higher gene expression levels than DI244 at early time points, which might be explanatory of its greater antiviral effect.

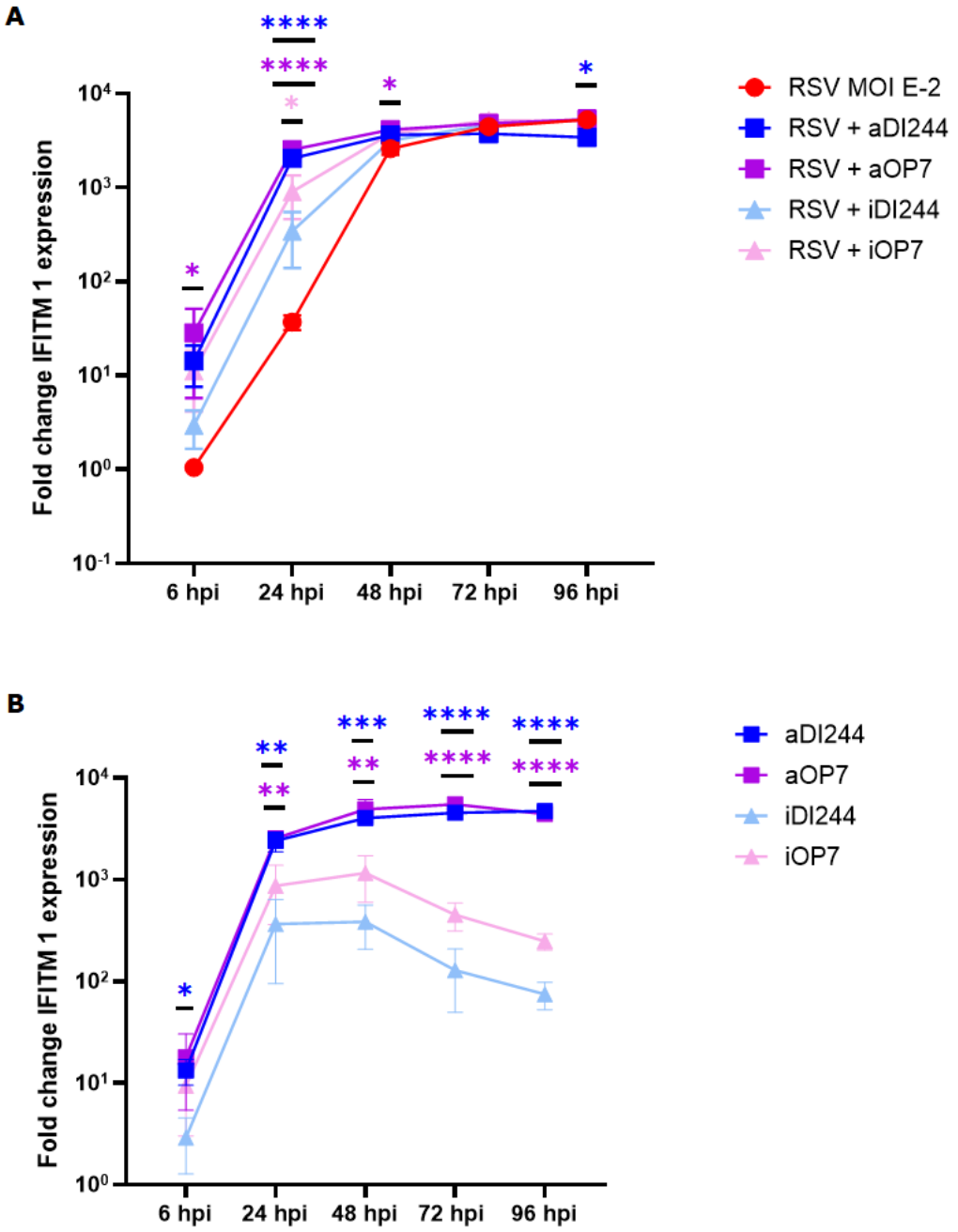

Figure 19 | Stimulation of IFITM1 expression.

Adherent A549 cells were either infected with RSV alone, coinfected with active or inactive DI244/OP7 or infected with DIPs alone. At the established time points cells were lysed, and intracellular mRNA was isolated. IFITM1 mRNA levels were subsequently measured via real-time RT-qPCR. The ΔΔCt method was used to calculate the fold change in gene expression. **(A)** Infection with RSV alone or coinfection with active or inactive DIPs at MOI 10^{-2}. **(B)** Infection with active or inactive DIPs alone. Means and sample standard deviations were generated from repeated experiments performed independently (n=3). For (A), statistical tests were conducted using one-way ANOVA and Dunnett's post-hoc test. Conditions were compared to RSV MOI E-2. For (B), Student's t-test was carried out. Values of active IAV DIPs were compared to those of inactive IAV DIPs. Asterisks indicate significance (ns $p \geq 0.05$, * (significant) $p < 0.05$, ** (very significant) $p < 0.01$, *** (highly significant) $p < 0.001$, **** (extremely significant) $p < 0.0001$).

5. Discussion

RSV causes more than 30 million acute respiratory infections each year, resulting in the death of at least 60000 infants every year[15]. To date, no vaccination strategy has yet been approved for the prevention of RSV infection. Moreover, the use of ribavirin, the only drug approved for treatment, is limited to high risk patients due to its cost inefficiency and safety issues[41].

In this study, we tested the antiviral potential of IAV DIPs DI244 and OP7 against RSV propagation *in vitro*. Because of the lack of efficient antiviral agents to treat RSV infection, new drugs are undergoing testing[1]. IAV DIP have been recently proposed as an inhibitory agent against several IFN-sensitive viruses, thus they could represent an effective and cost-efficient treatment against RSV infection[66,71,74,118]. We first produced a seed virus at low MOI to retrieve RSV with a low content of natural DIPs. We subsequently conducted a dynamic study in A549 and Vero cells – both permissive for RSV replication – and determined 72 and 96 hpi to be the best time points for infectious virus harvesting in coinfection studies. Moreover, we developed an *in vitro* interference assay to demonstrate the inhibitory effect of DI244 and OP7 against RSV propagation in human IFN competent A549 cells from the respiratory tract. Finally, to confirm that the inhibitory effect of IAV DIPs is dependent on the stimulation of the innate immune response, we measured the gene expression levels of key antiviral genes. RIG-I, IFN-β1, IFN-λ1, IFITM1 and Mx1 were found to be upregulated at early time points in a coinfection scenario with active DI244 and OP7.

5.1 Production of seed virus

The RSV strain A2 has been used throughout the course of this study. A2 is a live-attenuated, temperature sensitive strain that underwent cold passaging [110]. The virus' shut-off temperature is 40°C, and prolonged exposition to room temperature reduces RSV viability, function and infectivity[111,127–129].

Mundle *et al*. produced purified RSV stocks from cell lysates obtained via sonication at ice-cold temperatures. They state that cell lysate-derived

preparations present 2-fold more PFU per fraction compared to supernatant-derived ones[130]. To best preserve RSV preparations during the course of this study, the virus material was kept on ice at all times following sample thawing and until the time of use. This was particularly important during seed virus production: when carrying out low MOI passages, the seed virus was centrifuged at 4°C and kept on ice during vortexing. Moreover, the sonicator's sample support was kept at -20°C prior to use to avoid overheating. In order to further preserve virus viability, a sucrose solution (2% final concentration) was added to the seed virus stock, as it is reported to improve virus stability upon freezing[131,132]. Grosz *et al*. tested the protective effect of sucrose concentrations ranging from 0 to 20%: while higher concentrations are required if the virus undergoes nebulization, addition of 3% sucrose can fully preserve the material against freezing and thawing[132]. Lastly, to avoid crystal formation caused by slow freezing, which can rupture the envelope of RSV virions, RSV aliquots were snap frozen in liquid nitrogen and ultimately stored at -80°C, as it was suggested by Kast *et al*[133].

Following vRNA transcription, translation and replication, new filamentous RSV virions assemble at the cell surface in an actin-dependent manner. RSV mediates actin polymerization, resulting in the formation of filopodia that drive not only virion assembly but also cell to cell spreading[17,117]. This mechanism, however functional for virus replication in the host, limits the possibility to achieve high virus yields upon virus harvesting, both in the case of seed virus production and of vaccine manufacturing. Much like human immunodeficiency viruses (HIV) and modified vaccinia virus Ankara (MVA), RSV tends to remain associated to the cell membrane instead of being released into the supernatant following centrifugation[134,135]. For this reason, we tested several harvesting methods to establish which would grant the greatest virus release. When the supernatant was only pooled and centrifuged, we achieved the lowest virus release. On the other hand, when the supernatant was vortexed and sonicated prior to centrifugation, we could reach the greatest infectious virus titers. Sonication was the easiest procedure to carry out, but it was not selected as harvesting method because the combination of vortexing and sonication allowed greater cell

disruption – and supposedly greater virus release. Performing freeze-thawing cycles was the harshest method to retrieve RSV, and it was therefore not chosen as harvesting method to avoid loss of infectious material. Overall, breaking the cell membrane prior to virus harvesting allowed the greatest virus release according to our experiments. Parameters such as time, temperature, rpm and voltage most likely impact viral yields. According to literature, sonicating and freeze-thawing are the most common methods adopted to retrieve cell-associated virus upon harvesting[111,116,129,136–138].

It is known that naturally occurring RSV DIPs are able to stimulate the host innate immune response and hinder virus replication in some cases[69]. Because we needed to only assign the suppressing effect of the IAV DIPs DI244 and OP7 and not that of the DIPs present in the RSV seed, we produced a seed virus with the lowest content of natural DIPs that we could achieve. To do so, we carried out three passages at MOI 10^{-2}, which is considered the ideal low MOI for production of RSV with a low DVG content [116]. In a low MOI scenario, it is possible to produce a seed virus with a lower fraction of DIPs because less coinfections occur; therefore, DIPs cannot replicate and the STV can outcompete the DIPs. Performing infection at a lower MOI would result in low viral yields and virus degradation, as well as medium depletion, while high MOIs would result in accumulation of RSV DIPs. A stock virus of RSV A2 was used to perform the first infection, and harvested RSV material was always used to carry out the following infections. The seed virus production was a time consuming process, particularly because, before starting a new coinfection, it was necessary to determine the infectious virus titer of the previously produced viral material via $TCID_{50}$, which requires 7 days. Finally, we analyzed seed virus integrity via DIP RT-PCR. Gel electrophoresis was performed three times and, overall, the stock virus produced during the second low MOI passage was chosen as seed virus, as it presented the lowest content of DVGs (Figure 10). The FL band of each sample appeared smeared; this might be due to DNA overload on the gel, and diluting the DNA sample might resolve the issue. Alternatively, the protocol could be optimized by adjusting the concentration of reagents such as magnesium chloride in the master mix, or by using different primers for the RT reaction.

To summarize, we produced a seed virus at low MOI to obtain a stock virus with low content of RSV DIPs. To preserve virus viability, the virus was always handled on ice and kept at cold temperatures when possible, as well as being snap frozen to avoid crystal formation that could break virus particles and lower virus yields. Moreover, we determined that vortexing and sonicating the virus material prior to centrifugation allowed us to achieve the greatest virus release at the time of harvesting.

5.2 RSV infection dynamics

To investigate the propagation dynamics of RSV in A549 and Vero cells, we carried out a replication study at MOI 10^{-2}. As a result, we determined which time points yield the greatest RSV infectious virus titers for establishment of a coinfection assay.

The replication kinetics appeared to be faster in Vero cells. Our results are congruent with those observed by Straub *et al*: at 24 hpi, they recorded a titer of around 10^1 PFU/mL in A549 cells, and around 10^4 PFU/mL in Vero cells[139].
At 72 hpi, we detected infectious virus titers of $1.27*10^7$ $TCID_{50}$/mL in both cell lines, while at 96 hpi, titers of $7.11*10^6$ $TCID_{50}$/mL and of $2.25*10^7$ $TCID_{50}$ were obtained in A549 and Vero cells, respectively. While Tran *et al*., Straub *et al*. and Heumann *et al*. also reported considerably high titers at 72 and 96 hpi upon Vero cells infection, with values ranging from 10^6 to 10^7 PFU/mL, the same cannot be said for A549 cells[139–141]. In the IFN-competent cell line, the infectious virus titers reported in pre-existing literature were typically lower (10^4 PFU/mL)[139,142]. This difference is probably to be attributed to the different experimental setup of each study, as well as the different strains used – respectively, RSV D46/6120 and RSV A/Tracy(GA1). Each RSV strain is known to have their characteristic infection dynamics, and the quality and integrity of the seed virus can greatly affect the outcome of the experiment. For instance, a higher content of natural DIPs in the seed virus can result in lower infectious virus titers. The conditions upon such work is carried out can also have a significant impact. Each cell cultivation presents biological differences, and cell growth and confluency can have a major influence on virus production, as well

as the MOI chosen for infection, and the composition and handling of the medium selected for cell culture. Moreover, factors such as the coating of plastic disposables for cell attachment can also generate variation in virus spreading and therefore in detection of infectious virions.
In addition to this, our harvesting and freezing protocols for seed virus production likely contributed to optimize RSV virions release and maintenance upon freezing, whereas no particular methodology for harvest and virus conservation was reported in the above mentioned studies.

In conclusion, both A549 and Vero cells were susceptible to RSV. We showed that infectious RSV titers were considerably high both in A549 and Vero cells at 72 and 96 hpi. Because the titers were also comparable in between the two cell lines, we established that sampling for the interference assays will be carried out at these time points. Moreover, we stated that the number of infectious virions released into the extracellular fluid can variate greatly depending on the experimental setup.

5.3 Inhibitory effect of IAV DIPs in IFN competent cells

Based on the results of our dynamic study, we developed a coinfection assay to assess the inhibitory effect of IAV DIPs DI244 and OP7 against RSV replication *in vitro*. Since the antiviral effect of IAV DIPs is believed to be IFN-dependent, experiments have been carried out both in IFN-competent (A549 cells) and in IFN-deficient cells (Vero cells)[2,63,69–71].
A549 cells hold the ability to secrete IFNs type I, II and III and to elicit an immune response in the presence of an antigen[143]. A549 cells were a particularly prominent platform for this study, as RSV primarily infects epithelial cells of the respiratory tract.

In our study, active DI244 and active OP7 strongly inhibited RSV propagation in A549 cells. At 72 hpi, the infectious virus titer was reduced to $5.4*10^4$ $TCID_{50}$/mL with DI244, and an even further decrease was observed with OP7 ($7.07*10^3$ $TCID_{50}$/mL). Similar results were registered at 96 hpi. When cells were coinfected with inactivated DIPs, we also observed a 0.5 to 1 log reduction, and

OP7 in particular displayed a considerable residual inhibitory effect. Overall, OP7 displayed a stronger antiviral potential than DI244. This was also observed by Hein *et al*. in *in vivo* experiments[66,74]. IAV DIPs have been thoroughly tested for antiviral treatment of IAV, influenza B virus (IBV), SARS-CoV-2, pneumonia virus and YFV[66,71,74,77,118,144]. Hein *et al*. carried out *in vivo* coinfection studies in mice. When mice were infected with a dose of STV IAV of 1000 focus forming units (FFU) alone, all subjects lost body weight and died after a short period of time. However, mice that also received a dose of DI244 ($1.5*10^6$ PFU per mouse) or OP7 ($2.2*10^8$ Seg7 OP7 vRNA copies/mice) reported improved clinical scores, and they all survived the otherwise lethal infection as a result of the replication interference of IAV DIPs against IAV[66,74,126]. Moreover, IAV DIPs can inhibit virus propagation through interferon induction. Easton *et al*. reported that, when a single dose of DI244 was administered to mice who had been intranasally injected with 10 LD_{50} of pneumovirus, all animals survived[118]. Recently, the antiviral potential of DI244 and OP7 has been assessed *in vitro* against SARS-CoV-2 and YFV. Both studies reported an almost complete inhibition of the respective viruses upon coinfection with active IAV DIPs, and a residual inhibitory effect was observed when cells were coinfected with UV-inactivated DIPs[71,77]. Altogether, DI244 and OP7 substantially inhibited RSV replication; nonetheless, they presented a lower inhibitory effect against RSV compared to what Rand *et al*. observed in regard to SARS-CoV-2 and to what Marsall *et al*. reported for YFV[71,77]. One reason to this is that RSV displays a multitude of mechanisms that hinder the host's antiviral responses. For instance, NS1 and NS2 viral proteins can block the activation of IRFs, suppress RIG-I-mediated antiviral signaling and generally hinder IFN type I and type III-dependent signaling through the formation of a NS-degradasome. Furthermore, they can facilitate virus growth and suppress early apoptotic processes in infected cells[26,78,94,95].

In our experimental setup, we included cotreatment with IFN-β1a, IFN-λ1 or ribavirin as positive controls. In previous years, therapy with IFN has been proposed as a treatment for RSV infection: although Sung *et al*. reported promising results in infants, Higgins *et al*. did not register any beneficial effect

in the adult population[145,146]. Moreover, IFN therapy presents many side effects, and it is thus not commonly used as antiviral agent due to safety issues[147–149]. We reported a significant reduction ranging between 0.5 and 1.5 orders of magnitude in the infectious virus titer of A549 cells cotreated with 2000 U/mL of IFN-β1a or with 10 or 100 ng/mL of IFN-λ1, with the type I IFN displaying the greatest inhibitory effect. Zhang *et al*. cotreated Hep-2 cells with increasing concentrations of IFN-β at an MOI of 10^{-1} and observed a great reduction in the number of vRNA copies upon cotreatment with 2000 U/mL of IFN-β[112]. Furthermore, Okabayashi *et al*. reported significant reduction of infectious virus titer following cotreatment of telomerase reverse transcriptase-transfected human primary nasal epithelial cells (hTERT-NECs) with RSV and IFN-λ[113].
Ribavirin is the only licensed drug for the treatment of RSV infection. It has been reported to be particularly effective in inhibiting RSV propagation in numerous *in vitro* studies, as well as *in vivo* ones[36,150–154]. When we cotreated cells with 409 µM of ribavirin, we obtained an infectious virus titer of only 6 $TCID_{50}$/mL. Thus, ribavirin almost entirely inhibits virus replication. In line with our results, Dunn *et al*. report an almost complete inhibition of RSV following treatment with 100 µM of ribavirin[114].

We showed that the antiviral effect of IAV DIPs against RSV was IFN-dependent by cotreating cells with ruxolitinib, a JAK1/2 inhibitor. Rand *et al*. also included this condition in their experimental setup and showed that ruxolitinib administration to IFN-competent cells resulted in a complete inhibition of the antiviral effect of IAV DIPs[71]. In accordance with Rand *et al*., we also stated that there is no significant statistical difference between cotreatment of A549 cells with RSV, active IAV DIPs and ruxolitinib and RSV only infection. To further confirm our results, we also report that cotreatment of cells with ruxolitinib has been proposed as a method to maximize production of IFN-sensitive viruses[115]. Lastly, no cell or virus toxicity was detected via microscopy or $TCID_{50}$ assay upon cotreatment with EtOH, and this can thus be used to dissolve ruxolitinib.

In the future, it might be beneficial to investigate the antiviral effect of IAV DIPs in a high MOI coinfection scenario, as well as the pre-treatment of host cells

prior to infection. Easton *et al*. report that, when IAV DIPs are administered 48 hours following pneumovirus injection, mortality in mice was increased compared to when DI244 was administered at the time of infection[118]. This suggests that early administration of the antiviral drug is crucial for successful virus inhibition and positive clinical outcome. Pre-treatment has been reported to be beneficial in increasing the efficacy of protection against viruses and in reducing disease severity in mouse models[144].

Overall, our findings indicated that IAV DIPs could be an optimal antiviral for the treatment and prophylaxis of RSV, as well as heterologous IFN-sensitive viruses. Interestingly, OP7 reported the greatest antiviral potential. Moreover, treatment with ruxolitinib strongly suggested that the inhibitory effect of IAV DIPs is JAK/STAT-dependent.

5.4 Inhibitory effect of IAV DIPs in IFN deficient cells

In our coinfection assay, Vero cells were used as a negative control. While A549 cells can secrete IFNs, this cell line presents mutations – of which the most prominent is a 9 mega base pair (Mb) deletion on chromosome 9 – that affect the cells' ability to secrete class I and class III IFNs[122,124,155]. Because we believe the inhibitory effect of IAV DIPs to be IFN-dependent, we hypothesized that DI244 and OP7 should not interfere with RSV propagation in Vero cells.

In our study, we showed that IAV DIPs did not inhibit RSV propagation in Vero cells. These results are in line with what Marsall *et al*. reported in their study: upon coinfection with IAV DIPs, no interference against YFV replication was observed throughout the course of the experiment[77]. Moreover, to ensure that no IFN-dependent inhibition of IAV DIPs is observed in Vero cells, we also included a negative control in our experimental setup. Cells were cotreated with ruxolitinib and coinfected with active IAV DIPs, and they revealed infectious virus titers comparable to those of cells infected with RSV alone or coinfected with IAV DIPs. This evidence strongly suggested that a functioning IFN system is of crucial importance to elicit an antiviral response in the host when DI244 and OP7 are administered.

Vero cells present a large deletion on chromosome 12 that results in the cell line's inability to secrete type I IFNs. However, the cells still preserve type I IFN receptors, and are supposedly able to elicit an antiviral response upon administration of exogenous type I IFNs[124]. For instance, Hart *et al*. showed that IFN-β treatment can substantially inhibit Middle East respiratory syndrome coronavirus (MERS-CoV) replication in Vero cells[156]. In accordance with this, our results revealed that the infectious virus titers were significantly reduced following cotreatment of Vero cells with 2000 U/mL of IFN-β1a.

Ribavirin is a guanosine analog with broad spectrum antiviral activity. Upon uptake, ribavirin is metabolized via 5'-phosphorylation by cellular kinases into ribavirin mono-, di- or triphosphate[157,158]. In our study, we observed a limited inhibitory effect of ribavirin against RSV propagation. Following cotreatment, the infectious virus titer was $2.58*10^5$ $TCID_{50}$/mL, extremely close to that of cells infected with RSV only. Previous research highlighted that some lineages of Vero cells can present differences in metabolizing ribavirin, which ultimately result in limited ribavirin cell uptake and limited antiviral activity. Shah *et al*. reported this issue upon ribavirin treatment of Vero cells following vesicular stomatitis virus and sendai virus infection[158]. Moreover, Morgenstern *et al*. and Falzanaro *et al*. reported the same observation following treatment of Vero cells infected with SARS-CoV and human betacoronavirus, respectively[159,160]. The mechanism underlying this phenomenon is not yet clear; however, cotreatment of cells with both ribavirin and class I IFNs has been proposed as a possible treatment for ribavirin-resistant cells[160].

To summarize, IAV DIPs were unable to inhibit RSV replication in IFN-deficient Vero cells. However, when cells were treated with recombinant exogenous IFN-β1a, a reduction in the infectious virus titer could be observed. These results strongly implied that DI244 and OP7 can elicit an antiviral response by stimulating an innate immune response in the host. Moreover, we confirmed that a functioning host's IFN-system is crucial in successfully inhibiting RSV replication.

5.5 Innate immune response stimulation by IAV DIPs

Defective interfering particles are known to elicit an innate immune response in the host, and they have been proposed as a heterologous treatment for IFN-sensitive viruses[70,71,118]. Although the exact mechanism has not yet been elucidated, it is believed that the truncated vRNAs of IAV DIPs can be recognized by PRRs such as RIG-I receptors. This elicits increased production of type I and type III IFNs, which ultimately triggers the expression of hundreds of ISGs via JAK/STAT signaling[56,61,69,70,144]. In this study, we assessed the gene expression levels of RIG-I, IFN-β1, IFN-λ1, Mx1 and IFITM1 induced by IAV DIPs and RSV via RT-qPCR.

RIG-I, a cytosolic PRR, recognizes short dsRNAs linked to specific secondary structures[78,83]. Coinfection of A549 cells with IAV DIPs resulted in strong upregulation of RIG-I at early time points of infection – specifically, at 6 and 24 hpi – compared to RSV infection alone, which did not significantly induce RIG-I expression. These findings were consistent with those of Marsall *et al*. in regard to inhibition of YFV propagation[77]. From 48 hpi, gene expression levels were the same for both IAV DIPs coinfection and RSV only infection. At 2 dpi, RSV reached high viral loads, and therefore all genes linked to the innate immune response were highly upregulated due to abundant presence of viral progeny. When cells were infected with active IAV DIPs alone, we observed constant upregulation of RIG-I for the whole course of the experiment. However, no significant upregulation was detected when the infection was carried out with inactivated DI244 and OP7. Easton *et al*. also reported that UV inactivation damages the vRNA of DI244, ultimately leading to complete loss of antiviral activity[118].
It is very likely that early overexpression of RIG-I triggered by IAV DIPs leads to an antiviral response, thus implying that RIG-I is a key component for RSV abrogation. While we can hypothesize that DI244 is successfully recognized by RIG-I due to its large deletion on Seg1 of the vRNA, the same cannot be reported for OP7[2]. In fact, OP7 does not present a truncated genome, but rather 37 point mutations that do not affect the length of the vRNA segment[3]. The mechanism by which OP7 is recognized by RIG-I remains elusive but, due to the high

incorporation of Seg 7-OP7 by the superpromoter, it is possible that overexpressed short segments are recognized by RIG-I, hence eliciting the upregulation of this PRR[3,161]. In this regard, it would be interesting to investigate gene expression levels of other PRRs such as MDA5, to examine a possible correlation between their gene upregulation and the antiviral activity of IAV DIPs.
Overall, we reported that RSV does not trigger high RIG-I expression levels, whereas active IAV DIPs hold the ability to strongly upregulate the PRR's gene, leading to the stimulation of the innate immune response.

Following RIG-I activation, type I and type III antiviral IFNs are secreted. IFNs act on host cells both in an autocrine and a paracrine way, leading to the activation of the innate immune response[88,90,125,162]. We reported significant upregulation of IFN-β1 and IFN-λ1 upon active IAV DIPs coinfection. When cells were infected with DIPs alone, active DI244 and OP7 triggered high gene expression levels over the whole course of the experiment, whereas no significant upregulation was observed upon inactive IAV DIPs infection. In this study, it was not possible to determine ΔΔCt values for IFN-λ1 because the gene expression levels of IFN-λ1 in the mock controls were below the limit of detection. This this reason, Ct values were alternatively plotted and analyzed.
Even though type I IFNs are believed to be the main host factor contributing to virus abrogation, the importance of type III IFNs in the inhibitory process has been highlighted, particularly in the case of RSV infection. Type III IFNs have been reported to limit RSV replication, as well as reduce RSV-related symptoms[69,78,113].
Our findings were in line with what Rand *et al*. and Marsall *et al*. reported in their studies on SARS-CoV-2 and YFV[71,77]: significant uptake by host cells of active DI244 and OP7 resulted in concomitant upregulation of type I and type III IFNs at early time points of infection, thus motivating the inhibitory potential of active IAV DIPs.

Finally, we measured gene expression levels of ISGs[84,98,163]. Specifically, we investigated Mx1, which serves as an inflammasome sensor in epithelial airway

cells, and plays a critical role in inhibiting viral replication and transcription[104,106,107]. Moreover, we assessed gene expression levels of IFITM1, which interferes with virus-endosome fusion at the cell entry[100,102]. Both genes were found to be extremely upregulated at 6 and 24 hpi following coinfection with active IAV DIPs, and particularly with OP7. Infection with RSV alone did not result in overexpression of either Mx1 or IFITM1, suggesting that RSV did not elicit a strong innate immune response until 48 hpi, when high presence of progeny virions resulted in general upregulation of antiviral genes. Upon infection with IAV DIPs alone, we reported a strong gene upregulation elicited by active DI244 and OP7, which confirmed our coinfection findings. Moreover, infection with inactivated DIPs did not trigger significant gene overexpression. Our results were in compliance with those of Kupke *et al*., who also reported significant Mx1 upregulation in MDCK cells following OP7 coinfection[3]. Moreover, Hein *et al*. also stated that IAV DIPs present a strong inhibitory effect on IAV propagation in *in vivo* experiments, and that Mx1 is crucial for mice survival and IAV DIPs effectiveness[66,74]. Furthermore, Wang *et al*. reported that upregulation of IFITM proteins results in inhibition of IAV in A549 cells[164].

In future studies, it would be interesting to assess gene expression levels of other genes linked to the innate immune response, such as other PRRs and ISGs, to gain a better understanding of the immune processes underlying RSV inhibition by IAV DIPs. It would also be beneficial to get an insight of gene expression levels in Vero cells, particularly to elucidate defects in type I and type III IFNs. As OP7 stimulated greater gene expression levels than DI244 at 6 hpi, it would be beneficial to further investigate if such difference at very early time points motivates the strongest inhibitory effect of OP7 compared to DI244.

In conclusion, we state that RIG-I, type I and type III IFNs, Mx1 and IFITM1 were all strongly upregulated from early time points upon coinfection with active IAV DIPs. This confirms that the antiviral effect of IAV DIPs in JAK/STAT-dependent. Although further research must be carried out, specifically in animal models, IAV DIPs could represent a cost-effective antiviral for the treatment and prophylaxis of RSV infection. Due to the promising data on IAV DIPs inhibitory

potential against IFN-sensitive viruses, it would be beneficial to also investigate their antiviral potential against replication of viruses such as herpes simplex virus and hepatitis C virus.

6. Conclusion and Outlook

In this study, we produced a seed virus of RSV with a low content of RSV DIPs. The replication dynamics of RSV were assessed in A549 and Vero cells. *In vitro* coinfection studies were carried out to determine the antiviral potential of DI244 and OP7 against RSV propagation. In addition, we performed host cell gene expression analysis to confirm that the inhibitory effect of IAV DIPs is JAK/STAT-dependent.

We report that harvesting the virus by vortexing and sonicating the cell pellet prior to centrifugation enabled the highest virus release. To preserve virus viability, the virus material was additioned with sucrose and snap frozen. Virus integrity was investigated via RT-PCR and gel electrophoresis to select a seed virus with a low content of RSV DIPs, to evaluate the suppressive effect of IAV DIPs alone. Next, we established an *in vitro* interference assay at MOI 10^{-2}. Coinfection experiments were carried out in IFN-competent and IFN-deficient cells. IAV DIPs could substantially inhibit RSV propagation in A549 cells, whereas no antiviral effect was observed upon coinfection of Vero cells. In particular, OP7 achieved greater infectious virus titer reductions than DI244, demonstrating remarkable antiviral potential. Finally, we confirmed that the inhibitory effect of IAV DIPs is likely dependent on JAK/STAT signaling. By RT-qPCR, we measured the gene expression levels of antiviral genes RIG-I, IFN-β1, IFN-λ1, Mx1 and IFITM1. IAV DIPs could elicit early upregulation of all our designated targets, hence demonstrating that they can stimulate the host's innate immune response.

Further *in vitro* and *in vivo* studies must be carried out to confirm whether DI244 and OP7 could become a suitable antiviral for treatment and prophylaxis of RSV infection. For instance, coinfection experiments at high MOI should be carried out, as well as pre- and post-treatment assays. Moreover, it would be beneficial to assess gene expression levels of additional innate immune response-related targets. If future research will display positive outcomes, IAV DIPs could constitute a cost efficient treatment that could save thousands of lives each year, especially in low income countries.

7. References

1 Domachowske JB, Anderson EJ, Goldstein M. The Future of Respiratory Syncytial Virus Disease Prevention and Treatment. *Infectious Diseases and Therapy* 2021; **10**: 47–60.

2 Dimmock NJ, Easton AJ. Defective Interfering Influenza Virus RNAs: Time To Reevaluate Their Clinical Potential as Broad-Spectrum Antivirals? *Journal of Virology* 2014; **88**: 5217–5227.

3 Kupke SY, Riedel D, Frensing T, Zmora P, Reichl U. A Novel Type of Influenza A Virus-Derived Defective Interfering Particle with Nucleotide Substitutions in Its Genome. *Journal of Virology* 2019; **93**. doi:10.1128/jvi.01786-18.

4 Morris JA, Blount RE, Savage RE. Recovery of Cytopathogenic Agent from Chimpanzees with Goryza. *Proceedings of the Society for Experimental Biology and Medicine* 1956; **92**: 544–549.

5 Chanock R, Roizman B, Myers R. Recovery from infants with respiratory illness of a virus related to chimpanzee coryza agent (CCA): Isolation, properties and characterization. *American Journal of Epidemiology* 1957; **66**: 281–290.

6 Mufson MA, Orvell C, Rafnar B, Norrby E. Two distinct subtypes of human respiratory syncytial virus. *Journal of General Virology* 1985; **66**: 2111–2124.

7 Johnson PR, Spriggs MK, Olmsted RA, Collins PL. The G glycoprotein of human respiratory syncytial viruses of subgroups A and B: extensive sequence divergence between antigenically related proteins. *Proc Natl Acad Sci U S A* 1987; **84**: 5625–5629.

8 Gilca R, de Serres G, Tremblay M, Vachon ML, Leblanc E, Bergeron MG *et al.* Distribution and clinical impact of human respiratory syncytial virus genotypes in hospitalized children over 2 winter seasons. *Journal of Infectious Diseases* 2006; **193**: 54–58.

9 Pandaya MC, Callahan SM, Savchenko KG, Stobart CC. A Contemporary View of Respiratory Syncytial Virus. *Pathogens* 2019; **8**: 1–15.

10 Battles MB, McLellan JS. Respiratory syncytial virus entry and how to block it. Nature Reviews Microbiology. 2019; **17**: 233–245.

11 Borchers AT, Chang C, Gershwin ME, Gershwin LJ. Respiratory syncytial virus - A comprehensive review. *Clinical Reviews in Allergy and Immunology* 2013; **45**: 331–379.

12 Rima B, Collins P, Easton A, Fouchier R, Kurath G, Lamb RA *et al.* ICTV virus taxonomy profile: Pneumoviridae. *Journal of General Virology* 2017; **98**: 2912–2913.

13 van den Hoogen BG, de Jong JC, Groen J, Kuiken T, de Groot R, Fouchier RAM *et al.* A newly discovered human pneumovirus isolated from young children with respiratory tract disease. *Nature Medicine* 2001; **7**: 719–724.

14 Collins PL, Melero JA. Progress in understanding and controlling respiratory syncytial virus: Still crazy after all these years. *Virus Research* 2011; **162**: 80–99.

15 Jha A, Jarvis H, Fraser C, Openshaw PJM. 5. Respiratory Syncytial Virus. 2016; : 1–38.

16 Utley TJ, Ducharme NA, Varthakavi V, Shepherd BE, Santangelo PJ, Lindquist ME *et al.* Respiratory syncytial virus uses a Vps4-independent budding mechanism controlled by Rab11-FIP2. *Proc Natl Acad Sci U S A* 2008; **105**: 10209–10214.

17 Paluck A, Osan J, Hollingsworth L, At. E. Role of ARP2/3 Complex-Driven Actin Polymerization in RSV Infection. *Pathogens* 2022; : 1–12.

18 Gan SW, Tan E, Lin X, Yu D, Wang J, Tan GMY *et al.* The small hydrophobic protein of the human respiratory syncytial virus forms pentameric ion channels. *Journal of Biological Chemistry* 2012; **287**: 24671–24689.

19 Kiss G, Holl JM, Williams GM, Alonas E, Vanover D, Lifland AW *et al.* Structural Analysis of Respiratory Syncytial Virus Reveals the Position of M2-1 between the Matrix Protein and the Ribonucleoprotein Complex. *Journal of Virology* 2014; **88**: 7602–7617.

20 Sedeyn K, Schepens B, Saelens X. Respiratory syncytial virus nonstructural proteins 1 and 2: Exceptional disrupters of innate immune responses. *PLoS Pathogens* 2019; **15**: 1–18.

21 Swedan S, Musiyenko A, Barik S. Respiratory Syncytial Virus Nonstructural Proteins Decrease Levels of Multiple Members of the Cellular Interferon Pathways. *Journal of Virology* 2009; **83**: 9682–9693.

22 Krzyzaniak MA, Zumstein MT, Gerez JA, Picotti P, Helenius A. Host Cell Entry of Respiratory Syncytial Virus Involves Macropinocytosis Followed by Proteolytic Activation of the F Protein. 2013 doi:10.1371/journal.ppat.1003309.

23 Luisoni S, Greber UF. Biology of Adenovirus Cell Entry: Receptors, Pathways, Mechanisms. In: *Adenoviral Vectors for Gene Therapy: Second Edition*. Academic Press, 2016, pp 27–58.

24 Shahriari S, Gordon J, Ghildyal R. Host cytoskeleton in respiratory syncytial virus assembly and budding. *Virology Journal* 2016; **13**: 1–11.

25 Fuentes S, Tran KC, Luthra P, Teng MN, He B. Function of the Respiratory Syncytial Virus Small Hydrophobic Protein. *Journal of Virology* 2007; **81**: 8361–8366.

26 Bitko V, Shulyayeva O, Mazumder B, Musiyenko A, Ramaswamy M, Look DC *et al.* Nonstructural Proteins of Respiratory Syncytial Virus Suppress Premature Apoptosis by an NF-κB-Dependent, Interferon-Independent Mechanism and Facilitate Virus Growth. *Journal of Virology* 2007; **81**: 1786–1795.

27 Mehedi M, McCarty T, Martin SE, le Nouën C, Buehler E, Chen YC *et al.* Actin-Related Protein 2 (ARP2) and Virus-Induced Filopodia Facilitate Human Respiratory Syncytial Virus Spread. *PLoS Pathogens* 2016; **12**: 1–35.

28 Hall CB, Weinberg GA, Iwane MK, Blumkin AK, Edwards KM, Staat MA *et al.* The Burden of Respiratory Syncytial Virus Infection in Young Children. *New England Journal of Medicine* 2009; **360**: 588–598.

29 Obando-Pacheco P, Justicia-Grande AJ, Rivero-Calle I, Rodríguez-Tenreiro C, Sly P, Ramilo O *et al.* Respiratory syncytial virus seasonality: A global overview. *Journal of Infectious Diseases* 2018; **217**: 1356–1364.

30 Leung NHL. Transmissibility and transmission of respiratory viruses. *Nature Reviews Microbiology* 2021; **19**: 528–545.

31 Persson BD, Jaffe AB, Fearns R, Danahay H. Respiratory syncytial virus can infect basal cells and alter human airway epithelial differentiation. *PLoS ONE* 2014; **9**: 1–15.

32 Coultas JA, Smyth R, Openshaw PJ. Respiratory syncytial virus (RSV): A scourge from infancy to old age. *Thorax* 2019; : 986–993.

33 Wei L, Chan KH, Ip DKM, Fang VJ, Fung ROP, Leung GM *et al.* Burden, seasonal pattern and symptomatology of acute respiratory illnesses with different viral aetiologies in children presenting at outpatient clinics in Hong Kong. *Clinical Microbiology and Infection* 2015; **21**: 861–866.

34 Tregoning JS, Schwarze J. Respiratory viral infections in infants: Causes, clinical symptoms, virology, and immunology. *Clinical Microbiology Reviews* 2010; **23**: 74–98.

35 Lieberthal AS, Bauchner H, Hall CB, Johnson DW, Kotagal U, Light MJ *et al.* Diagnosis and management of bronchiolitis. Pediatrics. 2006; **118**: 1774–1793.

36 Walsh BK, Liu Y. Effect of Vibrating Mesh Nebulizer Aerosol Technology on the In Vitro Activity of Ribavirin Against Respiratory Syncytial Virus. *Respiratory Care* 2022; **67**: 421–427.

37 Behzadi MA, Leyva-Grado VH. Overview of current therapeutics and novel candidates against influenza, respiratory syncytial virus, and Middle East respiratory syndrome coronavirus infections. *Frontiers in Microbiology* 2019; **10**. doi:10.3389/fmicb.2019.01327.

38 Beaucourt S, Vignuzzi M. Ribavirin: A drug active against many viruses with multiple effects on virus replication and propagation. Molecular basis of ribavirin resistance. Current Opinion in Virology. 2014; **8**: 10–15.

39 Griffiths C, Drews SJ, Marchant DJ. Respiratory syncytial virus: Infection, detection, and new options for prevention and treatment. *Clinical Microbiology Reviews* 2017; **30**: 277–319.

40 Zhang Y, Jamaluddin M, Wang S, Tian B, Garofalo RP, Casola A *et al.* Ribavirin Treatment Up-Regulates Antiviral Gene Expression via the Interferon-Stimulated Response Element in Respiratory Syncytial Virus-Infected Epithelial Cells. *Journal of Virology* 2003; **77**: 5933–5947.

41 Mammas IN, Drysdale SB, Rath B, Theodoridou M, Papaioannou G, Papatheodoropoulou A *et al.* Update on current views and advances on RSV infection (Review). *International Journal of Molecular Medicine* 2020; **46**: 509–520.

42 Hu MJ, Bogoyevitch MA, Jans DA. Impact of respiratory syncytial virus infection on host functions: Implications for antiviral strategies. *Physiological Reviews* 2020; **100**: 1527–1594.

43 Varga SM, Wang X, Welsh RM, Braciale TJ. Immunopathology in RSV infection is mediated by a discrete oligoclonal subset of antigen-specific CD4+ T cells. *Immunity* 2001; **15**: 637–646.

44 Shan J, Britton PN, King CL, Booy R. The immunogenicity and safety of respiratory syncytial virus vaccines in development: A systematic review. *Influenza and other Respiratory Viruses* 2021; **15**: 539–551.

45 Mazur NI, Higgins D, Nunes MC, Melero JA, Langedijk AC, Horsley N *et al.* The respiratory syncytial virus vaccine landscape: lessons from the graveyard and promising candidates. *The Lancet Infectious Diseases* 2018; **18**: e295–e311.

46 Saso A, Kampmann B. Vaccination against respiratory syncytial virus in pregnancy: a suitable tool to combat global infant morbidity and mortality? *The Lancet Infectious Diseases* 2016; **16**: e153–e163.

47 Munoz FM, Piedra PA, Glezen WP. Safety and immunogenicity of respiratory syncytial virus purified fusion protein-2 vaccine in pregnant women. *Vaccine* 2003; **21**: 3465–3467.

48 McFarland EJ, Karron RA, Muresan P, Cunningham CK, Valentine ME, Perlowski C *et al.* Live-attenuated respiratory syncytial virus vaccine candidate with deletion of RNA synthesis regulatory protein M2-2 is highly immunogenic in children. *Journal of Infectious Diseases* 2018; **217**: 1347–1355.

49 Smith G, Raghunandan R, Wu Y, Liu Y, Massare M, Nathan M *et al.* Respiratory Syncytial Virus Fusion Glycoprotein Expressed in Insect Cells Form Protein Nanoparticles That Induce Protective Immunity in Cotton Rats. *PLoS ONE* 2012; **7**: e50852.

50 Fries L, Shinde V, Stoddard JJ, Thomas DN, Kpamegan E, Lu H *et al.* Immunogenicity and safety of a respiratory syncytial virus fusion protein (RSV F) nanoparticle vaccine in older adults. *Immunity and Ageing* 2017; **14**: 1–14.

51 GSK. GSK announces positive pivotal phase III data for its respiratory syncytial virus (RSV) vaccine candidate for older adults. 2022.https://www.gsk.com/en-gb/media/press-releases/gsk-announces-positive-pivotal-phase-iii-data-for-its-respiratory-syncytial-virus-rsv-vaccine-candidate-for-older-adults/ (accessed 20 Jun2022).

52 Henle W, Henle G. Interference of inactive virus with the propagation of virus of influenza. *Science (1979)* 1943; **98**: 87–89.

53 von Magnus P. Incomplete forms of influenza virus. *Zeitschrift fur Naturforschung - Section B Journal of Chemical Sciences* 1954; **17**: 749–750b.

54 Nayak DP, Chambers TM, Akkina RK. Structure of Defective-Interfering RNAs of Influenza Viruses and Their Role in Interference. *The Influenza Viruses* 1989; : 269–317.

55 Huang AS, Baltimore D. Defective Viral Particles and Viral Disease Processes. *Nature* 1970; **226**: 325–327.

56 Ziegler CM, Botten JW. Defective Interfering Particles of Negative-Strand RNA Viruses. *Trends in Microbiology* 2020; **28**: 554–565.

57 de Oliveira Resende R, de Haan P, van de Vossen E, de Avila AC, Goldbach R, Peters D. Defective interfering L RNA segments of tomato spotted wilt virus retain both virus genome termini and have extensive internal deletions. *Journal of General Virology* 1992; **73**: 2509–2516.

58 Mura M, Combredet C, Najburg V, Sanchez David RY, Tangy F, Komarova V. Nonencapsidated 5′ Copy-Back Defective Interfering Genomes Produced by Recombinant Measles Viruses Are Recognized by RIG-I and LGP2 but Not MDA5. *Journal of Virology* 2017; **91**: 1–22.

59 Marriott AC, Dimmock NJ. Defective interfering viruses and their potential as antiviral agents. *Reviews in Medical Virology* 2010; **20**: 51–62.

60 Dimmock NJ, Rainsford EW, Scott PD, Marriott AC. Influenza Virus Protecting RNA: an Effective Prophylactic and Therapeutic Antiviral. *Journal of Virology* 2008; **82**: 8570–8578.

61 Chaturvedi S, Vasen G, Pablo M, Chen X, Beutler N, Kumar A *et al.* Identification of a Therapeutic Interfering Particle — a single-administration SARS-CoV-2 antiviral intervention with a high barrier to resistance. *Cell* 2021; : 1–15.

62 Pfaller CK, Mastorakos GM, Matchett WE, Ma X, Samuel CE, Cattaneo R. Measles Virus Defective Interfering RNAs Are Generated Frequently and Early in the Absence of C Protein and Can Be Destabilized by Adenosine Deaminase Acting on RNA-1-Like Hypermutations. *Journal of Virology* 2015; **89**: 7735–7747.

63 Felt SA, Sun Y, Jozwik A, Paras A, Habibi MS, Nickle D *et al.* Detection of respiratory syncytial virus defective genomes in nasal secretions is associated with distinct clinical outcomes. *Nature Microbiology* 2021; **6**: 672–681.

64 Perrault J. Origin and replication of defective interfering particles. *Curr Top Microbiol Immunol* 1981; **93**: 151–207.

65 Lazzarini RA, Keene JD, Schubert M. The origins of defective interfering particles of the negative-strand RNA viruses. *Cell* 1981; **26**: 145–154.

66 Hein MD, Kollmus H, Marichal-Gallardo P, Püttker S, Benndorf D, Genzel Y *et al.* OP7, a novel influenza A virus defective interfering particle: production, purification, and animal experiments demonstrating antiviral potential. *Applied Microbiology and Biotechnology* 2021; **105**: 129–146.

67 Alnaji FG, Reiser WK, Rivera-Cardona J, te Velthuis AJW, Brooke CB. Influenza A Virus Defective Viral Genomes Are Inefficiently Packaged into Virions Relative to Wild-Type Genomic RNAs. *mBio* 2021; **12**. doi:10.1128/mBio.02959-21.

68 Laske T, Heldt FS, Hoffmann H, Frensing T, Reichl U. Modeling the intracellular replication of influenza A virus in the presence of defective interfering RNAs. *Virus Research* 2016; **213**: 90–99.

69 Sun Y, Jain D, Koziol-White CJ, Genoyer E, Gilbert M, Tapia K *et al.* Immunostimulatory Defective Viral Genomes from Respiratory Syncytial Virus Promote a Strong Innate Antiviral Response during Infection in Mice and Humans. *PLoS Pathogens* 2015; **11**: 1–21.

70 Dimmock NJ, Easton AJ. Cloned defective interfering influenza RNA and a possible pan-specific treatment of respiratory virus diseases. *Viruses* 2015; **7**: 3768–3788.

71 Rand U, Kupke SY, Shkarlet H, Hein MD, Hirsch T, Marichal-Gallardo P *et al.* Antiviral activity of influenza a virus defective interfering particles against sars-cov-2 replication in vitro through stimulation of innate immunity. *Cells* 2021; **10**. doi:10.3390/cells10071756.

72 Noble S, Dimmock NJ. Characterization of putative defective interfering (DI) A/WSN RNAs isolated from the lungs of mice protected from an otherwise lethal respiratory infection with influenza virus A/WSN (H1N1): A subset of the inoculum DI RNAs. *Virology* 1995; **210**: 9–19.

73 Wasik MA, Eichwald L, Genzel Y, Reichl U. Cell culture-based production of defective interfering particles for influenza antiviral therapy. *Applied Microbiology and Biotechnology* 2018; **102**: 1167–1177.

74 Hein MD, Arora P, Marichal-Gallardo P, Winkler M, Genzel Y, Pöhlmann S *et al.* Cell culture-based production and in vivo characterization of purely clonal defective interfering influenza virus particles. *BMC Biology* 2021; **19**: 1–18.

75 Dimmock NJ, Dove BK, Scott PD, Meng B, Taylor I, Cheung L *et al.* Cloned Defective Interfering Influenza Virus Protects Ferrets from Pandemic 2009 Influenza A Virus and Allows Protective Immunity to Be Established. *PLoS ONE* 2012; **7**. doi:10.1371/journal.pone.0049394.

76 Novel OP7 virus as an antiviral agent | Max Planck Institute for Dynamics of Complex Technical Systems. https://www.mpi-magdeburg.mpg.de/3939891/novel-op7-virus-as-an-antiviral-agent (accessed 24 May2022).

77 Thesis M. Yellow fever virus replication : Inhibition by Influenza A virus defective interfering particles. *Master's Thesis* 2021; : 1–112.

78 Sun Y, Lopez CB. Innate Immune Response to RSV: Understanding of Critical Viral and Host Factors. *Vaccine* 2018; **35**: 481–488.

79 Liu Y, Olagnier D, Lin R. Host and viral modulation of RIG-I-mediated antiviral immunity. Frontiers in Immunology. 2017; **7**: 1–12.

80 Essaidi-Laziosi M, Geiser J, Huang S, Constant S, Kaiser L, Tapparel C. Interferon-Dependent and Respiratory Virus-Specific Interference in Dual Infections of Airway Epithelia. *Scientific Reports* 2020; **10**: 1–9.

81 Onomoto K, Onoguchi K, Yoneyama M. Regulation of RIG-I-like receptor-mediated signaling: interaction between host and viral factors. *Cellular and Molecular Immunology* 2021; **18**: 539–555.

82 Johansson C. Respiratory syncytial virus infection: An innate perspective. F1000Res. 2016; **5**: 1–10.

83 Wu W, Zhang W, Duggan ES, Booth JL, Zou MH, Metcalf JP. RIG-I and TLR3 are both required for maximum interferon induction by influenza virus in human lung alveolar epithelial cells. *Virology* 2015; **482**: 181–188.

84 Carty M, Guy C, Bowie AG. Detection of Viral Infections by Innate Immunity. *Biochemical Pharmacology* 2021; **183**: 114316.

85 Goubau D, Deddouche S, Reis e Sousa C. Cytosolic Sensing of Viruses. *Immunity* 2013; **38**: 855–869.

86 Crosse KM, Monson EA, Beard MR, Helbig KJ. Interferon-Stimulated Genes as Enhancers of Antiviral Innate Immune Signaling. *Journal of Innate Immunity* 2018; **10**: 85–93.

87 Chan YK, Gack MU. Viral evasion of intracellular DNA and RNA sensing. Nature Reviews Microbiology. 2016; **14**: 360–373.

88 McNab F, Mayer-Barber K, Sher A, Wack A, O'Garra A. Type I interferons in infectious disease. *Nature Reviews Immunology* 2015; **15**: 87–103.

89 Lazear HM, Nice TJ, Diamond MS. Interferon-λ: Immune Functions at Barrier Surfaces and Beyond. *Immunity* 2015; **43**: 15–28.

90 Goritzka M, Makris S, Kausar F, Durant LR, Pereira C, Kumagai Y *et al.* Alveolar macrophage-derived type I interferons orchestrate innate immunity to RSV through recruitment of antiviral monocytes. *Journal of Experimental Medicine* 2015; **212**: 699–714.

91 Cormier SA, Shrestha B, Saravia J, Lee GI, Shen L, DeVincenzo JP *et al.* Limited Type I Interferons and Plasmacytoid Dendritic Cells during Neonatal Respiratory Syncytial Virus Infection Permit Immunopathogenesis upon Reinfection. *Journal of Virology* 2014; **88**: 9350–9360.

92 Liveenave R, Broadbent L, Douglas I, Lyons JD, Al. E. Induction and Antagonism of Antiviral Responses in Respiratory Syncytial Virus-Infected Pediatric Airway Epithelium. *Journal of Virology* 2015; **89**: 12309–12318.

93 Ioannidis I, Ye F, McNally B, Willette M, Flaño E. Toll-Like Receptor Expression and Induction of Type I and Type III Interferons in Primary Airway Epithelial Cells. *Journal of Virology* 2013; **87**: 3261–3270.

94 Bossert B, Marozin S, Conzelmann K-K. Nonstructural Proteins NS1 and NS2 of Bovine Respiratory Syncytial Virus Block Activation of Interferon Regulatory Factor 3. *Journal of Virology* 2003; **77**: 8661–8668.

95 Ban J, Lee NR, Lee NJ, Lee JK, Quan FS, Inn KS. Human respiratory syncytial virus NS 1 targets TRIM25 to suppress RIG-I ubiquitination and subsequent RIG-I-mediated antiviral signaling. *Viruses* 2018; **10**. doi:10.3390/v10120716.

96 Xu X, Zheng J, Zheng K, Hou Y, Zhao F, Zhao D. Respiratory syncytial virus NS1 protein degrades STAT2 by inducing SOCS1 expression. *Intervirology* 2014; **57**: 65–73.

97 Barik S. Respiratory syncytial virus mechanisms to interfere with type 1 interferons. *Current Topics in Microbiology and Immunology* 2013; **372**: 173–191.

98 Schoggins JW. Interferon-Stimulated Genes: What Do They All Do? *Annual Review of Virology* 2019; **6**: 567–584.

99 Au-Yeung N, Horvath CM. Transcriptional and chromatin regulation in interferon and innate antiviral gene expression. *Cytokine and Growth Factor Reviews* 2018; **44**: 11–17.

100 Smith SE, Busse DC, Binter S, Weston S, Soria CD, Laksono BM *et al.* Interferon-Induced Transmembrane Protein 1 Restricts Replication of Viruses That Enter Cells via the Plasma Membrane. *Journal of Virology* 2019; **93**: e02003-18.

101 Liang R, Li X, Zhu X. Deciphering the Roles of IFITM1 in Tumors. *Molecular Diagnosis and Therapy* 2020; **24**: 433–441.

102 Sun F, Xia Z, Han Y, Gao M, Wang L, Wu Y *et al.* Topology, antiviral functional residues and mechanism of IFITM1. *Viruses* 2020; **12**. doi:10.3390/v12030295.

103 Zhao Y, Pang D, Wang T, Yang X, Wu R, Ren L *et al.* Human MxA protein inhibits the replication of classical swine fever virus. *Virus Research* 2011; **156**: 151–155.

104 Lee SJ, Ishitsuka A, Noguchi M, Hirohama M, Fujiyasu Y, Petric PP *et al.* Influenza restriction factor MxA functions as inflammasome sensor in the respiratory epithelium. *Science Immunology* 2019; **4**: 1–12.

105 Haller O, Gao S, von der Malsburg A, Daumke O, Kochs G. Dynamin-like MxA GTPase: Structural insights into oligomerization and implications for antiviral activity. *Journal of Biological Chemistry* 2010; **285**: 28419–28424.

106 Haller O, Kochs G. Human MxA protein: An interferon-induced dynamin-like GTPase with broad antiviral activity. *Journal of Interferon and Cytokine Research* 2011; **31**: 79–87.

107 Daumke O, Gao S, von der Malsburg A, Haller O, Kochs G. Structure of the MxA stalk elucidates the assembly of ring-like units of an antiviral module. *Small GTPases* 2010; **1**: 62–64.

108 Cell Lines - IDT Biologika. https://idt-biologika.com/development-services/cell-lines/ (accessed 16 Jun2022).

109 Kim HW, Arrobio JO, Brandt CD, Wright P, Hodes D, Chanock RM *et al.* Safety and antigenicity of temperature sensitive (TS) mutant respiratory syncytial virus (RSV) in infants and children. *Pediatrics* 1973; **52**: 56–63.

110 Gerretsen HE, Sande CJ. Development of respiratory syncytial virus (RSV) vaccines for infants. *Journal of Infection* 2017; **74**: S143–S146.

111 Wright PF, Woodend WG, Chanock RM. Temperature-sensitive mutants of respiratory syncytial virus: In-vivo studies in hamsters. *Journal of Infectious Diseases* 1970; **122**: 501–512.

112 Zhang W, Zhang L, Zan Y, Du N, Yang Y, Tien P. Human respiratory syncytial virus infection is inhibited by IFN-induced transmembrane proteins. *Journal of General Virology* 2015; **96**: 170–182.

113 Okabayashi T, Kojima T, Masaki T, Yokota S ichi, Imaizumi T, Tsutsumi H *et al.* Type-III interferon, not type-I, is the predominant interferon induced by respiratory viruses in nasal epithelial cells. *Virus Research* 2011; **160**: 360–366.

114 Dunn MCC, Knight DA, Waldman WJ. Inhibition of respiratory syncytial virus in vitro and in vivo by the immunosuppressive agent leflunomide. *Antiviral Therapy* 2011; **16**: 309–317.

115 Stewart CE, Rall RE, Adamson CS. Inhibitors of the interferon response enhance virus replication in vitro. *PLoS ONE* 2014; **9**: 3–10.

116 Sun Y, Lopez CB. Preparation of Respiratory Syncytial Virus with High or Low Content of Defective Viral Particles and Their Purification from Viral Stocks. *Bio Protoc* 2016; **176**: 100–106.

117 Vanover D, Smith D v., Blanchard EL, Alonas E, Kirschman JL, Lifland AW *et al.* RSV glycoprotein and genomic RNA dynamics reveal filament assembly prior to the plasma membrane. *Nature Communications* 2017; **8**. doi:10.1038/s41467-017-00732-z.

118 Easton AJ, Scott PD, Edworthy NL, Meng B, Marriott AC, Dimmock NJ. A novel broad-spectrum treatment for respiratory virus infections: Influenza-based defective interfering virus provides protection against pneumovirus infection in vivo. *Vaccine* 2011; **29**: 2777–2784.

119 Thube MM, Shil P, Kasbe R, Patil AA, Pawar SD, Mullick J. Differences in Type I interferon response in human lung epithelial cells infected by highly pathogenic H5N1 and low pathogenic H11N1 avian influenza viruses. *Virus Genes* 2018; **54**: 414–423.

120 Tissari J, Sirén J, Meri S, Julkunen I, Matikainen S. IFN-α Enhances TLR3-Mediated Antiviral Cytokine Expression in Human Endothelial and Epithelial Cells by Up-Regulating TLR3 Expression. *The Journal of Immunology* 2005; **174**: 4289–4294.

121 Chew T, Noyce R, Collins SE, Hancock MH, Mossman KL. Characterization of the interferon regulatory factor 3-mediated antiviral response in a cell line deficient for IFN production. *Molecular Immunology* 2009; **46**: 393–399.

122 Desmyter J, Melnick JL, Rawls WE. Defectiveness of Interferon Production and of Rubella Virus Interference in a Line of African Green Monkey Kidney Cells (Vero). *Journal of Virology* 1968; **2**: 955–961.

123 Emeny JM, Morgan MJ. Regulation of the interferon system: Evidence that vero cells have a genetic defect in interferon production. *Journal of General Virology* 1979; **43**: 247–252.

124 Osada N, Kohara A, Yamaji T, Hirayama N, Kasai F, Sekizuka S *et al.* The genome landscape of the African Green Monkey kidney-derived vero cell line. *DNA Research* 2014; **21**: 673–683.

125 Hijano DR, Vu LD, Kauvar LM, Tripp RA, Polack FP, Cormier SA. Role of type I interferon (IFN) in the respiratory syncytial virus (RSV) immune response and disease severity. *Frontiers in Immunology* 2019; **10**: 1–14.

126 Arora P, Bdeir N, Gärtner S, Reiter S, Pelz L. Interferon induction and not replication interference mainly determines anti- influenza virus activity of defective interfering particles. *bioRxiv* 2021.

127 Crowe JE, Collins PL, London WT, Chanock RM, Murphy BR. A comparison in chimpanzees of the immunogenicity and efficacy of live attenuated respiratory syncytial virus (RSV) temperature-sensitive mutant vaccines and vaccinia virus recombinants that express the surface glycoproteins of RSV. *Vaccine* 1993; **11**: 1395–1404.

128 Crowe JE, Bui PT, Siber GR, Elkins WR, Chanock RM, Murphy BR. Cold-passaged, temperature-sensitive mutants of human respiratory syncytial virus (RSV) are highly attenuated, immunogenic, and protective in seronegative chimpanzees, even when RSV antibodies are infused shortly before immunization. *Vaccine* 1995; **13**: 847–855.

129 Gupta CK, Leszczynski J, Gupta RK, Siber GR. Stabilization of respiratory syncytial virus (SV) against thermal inactivation and freeze-thaw cycles for

development and control of RSV vaccines and immune globulin. *Vaccine* 1996; **14**: 1417–1420.

130 Mundle ST, Kishko M, Groppo R, DiNapoli J, Hamberger J, McNeil B *et al.* Core bead chromatography for preparation of highly pure, infectious respiratory syncytial virus in the negative purification mode. *Vaccine* 2016; **34**: 3690–3696.

131 Ajamian F, Ilarraza R, Wu Y, Morris K, Odemuyiwa SO, Moqbel R *et al.* CCL5 persists in RSV stocks following sucrose-gradient purification. *Journal of Leukocyte Biology* 2020; **108**: 169–176.

132 Grosz DD, van Geelen A, Gallup JM, Hostetter SJ, Derscheid RJ, Ackermann MR. Sucrose stabilization of Respiratory Syncytial Virus (RSV) during nebulization and experimental infection. *BMC Research Notes* 2014; **7**: 1–9.

133 Kast JI, McFarlane AJ, Głobińska A, Sokolowska M, Wawrzyniak P, Sanak M *et al.* Respiratory syncytial virus infection influences tight junction integrity. *Clinical and Experimental Immunology* 2017; **190**: 351–359.

134 Perlmutter JD, Hagan MF. Mechanisms of virus assembly. *Annual Review of Physical Chemistry* 2015; **66**: 217–239.

135 Lohr V. Characterization of the avian designer cells AGE1.CR and AGE1.CR.pIX considering growth, metabolism and production of influenza virus and Modified Vaccinia Virus Ankara (MVA). *PhD Dissertation* 2014; : 1–178.

136 Caidi H, Harcourt JL, Haynes LM. RSV growth and quantification by microtitration and qRT- PCR assays. In: *Methods in Molecular Biology*. Humana Press Inc., 2016, pp 13–32.

137 Hendry RM, McIntosh K. Enzyme-linked immunosorbent assay for detection of respiratory syncytial virus infection: Development and description. *Journal of Clinical Microbiology* 1982; **16**: 324–328.

138 Perez JW, Adams NM, Zimmerman GR, Haselton FR, Wright DW. Detecting respiratory syncytial virus using nanoparticle-amplified immuno-PCR. *Methods in Molecular Biology* 2013; **1026**: 93–110.

139 Straub CP, Lau WH, Preston FM, Headlam MJ, Gorman JJ, Collins PL *et al.* Mutation of the elongin C binding domain of human respiratory syncytial virus non-structural protein 1 (NS1) results in degradation of NS1 and attenuation of the virus. *Virology Journal* 2011; **8**: 1–12.

140 Tran KC, Collins PL, Teng MN. Effects of Altering the Transcription Termination Signals of Respiratory Syncytial Virus on Viral Gene Expression and Growth In Vitro and In Vivo. *Journal of Virology* 2004; **78**: 692–699.

141 Heumann R, Duncan C, Stobart CC, Kaschner S. Dynamical Differences in Respiratory Syncytial Virus. *Bulletin of Mathematical Biology* 2022; **84**: 1–16.

142 Rajan A, Piedra F, Aideyan L, Mcbride T, Robertson M, Johnson HL *et al.* Multiple Respiratory Syncytial Virus (RSV) Strains Infecting HEp-2 and A549 Cells Reveal Cell Line-Dependent Differences in Resistance to RSV Infection. *Journal of Virology* 2022; **96**: 1–20.

143 Jiao P, Fan W, Cao Y, Zhang H, Tian L, Sun L *et al.* Robust induction of interferon and interferonstimulated gene expression by influenza B/Yamagata lineage virus infection of A549 cells. *PLoS ONE* 2020; **15**: 1–18.

144 Scott PD, Meng B, Marriott AC, Easton AJ, Dimmock NJ. Defective interfering influenza A virus protects in vivo against disease caused by a heterologous influenza B virus. *Journal of General Virology* 2011; **92**: 2122–2132.

145 Sung RYT, Yin J, Oppenheimer SJ, Tam JS, Lau J. Treatment of respiratory sycytial virus infection with recombinant interferon alfa-2A. *Archives of Disease in Childhood* 1993; **69**: 440–442.

146 Higgins PG, Barrow GI, Tyrrell DAJ, Isaacs D, Gauci CL. The efficacy of intranasal interferonα-2a in respiratory syncytial virus infection in volunteers. *Antiviral Research* 1990; **14**: 3–10.

147 Sleijfer S, Bannink M, van Gool AR, Kruit WHJ, Stoter G. Side effects of interferon-α therapy. Pharmacy World and Science. 2005; **27**: 423–431.

148 Pichler Prof Dr. WJ, Campi P. Adverse side effects to biological agents. In: *Drug Hypersensitivity*. Karger Publishers, 2007, pp 151–165.

149 Manns MP, Wedemeyer H, Cornberg M. Treating viral hepatitis C: Efficacy, side effects, and complications. Gut. 2006; **55**: 1350–1359.

150 Kim YI, Pareek R, Murphy R, Harrison L, Farrell E, Cook R *et al.* The antiviral effects of RSV fusion inhibitor, MDT-637, on clinical isolates, vs its achievable concentrations in the human respiratory tract and comparison to ribavirin. *Influenza and other Respiratory Viruses* 2017; **11**: 525–530.

151 Hruska JF, Bernstein JM, Douglas RG, Hall CB. Effects of ribavirin on respiratory syncytial virus in vitro. *Antimicrobial Agents and Chemotherapy* 1980; **17**: 770–775.

152 Ventre K, Randolph AG. Ribavirin for respiratory syncytial virus infection of the lower respiratory tract in infants and young children. Cochrane Database of Systematic Reviews. 2007. doi:10.1002/14651858.CD000181.pub3.

153 Hall CB, McBride JT, Walsh EE, Bell DM, Gala CL, Hildreth S *et al.* Aerosolized Ribavirin Treatment of Infants with Respiratory Syncytial Viral Infection. *New England Journal of Medicine* 1983; **308**: 1443–1447.

154 Hruska JF, Morrow PE, Suffin SC, Douglas RG. In vivo inhibition of respiratory syncytial virus by ribavirin. *Antimicrobial Agents and Chemotherapy* 1982; **21**: 125–130.

155 Mosca JD, Pitha PM. Transcriptional and posttranscriptional regulation of exogenous human beta interferon gene in simian cells defective in interferon synthesis. *Molecular and Cellular Biology* 1986; **6**: 2279–2283.

156 Hart BJ, Dyall J, Postnikova E, Zhou H, Kindrachuk J, Johnson RF *et al.* Interferon-β and mycophenolic acid are potent inhibitors of middle east respiratory syndrome coronavirus in cell-based assays. *Journal of General Virology* 2014; **95**: 571–577.

157 Wu JZ, Larson G, Walker H, Shim JH, Hong Z. Phosphorylation of ribavirin and viramidine by adenosine kinase and cytosolic 5′-nucleotidase II: Implications for ribavirin metabolism in erythrocytes. *Antimicrobial Agents and Chemotherapy* 2005; **49**: 2164–2171.

158 Shah NR, Sunderland A, Grdzelishvili VZ. Cell type mediated resistance of vesicular stomatitis virus and sendai virus to ribavirin. *PLoS ONE* 2010; **5**. doi:10.1371/journal.pone.0011265.

159 Morgenstern B, Michaelis M, Baer PC, Doerr HW, Cinatl J. Ribavirin and interferon-β synergistically inhibit SARS-associated coronavirus replication in animal and human cell lines. *Biochemical and Biophysical Research Communications* 2005; **326**: 905–908.

160 Falzarano D, de Wit E, Martellaro C, Callison J, Munster VJ, Feldmann H. Inhibition of novel β coronavirus replication by a combination of interferon-α2b and ribavirin. *Scientific Reports* 2013; **3**: 1–6.

161 Belicha-Villanueva A, Rodriguez-Madoz JR, Maamary J, Baum A, Bernal-Rubio D, Minguito de la Escalera M *et al.* Recombinant Influenza A Viruses with Enhanced Levels of PB1 and PA Viral Protein Expression. *Journal of Virology* 2012; **86**: 5926–5930.

162 Taniguchi M, Yanagi Y, Ohno S. Both type I and type III interferons are required to restrict measles virus growth in lung epithelial cells. *Archives of Virology* 2019; **164**: 439–446.

163 Schoggins JW. Interferon-stimulated genes: Roles in viral pathogenesis. Current Opinion in Virology. 2014; **6**: 40–46.

164 Wang HF, Chen L, Luo J, He HX. KLF5 is involved in regulation of IFITM1, 2, and 3 genes during H5N1 virus infection in A549 cells. *Cellular and Molecular Biology* 2016; **62**: 65–70.

Elena Piagnani

Date of birth: 28/06/1997 | (+39) 3311043210 | elena.piagnani@student.uniri.hr |

https://www.linkedin.com/in/elena-piagnani-a4650019a/ | Via Campo di Marte 6A2, 06124, Perugia, Italy

About me: Biotechnology undergraduate with operational dexterity in research laboratories and a strong interest in medical research and molecular biology techniques. Used to working in an international environment. Able to combine academic knowledge and practical skills with a solution-oriented approach. Motivated, detail-oriented, fast learner and able to work both in a team and individually.

EDUCATION AND TRAINING

04/10/2020 – 28/07/2022 – Rijeka, Croatia
MASTER'S DEGREE IN BIOTECHNOLOGY FOR THE LIFE SCIENCES – University of Rijeka

31/01/2019 – 29/06/2019 – Riga, Latvia
ERASMUS+ EXCHANGE – University of Latvia

14/09/2016 – 11/02/2020 – Fano, Italy
BACHELOR'S DEGREE IN BIOTECHNOLOGY – Università degli Studi di Urbino Carlo Bo

09/09/2011 – 12/07/2016 – Perugia, Italy
CLASSICAL HIGH SCHOOL DIPLOMA – Liceo Classico e Musicale Annibale Mariotti

WORK EXPERIENCE

20/09/2021 – 20/06/2022 – Magdeburg, Germany
INTERNSHIP ""RESPIRATORY SYNCYTIAL VIRUS REPLICATION: INHIBITION BY INFLUENZA A VIRUS DEFECTIVE INTERFERING PARTICLES" – MAX PLANCK INSTITUTE FOR DYNAMICS OF COMPLEX TECHNICAL SYSTEMS

I assessed the antiviral potential of influenza A virus (IAV) defective interfering particles (DIPs) DI244 and OP7 against respiratory syncytial virus (RSV) propagation. I produced a seed virus with a low content of natural DIPs and carried out dynamics and coinfection studies in A549 and Vero cells. I carried out host cell gene expression analysis to investigate the gene expression levels of antiviral genes linked to the innate immune response, to confirm that the antiviral effect of IAV DIPs is interferon-dependant.

18/04/2021 – 03/06/2021 – Rijeka, Croatia
INTERNSHIP "IMMUNITY IN NEURODEGENERATIVE DISORDERS" – UNIVERSITY OF RIJEKA

I investigated the role of optineurin deficiency in protein aggregates accumulation in vitro. Wild type BV2 cells and a BV2 cell line in which the optineurin gene was knocked out using CRISPR-Cas9 technology were used. I induced endoplasmic reticulum (ER) stress with Tunicamycin, lipopolysaccharide and sodium arsenite and performed western blots for dose-response and pharmacokinetics experiments. I assessed the effect of ER stress on cells via fluorescence microscopy.

28/02/2021 – 15/04/2021 – Rijeka, Croatia
INTERNSHIP "DETECTION OF MICROPLASTICS IN SEAWATER" – UNIVERSITY OF RIJEKA

I researched a method for the determination of plastic polymers in seawater using Matrix-Assisted Laser Desorption/Ionization-Time of Flight mass spectrometry (MALDI) and Attenuated Total Reflectance Fourier-transform infrared spectroscopy (ATR-FTIR). I created a plastic library on an ATR-FTIR spectrometer. I developed a protocol for cleaning seawater plastic samples from organic and inorganic impurities and for dissolving polystyrene and polyvinyl chloride. I investigated the efficacy of several matrixes for analysis of plastic polymers on MALDI.

30/06/2018 – 19/08/2018 – Branca, Italy

INTERNSHIP AT USL UMBRIA 1 – USL UMBRIA 1 - BRANCA'S HOSPITAL

I worked in the medical laboratory of the hospital.
Highlights: bacterial cultures on petri dishes, sweat tests for the diagnosis of cystic fibrosis, antibiograms, observation of samples using the light microscope.

Branca, Italy

JOB-RELATED SKILLS

Job-related skills

- Experiment Planning
- Hypothesis Development
- Protocol Optimization
- Cell culture in a sterile environment
- Bacterial culture
- Virus production in vitro
- Coinfection assay
- TCID50
- Plaque assay
- RT-PCR
- RT-qPCR
- ELISA
- Western Blotting
- SDS-PAGE
- Gel Electrophoresis
- Plasmid Transformation
- Immunofluorescence Staining
- Fluorescence and Light Microscopy
- Mass Spectrometry
- Chromatography

DIGITAL SKILLS

My Digital Skills

Microsoft Office | Graph Pad Prism | ImageJ | BioRender | Google Drive

LANGUAGE SKILLS

Mother tongue(s): **ITALIAN**

Other language(s):

	UNDERSTANDING		SPEAKING		WRITING
	Listening	Reading	Spoken production	Spoken interaction	
ENGLISH	C1	C2	C1	C1	C2
FRENCH	B1	B2	A2	A2	B1
CROATIAN	A1	A1	A1	A1	A1

Levels: A1 and A2: Basic user; B1 and B2: Independent user; C1 and C2: Proficient user